INVESTIGATION OF THE EFFECTS OF FMOC AMINO ACIDS MODIFICATIONS TO OSTEOBLAST BEHAVIOUR ON RGO/Ti SURFACE

by

ELİF DÖNMEZ

B.S., Physics, Istanbul University, 2010

Submitted to the Institute of Biomedical Engineering
in partial fulfillment of the requirements
for the degree of
Master of Science
in
Biomedical Science

Boğaziçi University
2015

INVESTIGATION OF THE EFFECTS OF FMOC AMINO ACIDS MODIFICATIONS TO OSTEOBLAST BEHAVIOUR ON RGO/Ti SURFACE

APPROVED BY:

Assist. Prof. Dr. Bora Garipcan .....
(Thesis Advisor)

Assoc. Prof. Dr. Albert Güveniş .....

Assist. Prof. Dr. Ayşe Ak .....

DATE OF APPROVAL: 30 July 2015

ACKNOWLEDGMENTS

I would like to thank my committee members, Assist. Prof. Dr. Bora Garipcan, Assist. Prof. Dr. Ayşe Ak and Prof. Dr. Albert Güveniş for contribution and constructive comments.

I would like to offer my sincere thanks to Assist. Prof. Dr. Duygu Ege for her support, motivation and guidance. I would like to thank Assist. Prof. Dr. Ayşe Ak for teaching the cell studies and helping the cell experiments. I also would like to thank Assist. Prof. Dr. Hamdi Torun and his lab members for their helps.

I would like to thank the financial support of Bogaziçi University Scientific Research Fund (BAP) under Grant Number No.6701.

I specially thank my friends; Nazire Mercan, Öznur Taşlıyurt, Ecem Şahin, Fotaş Nacar, Hayriye Öztatlı, Sabra Rostami, Samet Kocatürk, Sezin Eren and BoNErve biomaterial group members for their support and motivation.

I would like to thank my beloved family members for the never-ending support, encouragement and love.

ABSTRACT

INVESTIGATION OF THE EFFECTS OF FMOC AMINO ACIDS MODIFICATIONS TO OSTEOBLAST BEHAVIOUR ON RGO/Ti SURFACE

In this thesis, adhesion, proliferation and morphology of osteoblast cells on functionalized RGO/Ti surface were investigated. Firstly, amino-functionalization with 3-aminopropyl phosphonic acid (APA) molecules on Ti surface was carried out. Graphene oxide flakes were immobilized on APA/Ti surfaces through interaction between the epoxy groups of GO and the amine groups of APA molecules. Reduced graphene oxide sheet on APA/Ti surface were performed by using hydrazine monohydrate treatment. In order to enhance further surface bioactivity, Fmoc amino acids having different the hydropathy indexes modified on RGO/Ti surface by the $\pi - \pi$ bond. The chemistry and morphology of unmodified and modified Ti surfaces were characterized by using Water Contact Angle (WCA) measurement, X-ray Photoelectron Spectroscopy (XPS), Raman Spectroscopy, Atomic Force Microscopy (AFM) and Scanning Electron Microscopy (SEM). According to characterization results, Ti surfaces were coated with GO and RGO, as well as the surface hydrophilicity was controlled by functionalization with Fmoc amino acids successfully. Then, cell viability, proliferation and morphology were examined by using the MTT, Alamar Blue Assays and SEM, respectively. The in vitro studies indicated that the surface chemistry and nanometric roughnesses on designed materials remarkably enhanced cell behavior, especially with respect to initial adhesion and proliferation. Consequently, the development of novel interface at cell/implant has a great potential for increasing osseointegration in the field of bone tissue engineering.

Keywords: Graphene Oxide (GO), Reduced Graphene Oxide (RGO), Titanium, Fmoc amino acids, $\pi - \pi$ interaction, Biocompatibility.

ÖZET

FMOC AMİNO ASİTLER İLE MODİFİYE EDİLMİŞ RGO/Ti YÜZEYLERIİNİN OSTEOBLAST HÜCRE DAVRANIŞLARI ÜZERİNDEKİ ETKİLERİNİN İNCELENMESİ

Bu tez çalışmasında, fonksiyonlandırılmış RGO/Ti yüzeyi üzerinde osteoblast hücrelerinin yapışma, çoğalma ve morfolojisi incelenmiştir. İlk olarak, 3-aminopropil fosfonik asit (AFA) molekülleri ile amino-işlevselleştirmesi gerçekleştirilmiştir. AFA moleküllerinin amin grubu ve GO'in epoksi grubunun arasındaki etkileşimi ile grafen oksit tabakları AFA/Ti yüzeyi üzerine immobilize edilmiştir. AFA/Ti yüzeyiüzerinde indirgenmiş grafen oksit tabakaları hidrazin monohidrat kullanarak kimyasal işlemi gerçekleştirilmiştir. Daha fazla yüzeyin biyolojik aktivitesini arttırmak için farklı hidropati endekslerine sahip Fmoc amino asitler $\pi - \pi$ bağı ile RGO/Ti yüzeyine modifiye edilmiştir. Su Temas Açısı ölçümleri, X-ışını Fotoelektron Spektroskopisi, Raman Spektroskopi, Atomik Güç Mikroskobu ve Taramalı Elektron Mikroskobu kullanılarak modifiye edilmemiş ve edilmiş Ti yüzeylerinin kimyası ve morfolojisi karakterize edilmiştir. Karakterizasyon sonuçlarına göre, Ti yüzeyleri GO ve RGO ile kaplanmış ve yüzey hidrofilisitesi Fmoc amino asitler ile başarıyla kontrol edilmiştir. Daha sonrasında, hücre canlılığı, çoğalması ve morfolojisi MTT, Alamar Blue analiz yöntemleri ve SEM kullanılarak incelenmiştir. In vitro hücre çalışmaları gösterdi ki tasarlanan malzemelerde yüzey kimyası ve nanometrik pürüzler özellikle ilk yapışma ve çoğalması ile ilgili olarak hücre davranışlarını önemli derecede geliştirmektedir. Sonuç olarak, hücre-implant arasında yeni geliştirilen arayüz, kemik doku mühendisliği alanında osseointegrasyonunu arttırmak için büyük bir potansiyele sahiptir.

Anahtar Sözcükler: Grafen Oksit (GO), İndirgenmiş Grafen Oksit (İGO), Titanyum, Fmoc amino asit, $\pi - \pi$ etkileşimi, Biyouyumluluk.

TABLE OF CONTENTS

ACKNOWLEDGMENTS iii
ABSTRACT iv
ÖZET v
LIST OF FIGURES viii
LIST OF TABLES xii
LIST OF SYMBOLS xiv
LIST OF ABBREVIATIONS xv
1. INTRODUCTION 1
1.1 Motivation 1
1.2 Objective 3
1.3 Outline 3
2. BACKGROUND 4
2.1 Surface Modification of Titanium and Titanium Alloys for Biomedical Applications 4
2.2 Self-Assembled Monolayers (SAMs) in Surface Engineering 6
2.3 General Overview of Graphene 9
2.4 Structure, Reduction, Functionalization and Applications of Graphene Oxide 9
2.4.1 Graphene and Graphene derivatives in Tissue Engineering . . . 12
2.5 Influence of Fmoc-terminated amino acid derivatives on cellular responses. 14
2.6 Adsorption of Fmoc-terminated amino acids on CNTs and graphene derivatives. 15
3. MATERIALS AND METHODS 18
3.1 Chemical Surface Modification 18
3.1.1 Modification of Titanium Surface with APA (3-aminopropyl phosphonic acid) molecules 18
3.1.2 Preparation of GO/Ti Nanocomposite 18
3.1.3 Preparation of Reduction of GO/Ti Nanocomposite 19

3.1.4 Modification of RGO/Ti Nanocomposite with Amino Acid conjugated Fmoc . . . 19
3.2 Surface Characterization . . . 21
3.2.1 Scanning Electron Microscopy (SEM) . . . 21
3.2.2 Atomic Force Microscopy (AFM) . . . 21
3.2.3 Water Contact Angle (WCA) Measurements . . . 21
3.2.4 X-ray Photoelectron Spectroscopy (XPS) . . . 22
3.2.5 Raman Spectroscopy . . . 22
3.3 Cell Studies . . . 22
3.3.1 Cell Culture . . . 23
3.3.2 Cell Viability and Proliferation . . . 23
4. RESULTS . . . 26
4.1 Surface Characterization . . . 26
4.1.1 Scanning Electron Microscopy (SEM) . . . 26
4.1.2 Atomic Force Microscopy (AFM) . . . 31
4.1.3 Water Contact Angle Measurements . . . 33
4.1.4 X-ray Photoelectron Spectroscopy (XPS) Analysis . . . 37
4.1.5 Raman Spectroscopy . . . 48
4.2 Cell Studies . . . 51
4.2.1 MTT Assay of unmodified and modified Ti surface . . . 51
4.2.2 Alamar Blue Assay of unmodified and modified Ti surface . . . 55
4.2.3 Cell Adhesion and Morphology of unmodified and modified Ti surface . . . 62
5. DISCUSSION . . . 68
5.1 Future Studies . . . 78
REFERENCES . . . 79

LIST OF FIGURES

Figure 2.1	Schematic diagram of Structures of Self-Assembled Monolayer on Substrate	7
Figure 2.2	Schematic view of some possible binding modes between phosphonic acid SAMs and Titanium dioxide (a monodentate P-O-M, bidentate P=O, tridentate P-OH bindings and bridging interactions)	8
Figure 2.3	a) Few-layered graphene or Graphite b) Graphene c) Graphene Oxide (GO) d) Reduced Graphene Oxide (RGO).	10
Figure 3.1	Schematic representation of (a) Bare Titanium, (b) Activated Ti surface, (c) APA modified Ti surface, (d) GO/Ti nanocomposite,(e) RGO/Ti nanocomposite, (f) Fmoc-Leu-OH/RGO/Ti nanocomposite, (g) Fmoc-Ser-OH/RGO/Ti nanocomposite.	20
Figure 4.1	SEM image of Graphene Oxide (GO).	26
Figure 4.2	SEM images of bare Ti surface and GO flakes on APA/Ti surfaces (left side).	27
Figure 4.3	SEM images of bare Ti surface and GO flakes on APA/Ti surfaces (right side).	28
Figure 4.4	SEM images of GO flakes on APA/Ti surfaces after doping Au particles.	29
Figure 4.5	SEM images of chemically Reduced GO flakes on APA/Ti surface.	29
Figure 4.6	SEM images of Fmoc-Ser-OH modified on RGO /Ti surface.	30
Figure 4.7	SEM images of Fmoc-Ser-OH modified on RGO /Ti surface.	30
Figure 4.8	AFM images and Surface profiles of RGO flakes on APA/Ti (a) deflection signal (b) height image (c) height profile.	31
Figure 4.9	3D AFM images of RGO flakes on APA/Ti surface: (d) deflection signal (e) height image.	32
Figure 4.10	Water contact Angle photographs of (a) bare Ti, (b) APA modified Ti.	33

Figure 4.11	Water Contact Angle photographs of (a) GO coating APA/Ti, (b) RGO coating APA/Ti.	34
Figure 4.12	Water Contact Angle photographs of Fmoc-Leu-OH modified on RGO/Ti surface with different dipping time : (a) 2h, (b) 8h, (c) 16h, (d) 24h.	35
Figure 4.13	Water Contact Angle photographs of Fmoc-Ser-OH modified on RGO/Ti surface with different dipping time : (a) 2h, (b) 8h, (c) 16h, (d) 24h.	35
Figure 4.14	Water contact angle degree of bare Ti, activated Ti, APA/Ti, GO/Ti, RGO/Ti, Fmoc-Ser-OH/RGO/Ti (24h) and Fmoc-Leu-Oh/RGO/Ti (24h).	36
Figure 4.15	XPS Survey Analysis of Ti.	37
Figure 4.16	XPS Survey Analysis of APA/Ti.	38
Figure 4.17	High-resolution spectra of oxygen peaks (O1s) for APA/Ti.	39
Figure 4.18	High-resolution spectra of phosphate peaks (P2p) for APA/Ti.	40
Figure 4.19	XPS Survey Analysis of GO/Ti.	40
Figure 4.20	High-resolution spectra of carbon peaks (C1s) for GO/Ti.	41
Figure 4.21	XPS Survey Analysis of RGO/Ti.	42
Figure 4.22	High-resolution spectra of carbon peaks (C1s) for RGO/Ti.	43
Figure 4.23	XPS Survey Analysis of Fmoc-Leu-OH modified on RGO/Ti.	44
Figure 4.24	High-resolution spectra of carbon peaks (C1s) for Fmoc-Leu-OH/RGO/Ti.	45
Figure 4.25	XPS Survey Analysis of Fmoc-Ser-OH modified on RGO/Ti.	46
Figure 4.26	High resolution spectra of carbon peaks (C1s) for Fmoc-Ser-OH/RGO/Ti.	47
Figure 4.27	Raman spectra of Bare Ti surface.	48
Figure 4.28	Raman spectra of GO/Ti and RGO/Ti surface.	49
Figure 4.29	Raman spectras of Ti, GO/Ti and RGO/Ti surface.	50
Figure 4.30	Raman spectras of Fmoc Amino Acids on RGO/Ti surfaces.	51
Figure 4.31	MTT assay results at 1st day. Data is expressed in means ± SE and represent the results of three independent experiments ($p < 0.05$).	52

Figure 4.32 MTT assay results at 3rd day. Data is expressed in means ± SE and represent the results of three independent experiments ($p < 0.05$). 53
Figure 4.33 MTT assay results at 5th day. Data is expressed in means ± SE and represent the results of three independent experiments ($p < 0.05$). 54
Figure 4.34 MTT assay for assessing cellular viability of osteoblasts on all experimental groups after 24h, 72h and 120h of application. 54
Figure 4.35 Alamar Blue assay results at 1st day. Data are presented as mean ± standard error of percentage viability compared to negative control (n=15, $p < 0.05$). 56
Figure 4.36 Alamar Blue assay results at 1st day. Data are presented as mean ± standard error of percentage viability compared to positive control (n=15, $p < 0.05$). 56
Figure 4.37 Alamar Blue assay results at 3rd day. Data are presented as mean ± standard error of percentage viability compared to negative control (n=15, $p < 0.05$). 58
Figure 4.38 Alamar Blue assay results at 3rd day. Data are presented as mean ± standard error of percentage viability compared to positive control (n=15, $p < 0.05$). 58
Figure 4.39 Alamar Blue assay results at 5th day. Data are presented as mean ± standard error of percentage viability compared to negative control (n=15, $p < 0.05$). 59
Figure 4.40 Alamar Blue assay results at 5th day. Data are presented as mean ± standard error of percentage viability compared to positive control (n=15,$p < 0.05$). 59
Figure 4.41 Alamar Blue assay for evaluating proliferation of osteoblasts compare to negative control group after 24h, 72h and 120h of incubation. 60
Figure 4.42 Alamar Blue assay for evaluating proliferation of osteoblasts compare to positive control group after 24h, 72h and 120h of incubation. 60

Figure 4.43 SEM images of cell morphologies on Ti (a,x1000; b,x2000; c,x5000 magnification), APA/Ti (d,x1000; e,x2000; f,x5000 magnification),GO/Ti (g,x1000; h,x2000; i,x5000 magnification), RGO/Ti (j,x1000; k,x2000; l,x5000 magnification), Fmoc-Leu-OH/RGO/Ti (m,x1000; n,x2000; o,x5000 and p,x1000; qx2000; r,x5000 magnification) and Fmoc-Ser-OH/RGO/Ti (s,x1000; t,x2000; u,x5000 and v,x500; w,x1000; x,x2000 magnification) after 1st day of culture. 63

Figure 4.44 SEM images of GO flakes modified on Ti surfaces (a,x200; b,x0100; c,x2000; d,e,f x5000 magnification) after 1st day of cell culture.) 64

Figure 4.45 SEM images of RGO flakes modified on Ti surfaces (a,x100; b,x1000; c,x2000; d,x5000; e,x10.000; f,x5000 (10kV) magnification) after 1st day of cell culture. 65

Figure 4.46 SEM images of cell morphologies on Ti (a,x100; b,x2000 magnification), APA/Ti (c,x100; d,x1000 magnification) and GO/Ti (e,x200; f,x2000 magnification) surfaces after 3rd day of culture. 66

Figure 4.47 SEM images of cell morphologies on RGO/Ti (g,x100; h,x2000 magnification), Fmoc-Ser-OH/RGO/Ti (i,x200; j,x1000 magnification), Fmoc-Leu-OH/RGO/Ti (k,x200; l,x1000 magnification) surfaces after 3rd day of culture. 67

LIST OF TABLES

Table 2.1	Hydropathy index for Standart Amino Side Chains.	17
Table 4.1	Water Contact Angle measurements of Bare, Activated and APA modified Ti.	33
Table 4.2	Water Contact Angle photographs of (a) Graphene oxide coating APA/Ti, (b) Reduced graphene oxide coating APA/Ti.	34
Table 4.3	Water Contact Angle Measurements of 5mM Fmoc-Leu-OH amino acids modified on RGO/Ti surface with different dipping times (2-24h).	35
Table 4.4	Water Contact Angle Measurements of 5mM Fmoc-Ser-OH amino acids modified on RGO/Ti surface with different dipping times (2-24h).	36
Table 4.5	Atomic percentages of APA/Ti surface.	38
Table 4.6	Parameters of APA/Ti showing binding energy (eV), full width at half maximum (FWHM, eV), relative % concentration and chemical bonds.	39
Table 4.7	Atomic percentages of GO coating APA/Ti surface.	41
Table 4.8	Parameters of GO/Ti showing binding energy (eV), full width at half maximum (FWHM, eV), relative % concentration and chemical bonds.	42
Table 4.9	Atomic percentages of RGO/Ti surface.	43
Table 4.10	Parameters of RGO/Ti showing binding energy (eV), full width at half maximum (FWHM, eV), relative % concentration and chemical bonds.	44
Table 4.11	Atomic percentages of Fmoc-Leu-OH/RGO/Ti.	45
Table 4.12	Parameters of Fmoc-Leu-OH/RGO/Ti showing binding energy (eV), full width at half maximum (FWHM, eV), relative % concentration and chemical bonds.	46
Table 4.13	Atomic percentages of RGO/Ti surface.	47

Table 4.14 Parameters of Fmoc-Ser-OH/RGO/Ti showing binding energy (eV), full width at half maximum (FWHM, eV), relative% concentration and chemical bonds. 48

LIST OF SYMBOLS

ε_{OX}	Molar extinction coefficient of AlamarBlue oxidized form (BLUE)
ε_{RED}	Molar extinction coefficient of AlamarBlue reduced form (RED)
A	Absorbance of test wells
A'	Absorbance of negative control well + without cells
A^o	Absorbance of positive growth control well
λ_1	Wavelenght (570nm)
λ_2	Wavelenght (595nm)

LIST OF ABBREVIATIONS

AFM	Atomic Force Microscopy
APA	3-Aminopropyl Phosphonic Acid
DMEM	Dulbecco's Modified Eagle's Medium
DMF	N, N-Dimethylformamide
DMSO	Dimethyl sulfoxide
FBS	Fetal Bovine Serum
Fmoc	N-(fluorenyl-9-methoxycarbonyl)
Fmoc-Leu	N-(fluorenyl-9-methoxycarbonyl) conjugated Leucine
Fmoc-Ser	N-(fluorenyl-9-methoxycarbonyl) conjugated Serine
GO	Graphene Oxide
RGO	Reduced Graphene Oxide
SAM	Self Assembled Monolayer
SEM	Scanning Electron Microscopy
TCPS	Tissue Culture Polystyrene
Ti	Titanium
XPS	X-ray Photoelectron Microscopy
WCA	Water Contact Angle

1. INTRODUCTION

1.1 Motivation

Graphene holds tremendous potential for nanoscience and nanotechnology because of its unique structure and excellent physical, chemical and mechanical properties. Graphene and its derivatives, the most known as graphene oxide (GO) and reduced graphene oxide (RGO) together with their chemically modified graphene sheets (CMGs), have been particularly investigated in interdisciplinary areas [1]. In addition to electronic and chemical applications, the use of graphene-based materials with chemical functionalization and modification have shed light on the novel developments in biomedical applications, such as drug/gene delivery, imaging, photothermal cancer therapy, biosensors, antibacterial agents, tissue engineering and and regenerative medicine [2, 3].

The developing bone tissue engineering substantially based on incoming advancements of material sciences and regenerative medicine. Graphene and graphene derivatives have been becoming popular materials due to exhibiting outstanding achievement for promoting the adhesion, proliferation of various cells (e.g.fibroblasts, osteoblasts, myoblasts, hMSCs, hNSCs and iPSCs etc.) and also differentiation. However, it can be difficult for graphene and its derivatives to be directly implanted in living tissue without the help of support materials such as polymers, nanoparticles etc. in bone tissue engineering [4]. Graphene and its derivatives combined with new support substrates for novel and useful composite materials have been still researched to increase their potential applications.

Titanium (Ti) and Ti alloys are mostly used as surgical implant materials in bone-tissue engineering for treatment of large bone defects owing to its excellent mechanical strength, chemical stability, corrosion resistance and biocompatibility. Despite of all properties, improvement of biocompatibility and bioactivity is required in order

to construct a new tissue-interface between Ti and host bone [5, 6]. The functionalization and modification of solid substrates provide change and supervision of the physico-chemical surface properties for tailoring smart interface at cell-implant material in bone-tissue engineering [7]. Therefore, graphene derivatives based Ti composite material has emerged as a promising alternative approach to organize and maintain cellular activity.

By non-covalent interactions such as $\pi - \pi$ stacking, cation-π, or van der Waals interactions, GO and RGO members of carbon nanomaterials family possess physical and chemical properties to bind biomolecules such as nucleic acids, peptides, and aromatic chemical compounds [8]. The use of Fluorenylmethoxycarbonyl (Fmoc) aromatic group protected amino acids or short peptides is believed to be an attractive strategy in tissue engineering and drug delivery due to its effective molecular gelator and protecting features [9]. The integration of graphene derivatives and Fmoc amino acids by utilizing the $\pi - \pi$ stacking interaction provides further improving the surface properties to cell behavior [10].

The development of surface chemistry and morphology of artificial bone substitutes is a critical point in success of implant surgery. Herein, novel composite materials were designed and characterized as well as biological response of osteoblasts cells on designed nanocomposite surfaces was described. The important parameters for interface at cell-implant material were addressed and discussed.

1.2 Objective

In this thesis, graphene derivatives-based materials were designed to elucidate the osteoblast cell behavior. In order to enhance the biocompatibility, RGO/Ti nanocomposite surfaces were modified by utilizing $\pi - \pi$ stacking interaction with Fmoc-amino acids (Fmoc-Serine and FMOC-Leucine selected as model biomolecules), respectively. Cellular behavior (adhesion, proliferation, viability etc.) were investigated. The main objectives of this thesis are :

- To improve the efficiency and feasibility of GO and RGO.
- To demonstrate the preparation and characterization of both GO and RGO modified Ti surfaces.
- To increase the biocompatibility of Ti surface by using GO, RGO and biomolecules (hydrophilic and hydrophobic amino acids) in biomedical applications.
- To investigate and control sv40 osteoblast cell behavior on designed nanocomposite materials by using SEM, MTT and Alamar Blue Assay.

1.3 Outline

The thesis is presented as follows: In chapter 2, background information about surface modification of Titanium, self assembled monolayer, graphene and its derivatives: structure, functinalization, applications and impacts together with Fmoc amino acids on cell behavior is given. In chapter 3, the experimental procedures are explained. In chapter 4, the results are presented. In chapter 5, the discussion of the results are given.

2. BACKGROUND

Biomaterial science is of paramount importance in the field of bone-tissue engineering to repair, maintain, or improve the function of damaged or deteriorating tissues or organs. Synthetic and natural biomaterials such as polymers, ceramics, metals and composites are being used as bone graft substitutes after large bone defects [11]. The ongoing researches for bone substitutes have exhibited, however, insufficient bioactivity of these conventional implant materials may entail the poor and incomplete osseointegration at the interaction bone-implant interface [12]. The development of quantity and quality of bone-implant interface with surface modification or coating at microscale and nanoscale is promising gateway to promote and accelerate the mechanism of osseointegration [13].

2.1 Surface Modification of Titanium and Titanium Alloys for Biomedical Applications

Bone lose induced traumatic injuries, tumor and other bone diseases are crucial health problems. To address the large bone deficiencies, one of the current clinical treatments is implantation of metallic structures such as platinum, titanium (Ti). By virtue of an outstanding mechanical strength, corrosion resistance, chemical stability, low toxicity and bioinertness, titanium and its different alloys are being routinely preferred as surgical implants, especially orthopedic implant materials and dentistry as well as maxillofacial, cardiac and cardiovascular applications [14]. However such conventional and invasive implant materials need bioactivity to improve interactions between implant surface and tissue surrounding the implant in bone-tissue engineering. There occurs osseointegration which known as the firm and stable anchorage of a surgical implant by the growth of bone tissue at the bone-implant interface [13].

The spontaneously formed natural oxide layer (TiO_2) having 2-5 nm thickness on the pure Ti surface partially provides bioactivity [15]. However, such level of bioactivity is inadequate to prevent against inflammation, fibrosis, thrombosis and infection induced implant material and to obtain cell adhesion or tissue growth on implant surface. Therefore; appropriate and suitable physical or chemical changes of titanium implant surface are important factor for stimulating cell behaviour such as adhesion, migration, orientation, guidance, growth, proliferation and differentiation. In order to alter substrate surfaces, there are three major techniques are used and classified as morphological, physico-chemical, biochemical modification [16, 17].

The physico-chemical, topographical and biochemical properties of implanted a biomaterial including surface-free energy, chemical composition, microstructure, roughness, corrosion resistance, bio-compatibility and wettability (hydrophilicity or hydrophobicity) have considerable effects on biological responses and processes (protein adsorption, cell-surface material interaction, tissue development etc.) for achieving tissue healing in a short time, initial and long-term efficacy in appropriate applications [5].

Functionalization and modification with bioactive molecules on material surface are significant in biomaterial research to further enhance the surface biocompatibility and bioactivity For this purpose, different surface modification techniques such as hydroxyapatite-coated surface [18], sol-gel deposition [19], chemical (alkali/acid) treatment [20], anodization, plasma spray [21], and self-assembled monolayers [22] have been developed. Nevertheless, initial and long-term integration of the implant material with host bone have been still researched to improve clinical success in biomedical applications.

2.2 Self-Assembled Monolayers (SAMs) in Surface Engineering

Self-assembled monolayers (SAMs) represent a single layer of ordered molecular assemblies that are formed by spontaneous self-organization of organic molecules on the surface of appropriate substrates. The construction of more highly ordered molecules on surfaces of substrates occurred by using self assembly process which is a controllable technique on the molecular level. SAMs have been applied in chemical synthesis, biosensor, polymer science and surface engineering [23, 24].

Material surface properties including chemistry, micro-topography, biocompatibility and wettability etc. can be varied and controlled by using SAMs to build up the smart interfaces of material substrates in possible applications such as biomaterial science. The chemisorption of the surfactants on substrate surfaces could be created by either covalent or non-covalent bindings. In recent years, the two methods are commonly used to create the modification of active organic molecules on solid surfaces. These methods are called as Langmuir-Blodgett and self-assembly technique for depositing molecules as a monolayer. These dynamic systems present a powerful and highly flexible surface modification with densely-packed two-dimensional arrays of molecules [23, 24].

The structure of an active surfactant is formed by a head-group, a backbone or spacer which is usually with an alkyl group, and a reactive tail group (Figure 2.1) [24, 25]. SAMs are mainly based on the specific interaction between head-group and the substrate surface. By the aid of the alkyl chain, a monolayer structure on surface can remain its stability because of van der Waals interactions. SAMs modifications of the surfactants on a solid surface are performed from either liquid or a gas phase reaching the minimum surface energy that is associated with the chemisorption [23]. The terminal end group called as the reactive functional groups give rise to highly physical and chemical changes of surfaces. The reactive functional groups (i.e. -OH,-CH_3, -COOH, or -NH_2) have also enabled the modification of a variety of biomoleculus such as proteins, peptides, DNA, carbohydrates and antibodies and cells-surfaces interactions in biomedical science [26, 27].

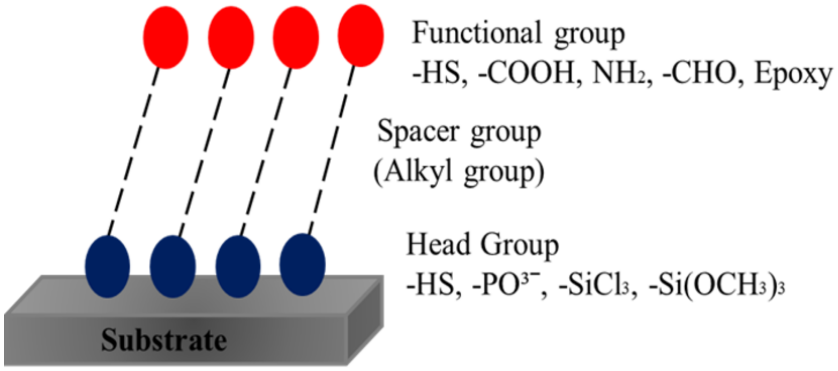


Figure 2.1 Schematic diagram of Structures of Self-Assembled Monolayer on Substrate

Interfacial reactions depend on the convenient affinity of anchor group of surfactant molecules, preparation conditions and surface morphology of substrate. The functionalization of solid substrates have been still studied with monolayer self-assembly systems including alkanethiols on noble metals (especially gold) [28], alkylsilanes on hydroxy functionalized surfaces (especially silicon) [29], isonitriles on platinum [30], and phosph(on)ates on metal oxides [31] according to their versatility and stability.

The stability of organic molecules on substrates is crucial for initial and long-term success of an implant materials in biomedical applications. Recently phosphonic acid (or an alkylphosphoric acid) molecule has been introduced for SAM formation on appropriate surfaces. Self-assembled construction of phosphonate anchor groups on a wide range of oxide surfaces can provide alternative solutions to overcome the limitation of thiol and silane systems in terms of a robustly ordered and fully covering self assembled monolayer [32]. PAs (Phosphonic Acids) are covalently attached to metal oxide surface thanks to process of an acid-base reaction with the hydroxyl groups on surface [33]. Schwartz et al. reported that the strong bonding of self-assembled monolayers of phosphonates to Ti or Ti alloy surfaces exhibited because of more hydrolyticly stability under physiological condition. Furthermore, previous studies have suggested that silane terminated monolayers on metal substrates showed less tendency to preserve physical and chemical stability in contrast to PAs terminated monolayers [32].

Chemical modification of the native oxide surface of Ti implant material have been carried out by using self-assembled monolayers (SAMs) of silane-, phosphonate-, or phosphonic acid- based molecules because of their affinity toward metal oxide surfaces. In addition to formation of phosphate- or phosphonic acid based SAM on Ti substrates, SAM formation of phoshonic acids on substrate surfaces (e.g.Al_2O_3, ZnO, Indium tin oxide (ITO), planar mica, and SiO_2)has been studied [25]. The some possible binding modes between PAs and TiO_2 were shown in Figure 2.2 [25]

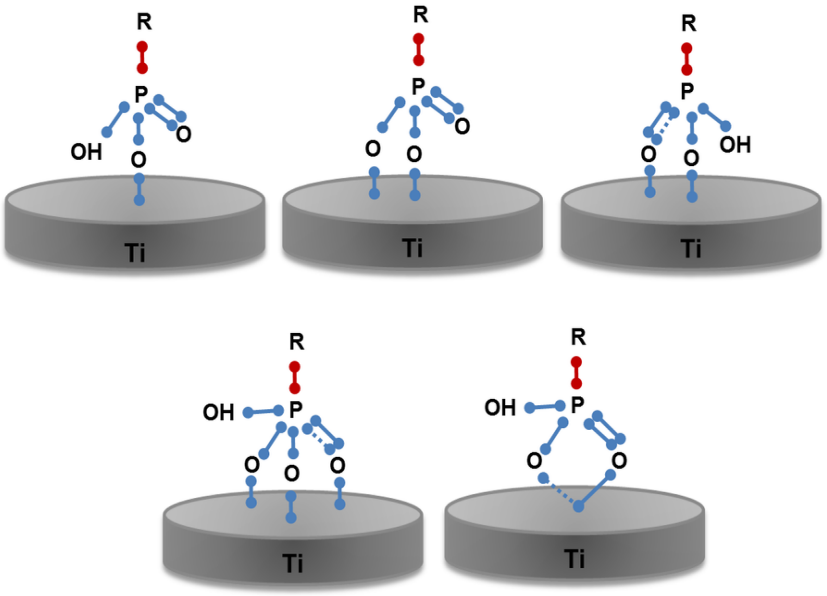


Figure 2.2 Schematic view of some possible binding modes between phosphonic acid SAMs and Titanium dioxide (a monodentate P-O-M, bidentate P=O, tridentate P-OH bindings and bridging interactions)

The strategies of PAs-based SAMs on substrates were investigated in biomedical applications. Besides, PAs-based SAMs platforms have been designed for various applications such as surface patterning, surface work function modification, small molecule detection, catalysis, corrosion resistance, biosensors, and electrical sensors [34].

2.3 General Overview of Graphene

Graphene (G), described as the form of one-atom thick monolayer of carbon atoms arranged in a two dimensional (2D) honeycomb crystal lattice, has attracted much attention in the recent years because of its unique structure and excellent physical, chemical, mechanical properties and huge specific surface area. Graphene-based research has merited the 2010 Nobel Prize in physics. This discovery is an important milestone in the world of nanotechnology. Up to now, graphene has been produced by using various physical and chemical methods such as epitaxial growth, mechanical or thermal exfoliation and Chemical Vapor Deposition (CVD). This extremely thin nanomaterial possesses a high intrinsic mechanical strength. Its fracture strength is 130 GPa, about 100 times larger than typical steels. Its Youngs modulus was measured to be 1.0 TPa by atomic force microscopy (AFM) (by Lee et al). Graphene including outstanding strength and stiffness for mechanical reinforcements, a large theoretical specific surface area (2630 m^2 g^{-1}), intrinsic mobility values as high as (200 000 cm^2 v^{-1} s^{-1}) at low temperature with a suspended geometry, high thermal conductivity (5000 Wm^{-1} K^{-1}), good optical transparency (97.7%) and impressive transport phenomena such as the quantum Hall effect contributes to develop the performance of nanosystems [1].

2.4 Structure, Reduction, Functionalization and Applications of Graphene Oxide

2D carbon nanomaterial Graphene oxide (GO), exhaustive oxidative form of graphene, can be synthesized from natural graphite flakes by utilizing one of three basic methods: the Brodie, Staudenmaier, and Hummers, respectively. The oxidative form of graphene is found to be partially hydrophobic domains capable of $\pi - \pi$ interactions, shown in Figure 2.3 [4], and exhibits well-dispersed in water and physiological environments due to the presence of the oxygen functionalities such as epoxy, carbonly, carboxyl and hydroxyl group that provide anchor sites for the immobilization of various

biomolecules via covalent bonds [1, 35].

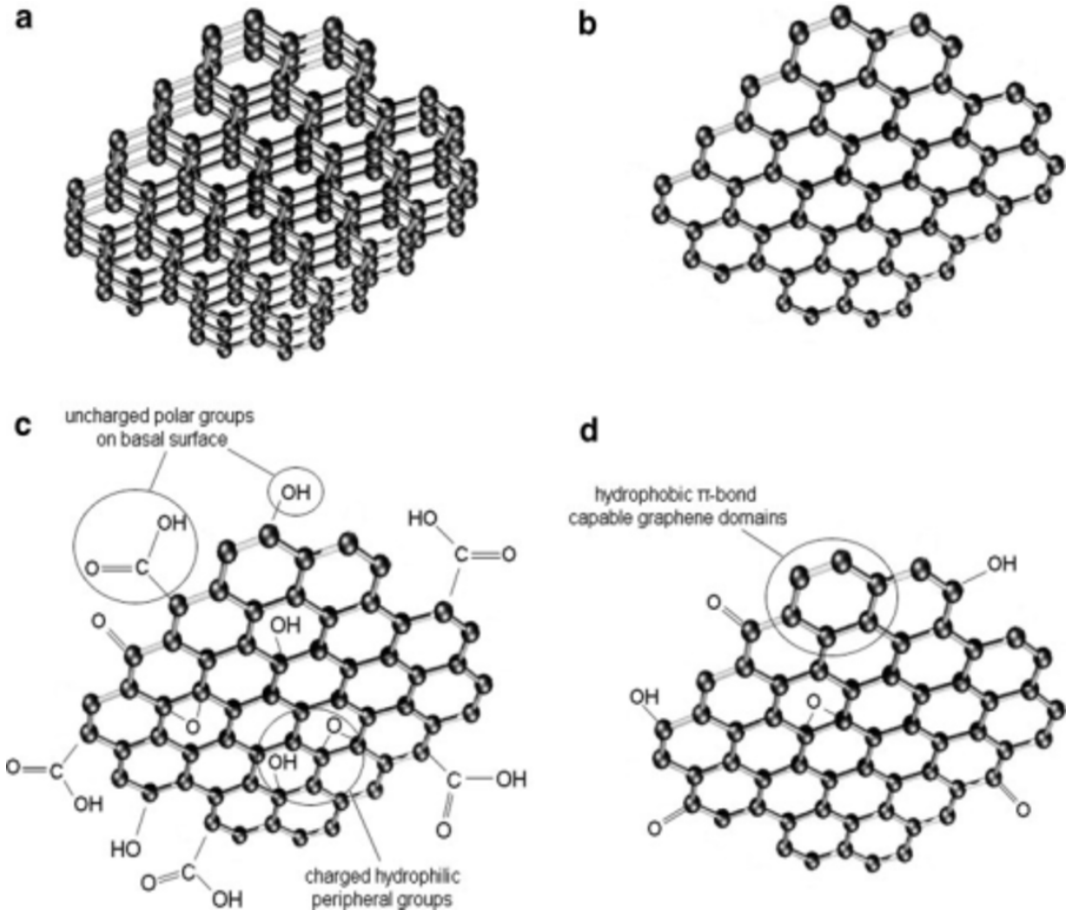


Figure 2.3 a) Few-layered graphene or Graphite b) Graphene c) Graphene Oxide (GO) d) Reduced Graphene Oxide (RGO).

Developing reduction process has grown extremely in reputation due to the remarkable similarities between reduced graphene oxide (RGO) and pure graphene properties. The surface of RGO flake is shown in Figure 2.3. Reduced graphene oxide , removing oxygen groups from GO, is efficiently obtained by using thermal annealing, electrochemical, and photo-irradiation techniques and numerous chemical agents such as hydrazine, hydriodic acid (HI), NaOH, $NaBH_4$, glucose, ascorbic acid, pyrrole, tetrathiafulvalene and thiophene [36, 37]. Reduction process cause the decrease of hydrophilicity and surface charge. RGO ensures to renovate the electrical conductivity, optical absorbance in GO. By controlling the degree of reduction, the electric and optoelectric properties could be decided [1].

G, GO and RGO sheets were used to modified or coated on noble, metal and meatal oxide nanoparticles (Au, Ag, Pd, Pt, Ni, Cu, TiO_2, ZnO, MnO_2, Co_3O_4, Fe_3O_4 etc.), quantum dots [38], plate surfaces (PDMS, SiO_2, glass, mica etc.) [39], [40], [41] and used as support materials with natural and synthetic polymers such as chitosan, gelatin, poly(vinyl alcohol) (PVA), poly(methyl methacrylate) (PMMA), polyaniline, poly(2-methoxystyrene), polyacrylate, poly(3-caprolactone) (PCL), poly(L-lactic acid) (PLA), polyethylene (PE), poly(acrylic acid) (PAA), poly(etherimide) (PEI), polyethylene glycol (PEG) etc. by utilizing different techniques to improve the graphene-based composite materials in a variety of technologies [42].

The strategy of functionalization for any graphene family member is aim to improve specific properties. For design of graphene based nanocomposite structures, chemical functionalization of GO specifically includes that the epoxy groups at the basal planes of sheets covalently linked to biomoleculus through ring opening reactions (S_N2 nucleophilic substitution) of amines. Carboxylic acid groups where situated usually at the edges of GO sheets covalently bind with biomoleculus using nucleophiles such as amine or hydroxyl groups. The structure of GO sheets leads to negative charges on the surface owing to its polarity arising from these functional groups. GO sheets can be also functionalized non-covalently through using free π-electrons which let the $\pi - \pi$ stacking, hydrophobic interactions or electrostatic interaction, van der Waals interaction with polymers, small molecules etc. [35, 39].

Functionalizations of RGO sheets are primarily possible with non-covalent attachments such as $\pi - \pi$ stacking or van der Waals interactions. It was reported that tetracyanoquinodimethane (TCNQ), sulfonated poly(aniline) (SPANI), amphiphilic polymer, poly(sodium 4-styrenesulfonate) (PSS), poly(Nisopropylacrylamide) (PNIPAAm), pyrene and its derivatives and other aromatic species could be used to obtain non-covalently functionalized RGO surface by $\pi - \pi$ stacking interactions. In several applications, van der Waals interactions between electrostatically neutral, aliphatic copolymers and RGO could be occurred [35, 42].

Graphene and its derivatives, the most known as GO and RGO together with their chemically modified surfaces, are used for many applications as depending on their excellent properties, some of which is altered after oxides processes of reduction and oxidation of graphene. Chemically modified graphenes (CMGs) including graphene oxide, reduced graphene and their derivatives have been developed to expand the use of different application areas including not only electronic and chemical applications but also biomedical applications [3].

Two-dimensional graphene-based structure is able to be used as versatile material in biomedical applications such as in gene and drug delivery, imaging, photothermal cancer therapy, biosensor and tissue engineering (Figure 2.4). Besides, antibacterial properties of graphene-based materials have been investigated to prevent infection upon implantation of material. Cytotoxicity of graphene-based materials at implant applications in vitro and in vivo can be controlled because of depending its dose that exhibits insignificant effect at a low concentration for mammalian cells [2, 3].

2.4.1 Graphene and Graphene derivatives in Tissue Engineering

Tissue engineering focus to design novel scaffold with help of regenerative medici ne system to replace and restore the functions of diseased or damaged tissue. Graphene and graphene derivatives render possible ascendent biocompatible scaffolds for cells. Physico-chemical properties of graphene and graphene derivatives affect cellular behavior, such as adhesion, proliferation and differentiation [4].

The behavior of mammalian NIH-3T3 fibroblast cells on various carbon nanomaterials (GO, RGO, and carbon nanotubes etc.) coated substrates have been investigated. Increase of biocompatibility and gene transfection efficiency affected by the carbon nanomaterials coated substrates have been also observed [43]. Graphene was shown to be an appropriate substrate for accelerating differentiation of human mesenchymal stem cells (hMSCs) comparable to common growth factors (e.g. dexamethasone, β-glicerophosphate [39, 44]. Park et al. first reported the positive influence

of graphene on neural stem cells (NSCs).The increased differentiation of human neural stem cells (hNSCs) to neurons on graphene coating glass was indicated [45].

Anchorage-dependent cells such as osteoblasts require good adhesion in order to lead off subsequent cell functions at the cell/material interface. Kalbacova et al. observed that graphene-coated SiO_2 surface by CVD increased proliferation of human osteoblasts and mesenchymal stromal cells (MSCs) compared to uncoated silica (SiO_2) [46]. Biris et al. reported thar osteoblast cells (MC3T3-E1) have an ability to promote the adhesion, proliferation on graphene film [47].

GO sheets based platforms influence enhanced/accelerated cell attachment, growth and differentiation. Previous studies have shown that GO based materials promotes the adhesion and proliferation of L929 fibroblasts, osteoblasts and embryonic cells [4]. Chen et al. demonstrated that the surface properties of GO provided better attachment, proliferation and differentiation of induced pluripotent stem cells (iPSCs) than graphene because of the presence of abundant oxygen functionalities. The effects of GO-coated surfaces for the differentiation of iPSCs toward endodermal lineage (hepatocytes and insulin-producing β cells) have been evaluated [48]. GO surface has been exhibited to be effective preconcentration for the differentiation of hMSCs to adipocytes. Graphene and GO acted as preconcentrate growth factors and accelerated chondrogenic differentiation of hMSCs [49].

Reduced graphene oxide (RGO) have been reported to be more biocompatible than single-wall carbon nanotubes (SWCNTs) in different cell lines including neuroendocrine PC12 cells, oligodendroglia, or osteoblasts by Agarwal and co-workers [50]. Akhavan and Ghaderi at al. reported that the photocatalytically reduced graphene oxide sheets coated on TiO_2 film accelerated neuronal differentiations of hNSCs [51]. Ku and Park et al. have evaluated that GO and RGO modified glass substrates affected mouse myoblast C2C12 cell behavior, including adhesion, proliferation, and differentiation [41].

Though the influences of graphene and its derivatives on protein adsorption and cellular activities have been observed, recent studies have shown that bioactivities of GO and RGO structures could be highly enhanced by using biomolecules according to fields of their applications. Graphene and its derivatives could be functionalized with aptamers, small molecules, avidin-biotin, peptides, proteins, bacteria, and cells via acting physical adsorption or chemical conjugation have been reported in order to design advanced platforms in biosensors, biodevices and biomaterials [3].

2.5 Influence of Fmoc-terminated amino acid derivatives on cellular responses.

The 9-Fluorenylmethoxycarbonyl (Fmoc), introduced in 1970 by Carpino and Han, is used as a protecting group for primary and secondary amines and especially for amino acids [52]. The properties of different classes of amino acids and their connection with Fmoc-side were shown in Table 2.1 [53]. It is employed widely as a protecting group in solid phase synthesis [54]. The formation of hydrogels with Fluorenylmethoxycarbonyl (Fmoc)-protected amino acids and dipeptides were first reported in 1995 by Vegners [55]. Fmoc amino acids, specifically Fmoc-tyrosine and Fmoc-phenylalanine, are known as very simple class of low molecular weight hydro-gelators [56, 57]. Also, Burch et al. reported that anti-inflammatory effect of some Fmoc-amino acids were displayed [55]. The design of nanocomposite material with low molecular weight hydrogelators (LMWGs) is believed to attain success in biomedical applications such as wound treatment, drug delivery, and tissue engineering.

Recent studies reported that structures of terminally protected peptide or amino acids with synthetic aromatic groups such as pyrenyl, perylene, benzyloxycarbonyl (Cbz), naphthalene (Nap) and Fmoc-(N-(fluorenyl-9-methoxycarbony)) as stable gelators or hydrogels have been investigated for various applications. Among the molecular hydrogelators, Fmoc-protected amino acids or short peptides were presented to be the structure of molecular hydrogels that could be achieved the strong candidate for

in vitro cell cultures and drug delivery to be as scaffolds and carrier. For instance, the hydrogel forms of Fmoc-l-phenylalanine and Fmoc-diphenylalanine have been used for drug delivery and cell culture studies [58]. Jayawarna et al. previously demonstrated that Fmoc-diphenylalanine considered as a suitable matrix for two-dimensional (2D) or three-dimensional (3D) culture of primary bovine chondrocytes [59]. Zhou et al. reported that the design of biomimetic nanofibrous hydrogel based on a mixture of Fmoc-FF (Fluorenylmethoxycarbonyl-diphenylalanine) and Fmoc-RGD (arginine-glycine-aspartate) as the simplest self-assembling moieties promote adhesion of cells. Hamley and coworkers reported hydrogel structure of Fmoc-tripeptides used as a support for bovine fibroblasts. Enzyme-catalyzed formation of hydrogels based on Fmoc-peptides has been reported by Ulijn and co-workers [57].

2.6 Adsorption of Fmoc-terminated amino acids on CNTs and graphene derivatives.

Carbon family members such as graphene, CNTs and fullerene are disposed to protect their natural properties (e.g.structural and functional properties) when functionalized and modified with surfactants and polymers. Therefore, the noncovalent binding such as $\pi - \pi$ stacking, hydrophobic interactions, electrostatic adsorption and hydrogen bonding are naturally selected in contrast to covalent attachment [60].

The previous studies of aromatic ligands of surfactants that could self-assemble into CNTs via $\pi - \pi$ stacking have been presented. Li et al. have demonstrated that CNT-SiO_2 nanohybrids noncovalently immobilized with biofunctional molecule 1-aminopyrene through $\pi - \pi$ stacking. Reches and Gazit have previously reported that aromatic dipeptides FF (Phe-Phe) self-assembled into straight nanotubes by $\pi - \pi$ stacking. Cousins et al. have reported that homogeneous CNT dispersions attached well to the aromatic fluorenyl rings of N-(fluorenyl-9-methoxycarbonyl) terminated aromatic amino acids (Fmoc-AAs) [61]. Fmoc-terminated amino acid derivatives suh as histidine, tryptophan, tyrosine, phenylalanine, glycine were selected as a model system

to beef up hydrophilic effect in composite materials. Adhikari and Banerjee et al. reported that reduced graphene oxide (RGO) successfully incorporated with N-terminally Fmoc protected dipeptides to produce stable hybrid hydrogel systems [10]. In carbon family members, two-dimensional graphene oxide and reduced graphene oxide sheets also act as the reactive sites (hydrophilic or hydrophobic domains) for architecting chemically modified graphene (CMG) sheets. Therefore, 2D-carbon structures put forward attractive material science applications. 1D carbon nanomaterials, such as fullerenes and Carbon Nanotubes (CNTs) are found to be rather cytotoxic compare with 2D graphene and its derivatives, so graphene and its derivatives are more suitable and preferred for biomedical applications [2, 62].

Table 2.1
Hydropathy index for Standart Amino Side Chains.

Amino Acids	Hydropathy index
Nonpolar, Aliphatic R groups	
Glycine	-0.4
Alanine	1.8
Valine	4.2
Leucine	3.8
Isoleucine	4.5
Methionine	1.9
Aromatic R groups	
Phenylalanine	2.8
Tyrosine	-1.3
Tyrptophan	-0.9
Polar, Uncharged R groups	
Serine	-0.4
Proline	1.6
Theonine	-0.7
Cysteine	-2.5
Asparagine	-3.5
Glutamine	-3.5
Positively charged R groups	
Lysine	-3.9
Histidine	-3.2
Arginine	-4.5
Negatively charged R grops	
Aspartate	-3.5
Glutamate	-3.5

3. MATERIALS AND METHODS

3.1 Chemical Surface Modification

3.1.1 Modification of Titanium Surface with APA (3-aminopropyl phosphonic acid) molecules

Titanium surfaces were treated and activated by using oxygen (O_2) plasma technique (March Plasma Systems, PM-100). Treatment was performed for 10 min at 200 mT and 50 sccm flow of oxygen to remove organic impurities and to form hydroxyl groups (-OH) on Ti surfaces.

3-aminopropyl phosphonic acid molecules (APA, Sigma-Aldrich) were modified to prepare self assembly monolayer (SAM) on Ti surfaces. APA molecules specifically conjugate the Ti surfaces [63, 64].

The cleaned Ti substrates were dipped into a 10 mM APA solution (in dI H_2O) at 80 °C for 4 h. Amino (-NH_2) groups were formed the Ti surface after APA conjugation. APA modified on Ti surfaces were baked at 125 °C to stabilize SAM. The surfaces of Ti substrates were removed any physically absorbed APA molecules from the solution and rinsed with dI H_2O and dried under a stream of N_2 gas [65, 66].

3.1.2 Preparation of GO/Ti Nanocomposite

Graphene oxide (GO, Sigma-Aldrich) sheets were immobilized by immersing APA-modified Ti surface into GO aqueous solution (0.5 mg/ml) for 1 h at room temperature. After this step, the surface of Ti/GO substrates were rinsed with dI H_2O and dried with an N_2 gas. The epoxy rings can be easily opened under acidic conditions or by nucleophilic attack [41]. GO sheets containing the epoxy, carbonly, carboxyl and

hydroxyl groups were modified on APA/Ti through S_N2 nucleophilic reactions between the epoxy groups of the surface of GO and the amine groups of APA [35].

3.1.3 Preparation of Reduction of GO/Ti Nanocomposite

Reduced graphene oxide, removing O_2 from graphene oxide, was efficiently obtained through using chemical, thermal annealing, electrochemical, and photo-irradiation techniques. In this step, reduced graphene oxides (RGO) flakes incorporated APA/Ti surface were formed by using chemical reaction with hydrazine monohydrate (Sigma-Aldrich). GO/Ti nanocomposite surface was reduced by immersing into 20% hydrazine monohydrate in DMF for 24 h at 80 °C , and rinsed with DMF, ethanol and dI H_2O and then dried with an N_2 gas [37, 41, 48, 67].

3.1.4 Modification of RGO/Ti Nanocomposite with Amino Acid conjugated Fmoc

Fluorenylmethoxycarbonyl (Fmoc) aromatic group was shown to be effective molecular gelators. In this step, the $\pi-\pi$ stacking interaction between the N-(fluorenyl-9-methoxycarbonyl) conjugated amino acid and RGO modified APA/Ti was investigated. RGO/Ti samples separately were placed into petri dish containing 5mM Fmoc-Leu-OH (Sigma-Aldrich) in DMSO and 5mM Fmoc-Ser-OH (Sigma-Aldrich) in ethanol with different dipping time (2h-24h). All samples were rinsed with ethanol and dI H_2O and then dried at ambient temperature [10, 68].

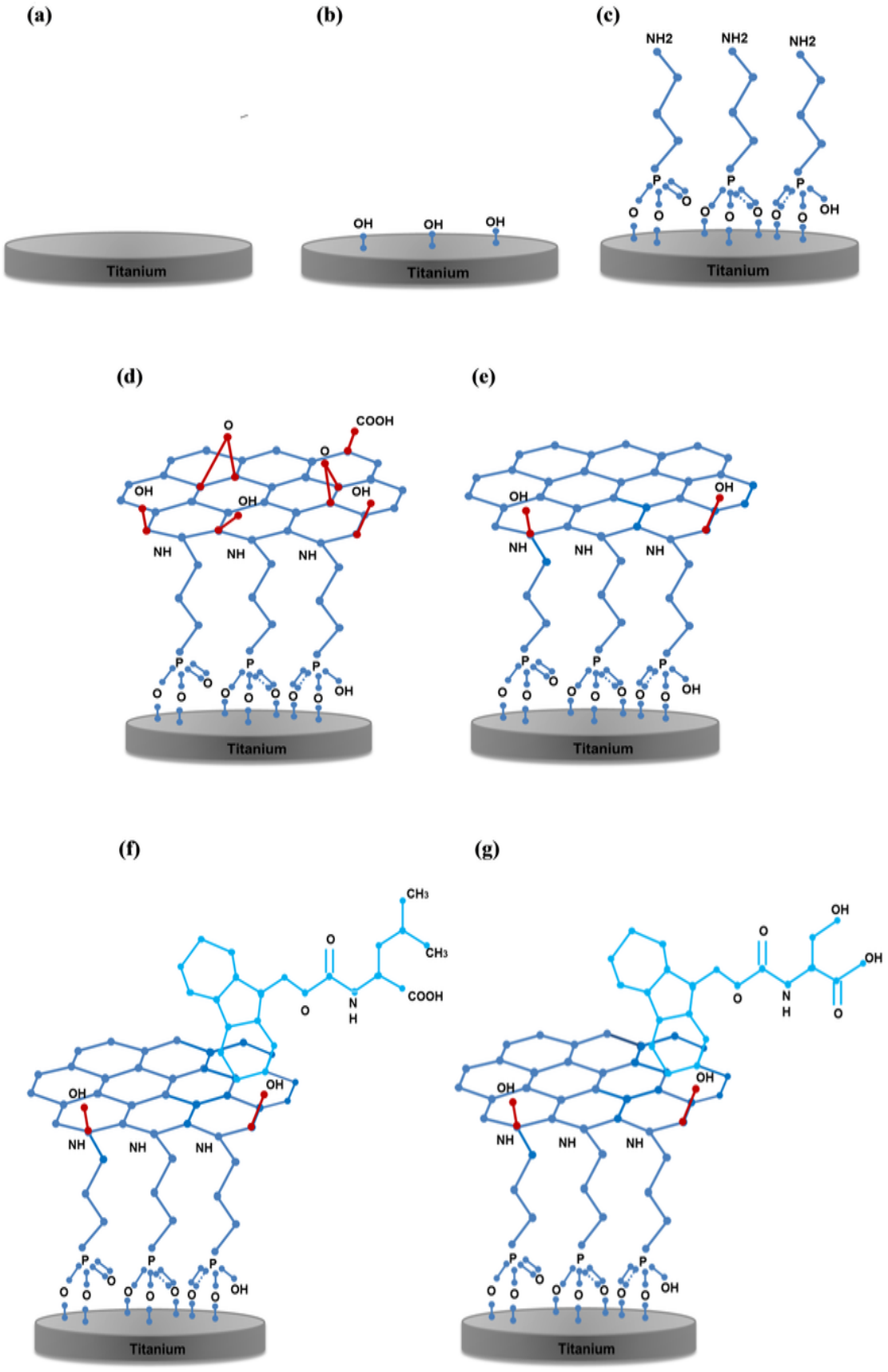


Figure 3.1 Schematic representation of (a) Bare Titanium, (b) Activated Ti surface, (c) APA modified Ti surface, (d) GO/Ti nanocomposite,(e) RGO/Ti nanocomposite, (f) Fmoc-Leu-OH/RGO/Ti nanocomposite, (g) Fmoc-Ser-OH/RGO/Ti nanocomposite.

3.2 Surface Characterization

3.2.1 Scanning Electron Microscopy (SEM)

The morphology and structure of GO and RGO flakes modified APA/Ti surfaces were investigated by using Scanning electron microscopy (SEM) (Philips XL30 ESEMFEG/EDAX) at Bogazici University Research and Development Center Electron Microscopy and Microanalysis Unit, İstanbul, Turkey

3.2.2 Atomic Force Microscopy (AFM)

Atomic Force Microscopy (AFM) (Bruker Dimension Edge) were used to observe RGO modified Ti surfaces topography at the nanometer scale. The surface morphologies of graphene derivatives incorparated Ti surfaces was determined by AFM in tapping mode or contact mode at the room temperature. The measurements by using contact mode of AFM were performed at Electrical and Electronics Engineering Department, Bogazici University, İstanbul, Turkey.

3.2.3 Water Contact Angle (WCA) Measurements

Water contact angles measurements of Bare Titanium, APA modified Ti, GO coating APA/Ti surface, RGO coating APA/Ti surface, Fmoc-Ser-OH modified on RGO/Ti, and Fmoc-Leu-OH modified on RGO/Ti were taken to investigate the hydrophobicity and hydrophilicity of the surfaces by using CAM 100, USA. Water contact angles of the distilled water droplets on the surface were recorded and measured by using the digital camera which captured 10 images with 1 s time intervals and software of the device. Measurements were repeated at least 2 times on the different points of surface of each sample and averaged. WCA measurements were performed at Bogazici University, Department of Chemistry, İstanbul, Turkey.

3.2.4 X-ray Photoelectron Spectroscopy (XPS)

XPS (Thermo Scientific K-Alpha X-ray Photoelectron Spectrometer technique) was used to examine the surface elemental composition of different specimens since XPS provides information about chemical bonds and molecular composition of the material surfaces, combined with a high surface specificity. The XPS spectra was recorded utilizing a monochromatic Al K-Alpha X-ray radiation source at 72 W, 400 μm spot size, 90° angle and with a 128-channel detector. All measurements were performed by using X-ray Photoelectron Spectrometer (XPS) at Advanced Technologies Research and Development Center, Bogazıcı University, İstanbul, Turkey.

3.2.5 Raman Spectroscopy

Raman spectroscopy measurements were performed by using Witec Alpha 300S, Raman Module, 532 nm laser excitation to characterize the activated and the modified Ti surfaces. The Raman spectroscopy measurements were performed at Unam, Bilkent University, Ankara, Turkey.

3.3 Cell Studies

The sv40osteoblast cells (ATTC, USA) were cultured for 1st, 3rd, and 5th days on Fmoc-Ser-OH/RGO/Ti, Fmoc-Leu-OH/RGO/Ti, RGO/Ti, GO/Ti, APA/Ti, Ti surfaces and TCPS in DMEM/F12 with 10% fetal bovine serum (FBS) and 1% antibiotic to investigate the effects of their surface properties on cell behaviour. After cell culture, the substrate surfaces were analyzed by MTT, Alamar Blue Assay and SEM to observe viability, adhesion, proliferation, and morphology of osteoblast cells.

3.3.1 Cell Culture

The cell culture studies were carried out by using osteoblast cell line. Cells ($4x10^4$) were seeded on each samples in 24-well tissue culture plates. The osteoblast cells were cultured in DMEM/F12 (Dulbecco's Modified Eagle's Medium/F12) supplemented with 10% FBS and 1% antibiotic and incubated in a humidity at 37°C under 5% CO_2 and 95% air atmosphere.

3.3.2 Cell Viability and Proliferation

- **MTT Assay**

MTT assay, a colorimetric method, is used to measure the activity of mitochondrial enzymes in living cells In this process, MTT, a tetrazolium dye, is reduced to insoluble formazan, giving a purple color [69]. In order to evaluate cell viability for TCPS, unmodified and modified Ti surfaces, osteoblast cells were seeded at a density of $4x10^4$. After cell incubation at 37 °C and in 5% CO_2 atmosphere for 1st, 3rd and 5th days that allowed cells to attach and proliferate on prepared samples surfaces, viability of the cells cultured on these samples was analyzed by using the MTT 3-(4,5-dimethylthiazol-2-yl)-2,5 diphenyltetrazolium bromide (Sigma-Aldrich) assay. An MTT stock solution was prepared by dissolving MTT reagent in PBS, filtered through a 0.2 μm filter and stored in the dark at 4 °C. MTT (20 μl, 5 mg/ml) solution and was added to each well and cultures continued for 3h at 37 °C. MTT reagent in normal media was removed and replaced with 100 μL acidified isopropanol solutions and solutions in 24-well were transferred to a 96-well plates. The optical density of formazan production induced from the reagent effect on cells at 570 nm and 750nm (a reference wavelength) was measured by using a micro plate reader spectrophotometer (BIO-RAD iMark, Microplate Reader).

• **Alamar Blue Assay**

Alamar Blue (Sigma-Aldrich) cell viability reagent is used to quantitatively measure cell proliferation and cytotoxicity [70]. After cell incubation for 1st, 3rd and 5th days, the culture medium supplemented with 10 vol.% Alamar Blue fluorescent dye and followed by 4h incubation at 37 °C and in 5% CO_2 atmosphere. 100 μL solution was taken from each 24-well and transferred into 96-well. Absorbance was read at a wavelength of 570 nm and 595 nm by using a microplate reader (BIO-RAD iMark, Microplate Reader). Alamar Blue fluorescent dye was also added to a medium without cells, as a negative control. According to the manufacture's protocol, cell proliferation and viability were calculated. The percentage of reduction of Alamar Blue (AB) is expressed by equation.

$$\%Reduced = \frac{(\varepsilon_{OX})\lambda_2 A\lambda_1 - (\varepsilon_{OX})\lambda_1 A\lambda_2}{(\varepsilon_{OX})\lambda_1 A'\lambda_2 - (\varepsilon_{OX})\lambda_2 A'\lambda_1} \times 100 \tag{3.1}$$

where are $\varepsilon\lambda_1$ and $\varepsilon\lambda_2$ constants representing the molar extinction coefficient of Alamar Blue oxidized ε_{OX} and ε_{RED} reduced forms at 570 and 595nm, respectively. Absorbance of test wells are represented as $A\lambda_1$ and $A\lambda_2$ at 570 and 595 nm, respectively. Absorbance of negative control wells (media plus Alamar Blue but no cells) are represented as A'λ_1 and A'λ_2 at 570 nm and 595 nm, respectively.

$$Percentdifferenceinreduction = \frac{(\varepsilon_{OX})\lambda_2 A\lambda_1 - (\varepsilon_{OX})\lambda_1 A\lambda_2}{(\varepsilon_{OX})\lambda_1 A^o\lambda_2 - (\varepsilon_{OX})\lambda_2 A^o\lambda_1} \times 100 \tag{3.2}$$

• **Adhesion and Morphology**

Cell adhesion and morphology on unmodified and modified Ti surfaces were investigated for 1st and 3rd days by using SEM. Osteoblast cells were seeded in DMEM-F12 (with 10% FBS and 1% antibiotics) at 37 °C in 5% CO_2 for 24 h. Before taking SEM images, the cells-materials were rinsed twice in PBS at pH 7.4 without NaCl, and primary fixation was carried out by immersing into 2.5% glutaraldehyde (50% v/v, Sigma Aldrich, USA) in distilled water at room temperature. The cells were then dehydrated through a graded concentrations of ethanol (10, 30, 50, 70, 95, and 100%) for 2 min in each solution. After this process, the cells-materials were air-dried, samples were sputter-coated with gold and images were taken by using SEM (Philips XL30 ESEMFEG/EDAX) at Bogazici University Research and Development Center Electron Microscopy and Microanalysis Unit [71].

• **Statistical Analysis**

Statistical analysis was performed by using ANOVA method to define the level of the statistical significance between groups. The value of $p<0.05$ was considered statistically significant. Tukeys multiple comparison tests were used. The data were demonstrated to be as means ± standard deviation or standard error.

4. RESULTS

4.1 Surface Characterization

4.1.1 Scanning Electron Microscopy (SEM)

• SEM images of GO/Ti and RGO/Ti nanocomposites.

SEM image of graphene oxide flakes in water was taken before preparing the dispersion and size distribution of GO monolayer on Ti surface.

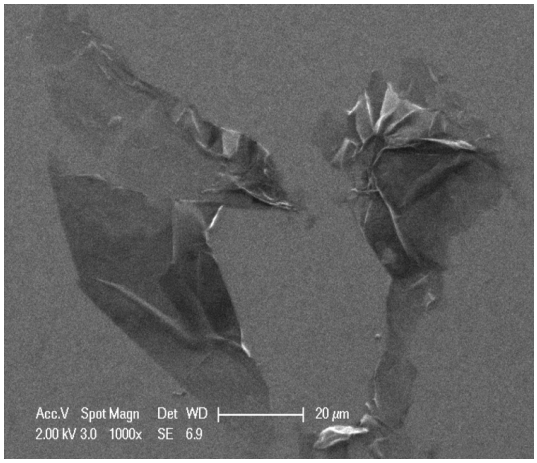


Figure 4.1 SEM image of Graphene Oxide (GO).

The morphology and structure of GO and RGO flakes modified on APA/Ti surfaces were examined by using SEM. Fig 4.2 and Fig. 4.3 have shown SEM images of two sides (left and right) of GO/Ti surface.

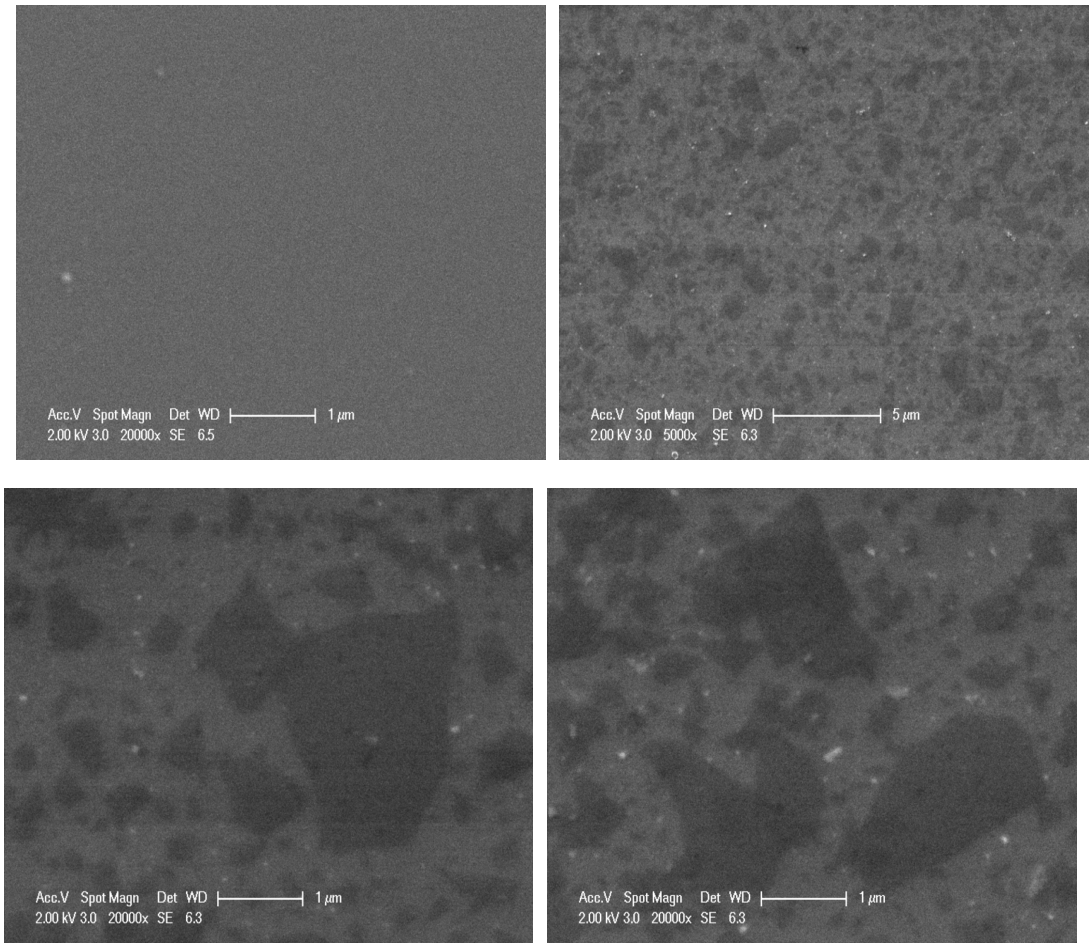


Figure 4.2 SEM images of bare Ti surface and GO flakes on APA/Ti surfaces (left side).

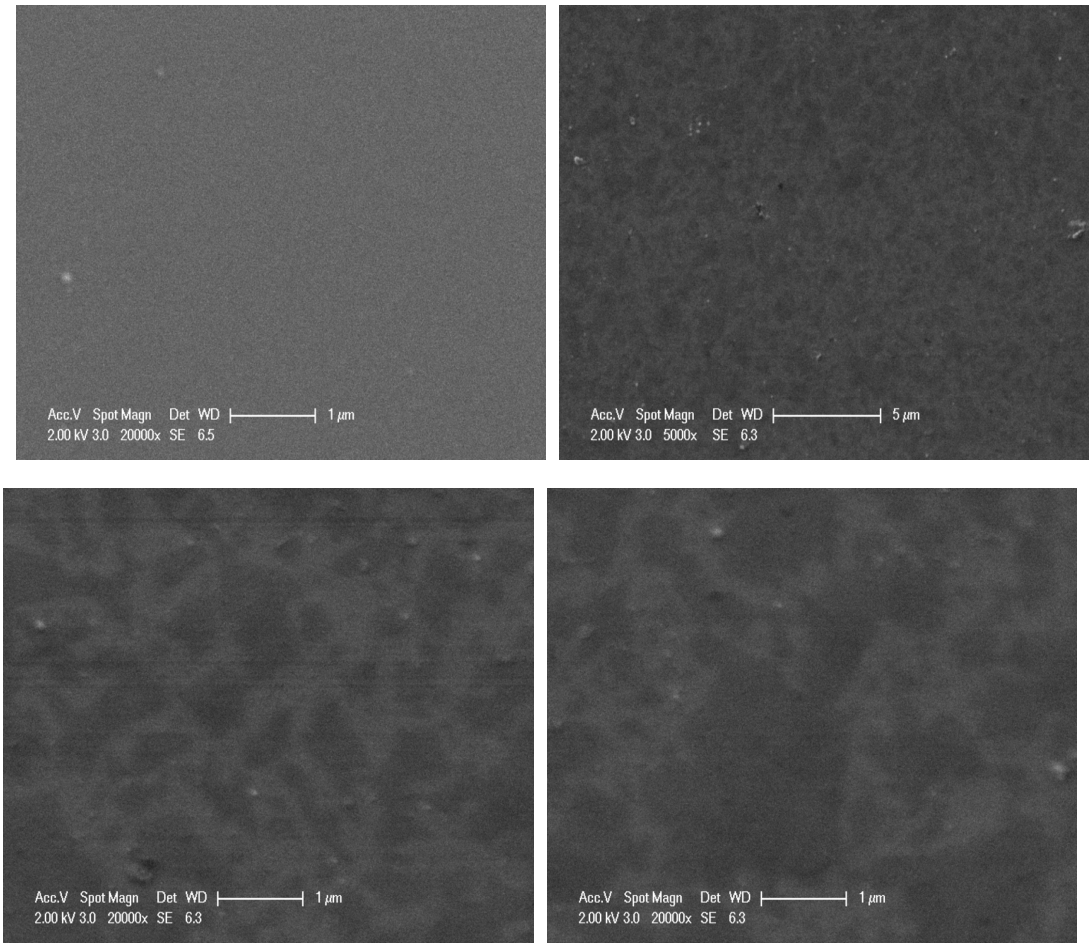


Figure 4.3 SEM images of bare Ti surface and GO flakes on APA/Ti surfaces (right side).

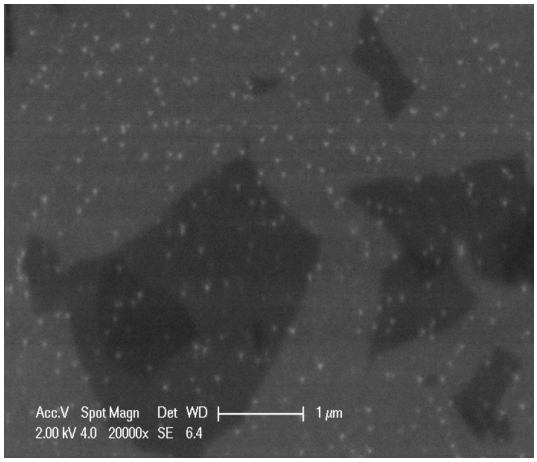


Figure 4.4 SEM images of GO flakes on APA/Ti surfaces after doping Au particles.

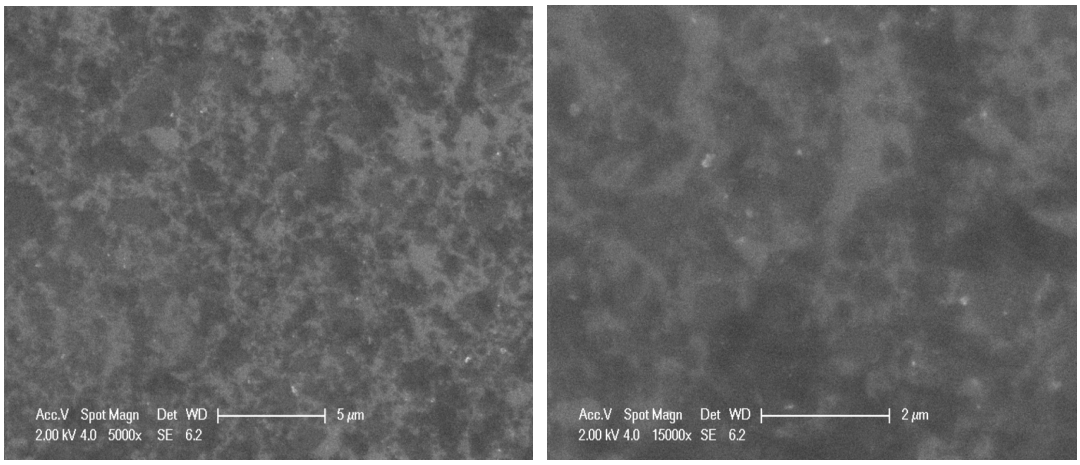


Figure 4.5 SEM images of chemically Reduced GO flakes on APA/Ti surface.

To obtain well-distinguished graphene flakes modified on APA/Ti surfaces was investigated by SEM at 2 kV after doping Au particles on the surface. The single and multilayer GO flakes modified on APA/Ti surface were more clearly shown by the color contrast in Figure.4.4.

The effect of chemical reduction were investigated by using SEM. The planar structure of RGO flakes on APA/Ti surface was observed to remain stable after chemical reduction.

• **SEM images of RGO/Ti nanocomposite with amino acid conjugated Fmoc amino acids**

Fmoc aromatic group was known to be effective molecular gelators. After, Fmoc amino acids modified on RGO/Ti surface, the morphology and structure of surfaces were investigated by using SEM

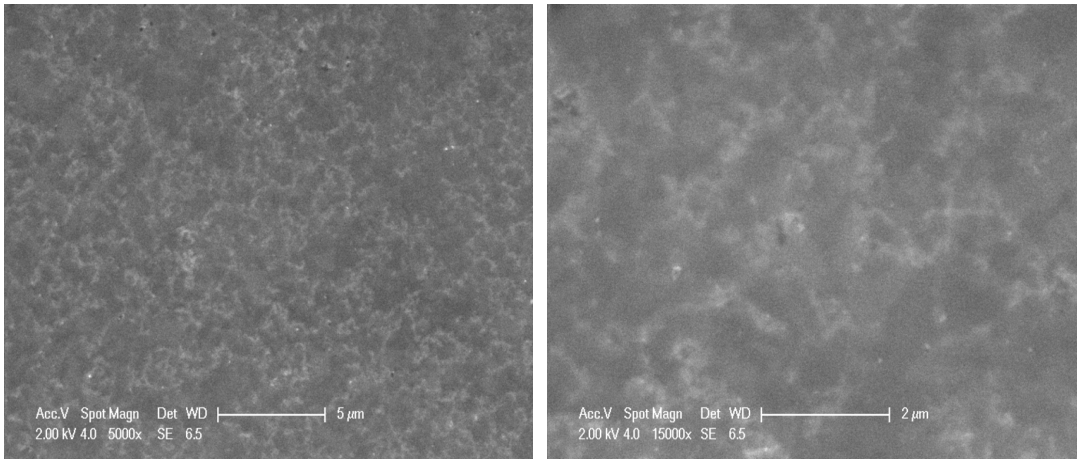


Figure 4.6 SEM images of Fmoc-Ser-OH modified on RGO /Ti surface.

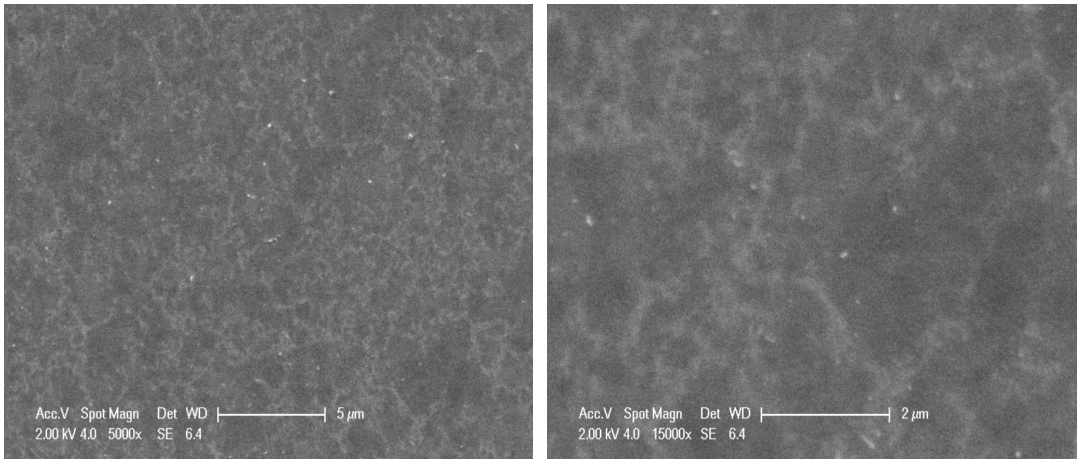


Figure 4.7 SEM images of Fmoc-Ser-OH modified on RGO /Ti surface.

4.1.2 Atomic Force Microscopy (AFM)

- **AFM images of RGO/Ti nanocomposites**

The thickness and morphology of RGO/Ti surface were investigated under ambient condition by using AFM. The 2D and 3D AFM image were shown in Figure 4.8 and Figure 4.9, respectively.

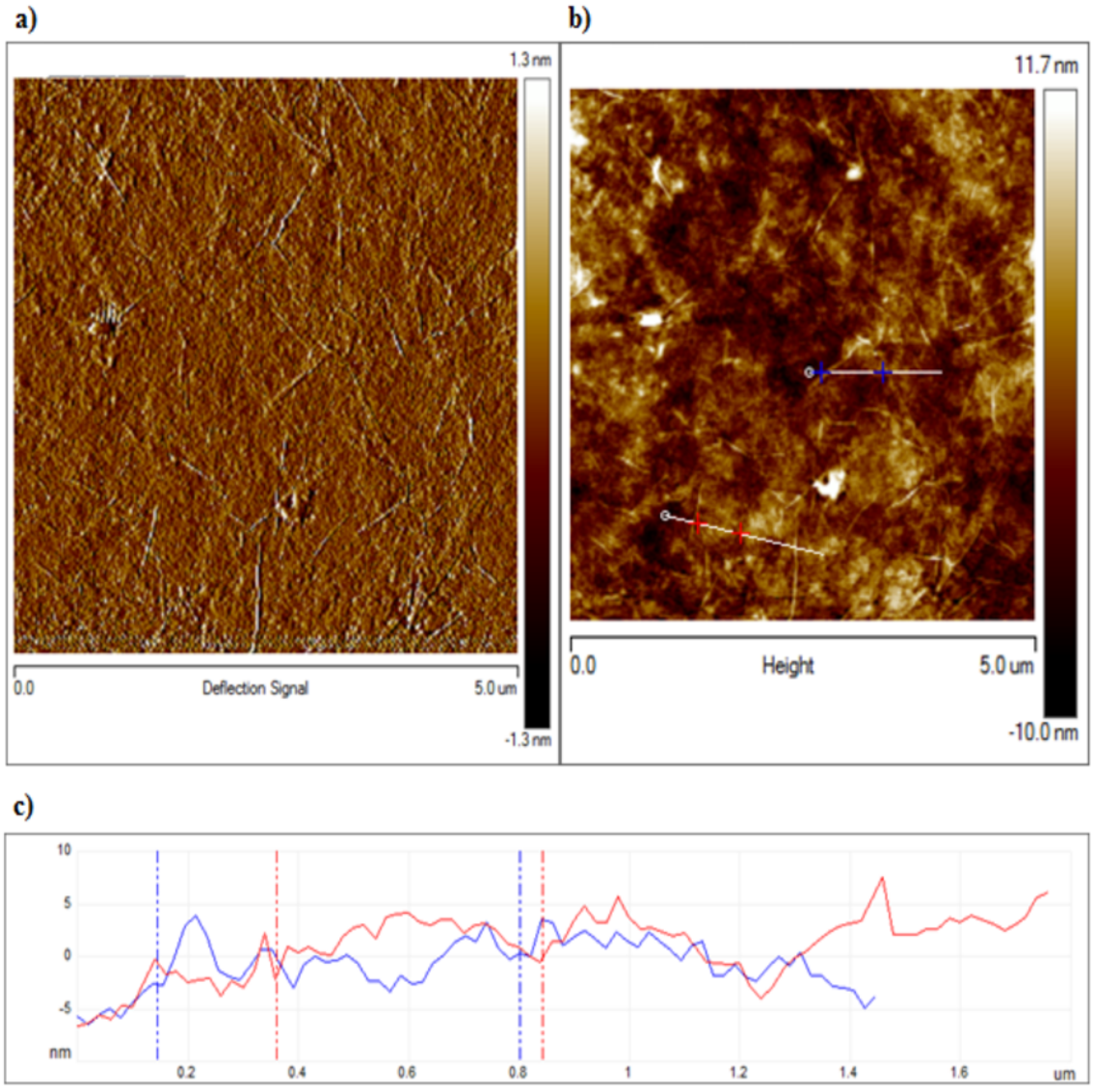


Figure 4.8 AFM images and Surface profiles of RGO flakes on APA/Ti (a) deflection signal (b) height image (c) height profile.

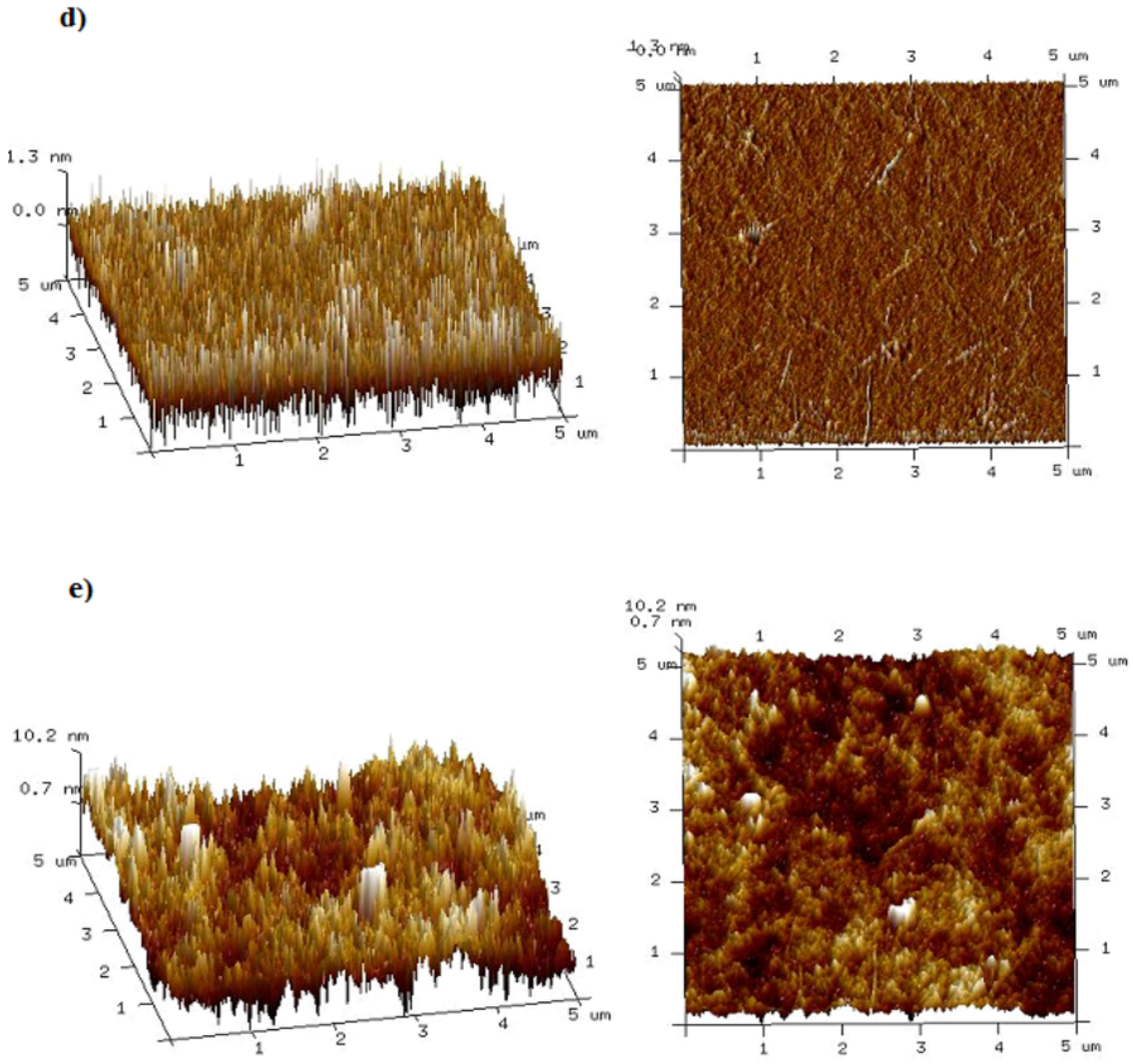


Figure 4.9 3D AFM images of RGO flakes on APA/Ti surface: (d) deflection signal (e) height image.

4.1.3 Water Contact Angle Measurements

• **Water Contact Angle Measurements of Bare, Activated and APA modified on Ti surface**

Water contact angles (WCAs) of bare, activated and APA modified Ti surfaces were investigated by using CAM 100, USA. The bare, activated Ti surfaces and self-assembled monolayers of APA molecules modified Ti were analyzed at 71.85° ± 2.76°, 8° ± 0.2°, 33.45° ± 3.3° taken off angles, respectively. The results were shown in the Table 4.1 and WCA photographs of bare Ti and APA modified Ti were shown in the Figure 4.10.

Table 4.1
Water Contact Angle measurements of Bare, Activated and APA modified Ti.

Surface	Contact Angle (°)
Bare Ti	75.85 ± 2.76
Activated Ti	0
APA modified Ti	33.45 ± 3.3

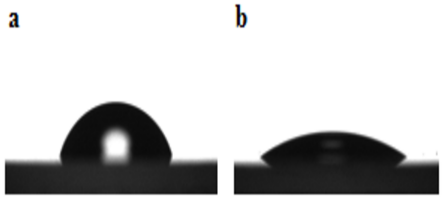


Figure 4.10 Water contact Angle photographs of (a) bare Ti, (b) APA modified Ti.

• Water Contact Angle Measurements of GO/Ti and RGO/Ti nanocomposites

Water contact angles (WCAs) of both GO and RGO deposited on APA/Ti surfaces were investigated by using CAM 100, USA. After the measurements, water contact angles were calculated to be 21.1° ± 4.3° and 69.96° ± 0.1° shown in the Table 4.2. WCA photographs of GO coating APA/Ti and chemically reduction of GO coating APA/Ti shown in the Figure 4.11. WCA data indicated that hydrophilicity of the surface decreased after chemically reduction of GO/Ti surface.

Table 4.2
Water Contact Angle photographs of (a) Graphene oxide coating APA/Ti, (b) Reduced graphene oxide coating APA/Ti.

Type of Modification	Contact Angle(°)
GO coating APA/Ti	21.1 ± 4.3
RGO coating APA/Ti	69.96 ± 0.1

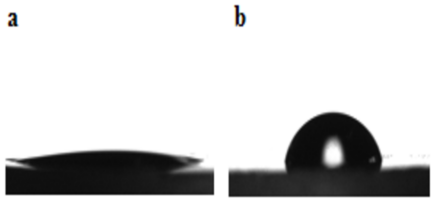


Figure 4.11 Water Contact Angle photographs of (a) GO coating APA/Ti, (b) RGO coating APA/Ti.

• **Water Contact Angle Measurements of Fmoc amino acids modified on RGO/Ti nanocomposite**

Water contact angles (WCAs) of Fmoc amino acids modified on RGO/Ti surfaces were investigated by using CAM 100, USA. The effects of increasing dipping times were investigated for 5 mM Fmoc amino acids modified on RGO/Ti surfaces. After measurements of 5mM Fmoc-Leu-OH amino acids modified on RGO/Ti surfaces, WCAs were calculated for different dipping times (2h-24h) and shown in the Table 4.3. To investigate the hydrophilicities of the surfaces of 5mM Fmoc-Ser-OH modified on RGO/Ti nanocomposites, water contact angles were calculated for different dipping times (2h-24h) and shown in the Table 4.4. WCA photographs of Fmoc-Leu-OH and Fmoc-Ser-OH modified on RGO/Ti surface with increasing dipping time shown in the Figure 4.12 and Figure 4.13, respectively.

Table 4.3
Water Contact Angle Measurements of 5mM Fmoc-Leu-OH amino acids modified on RGO/Ti surface with different dipping times (2-24h).

Dipping Time (h)	Contact Angle (°)
2	75.91 ± 3.51
8	72.08 ± 0.28
16	63.13 ± 3.58
24	55.57 ± 4.17

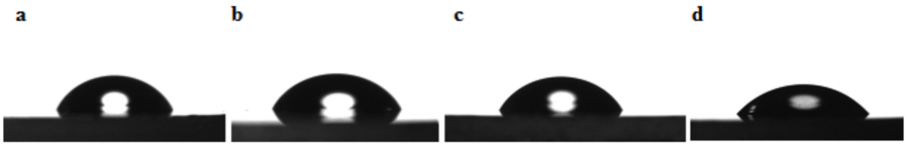


Figure 4.12 Water Contact Angle photographs of Fmoc-Leu-OH modified on RGO/Ti surface with different dipping time : (a) 2h, (b) 8h, (c) 16h, (d) 24h.

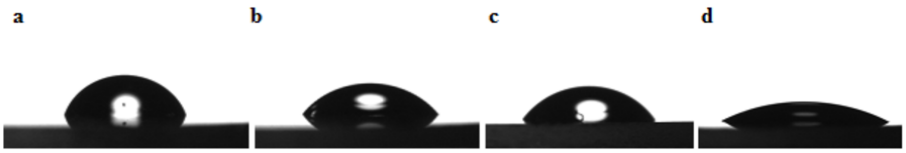


Figure 4.13 Water Contact Angle photographs of Fmoc-Ser-OH modified on RGO/Ti surface with different dipping time : (a) 2h, (b) 8h, (c) 16h, (d) 24h.

Table 4.4
Water Contact Angle Measurements of 5mM Fmoc-Ser-OH amino acids modified on RGO/Ti surface with different dipping times (2-24h).

Dipping Time (h)	Contact Angle (^{o})
2	63.58 ± 2.33
8	56.1 ± 2.69
16	55.79 ± 1.39
24	30.24 ± 3.17

As a result of an increase in dipping time, water contact angle values shown that surfaces of modified nanocomposites become more hydrophilic surface which resulted from the carboxylic acid and hydroxyl group of the adsorbed Fmoc amino acids. Moreover, the modification of Fmoc amino acids on nanocomposite surface suggested that $\pi - \pi$ interaction between aromatic ligands of Fmoc amino acid and hydrophobic domains of RGO was carried out (Fig.4.14).

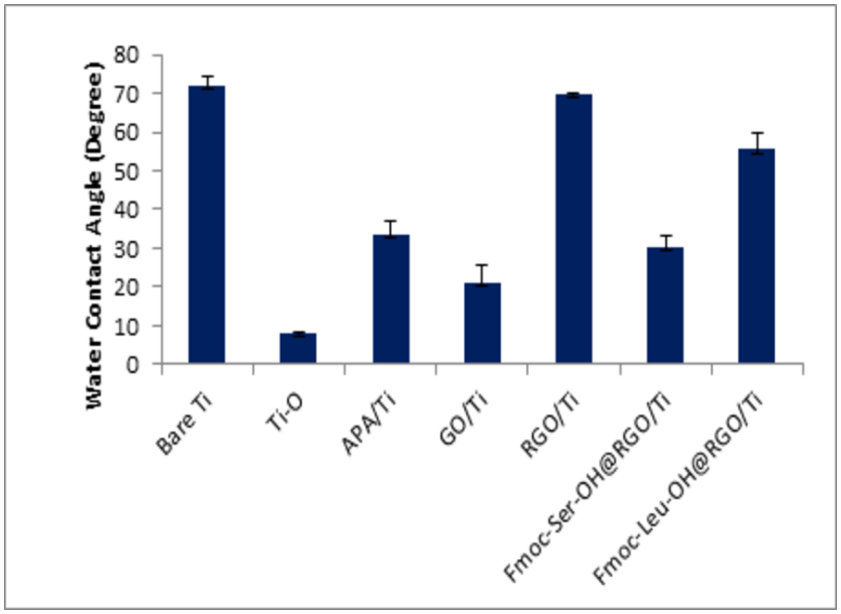


Figure 4.14 Water contact angle degree of bare Ti, activated Ti, APA/Ti, GO/Ti, RGO/Ti, Fmoc-Ser-OH/RGO/Ti (24h) and Fmoc-Leu-Oh/RGO/Ti (24h).

4.1.4 X-ray Photoelectron Spectroscopy (XPS) Analysis

- **XPS Analysis of Ti and APA modified on Ti surface**

Chemical compositions prior and after the modification on Ti surfaces were analyzed by using Thermo Scientific K-Alpha XPS. The XPS analysis were performed to demonstrate the C1s, O1s and Ti2p levels of unmodified Ti surface (Figure 4.15).

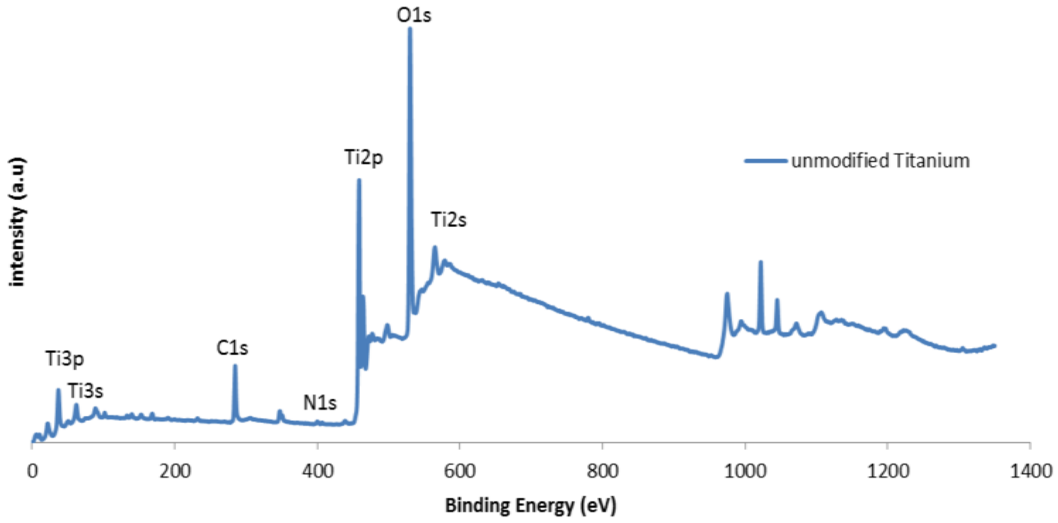


Figure 4.15 XPS Survey Analysis of Ti.

The XPS survey peaks and the deconvolutions of O1s, Ti2p, C1s, N1s and P2p will give more information about modification of self assembly monolayer (SAM) on Ti surface. After modification of APA molecules on Ti surfaces, N1s and P2p were markedly shown. The analysis of XPS survey spectrum of APA modified Ti surface was presented in the Figure 4.16.The presence of amino (-NH_2) groups on Ti surface was confirmed by XPS survey spectrum.

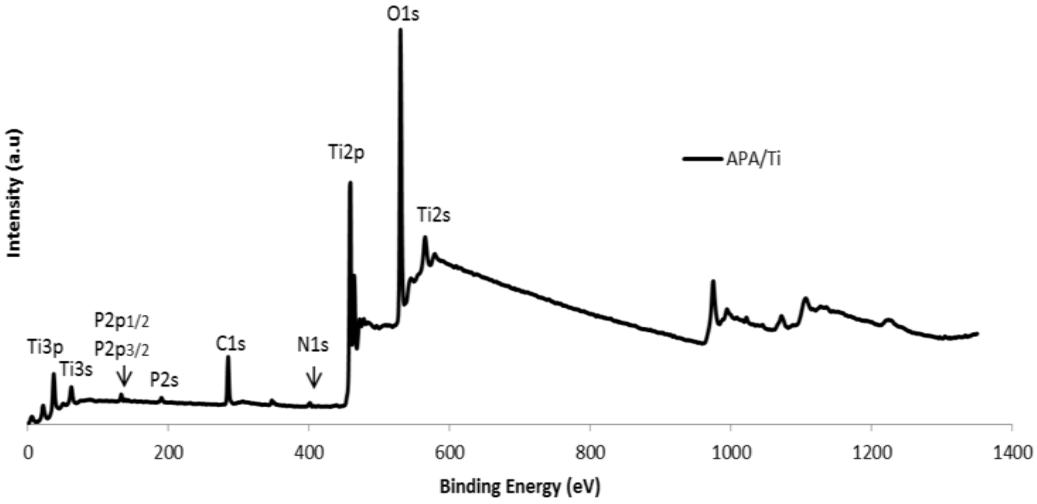


Figure 4.16 XPS Survey Analysis of APA/Ti.

Table 4.5
Atomic percentages of APA/Ti surface.

Atoms	Atomic%
C1s	25.55
O1s	51.61
Ti2p	18.08
P2p	3.18
N1s	1.58

The atomic percentages of C1s, O1s, Ti2p, P2p and N1s were measured to be as 25.55%, 51.61%, 18.08%, 3.18% and 1.58%, respectively (Table 4.5). The O1s core-level spectra of APA/Ti surface was resolved into three peak components at 529.96 eV, 531 eV and 531.98 eV which are assigned to TiO_2, P-O-Ti/P=O and P-OH [72, 73, 74, 75],respectively and shown in Figure 4.17 and Table 4.6.

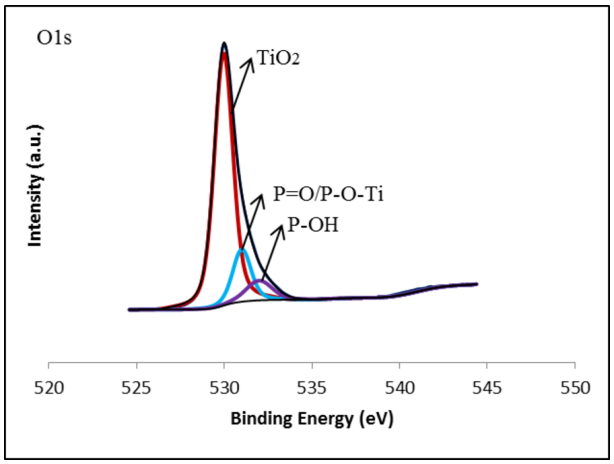


Figure 4.17 High-resolution spectra of oxygen peaks (O1s) for APA/Ti.

Table 4.6
Parameters of APA/Ti showing binding energy (eV), full width at half maximum (FWHM, eV), relative % concentration and chemical bonds.

Element	Binding Energy(eV)	FWHM	Relative Conc. (Atomic%)	Bond Assign Assignment (Chemical State)
O1s	529.96	1.26	76.23	TiO2
	531	1.24	15.48	P-O-Ti/P=O
	531,98	1.75	8.29	P-OH

In the analysis of P2p core level, three phosphorus signals at, 132.94 eV, 133.91 eV and 138.57 eV were obtained and represented in Figure 4.18. The peaks at 132.94 eV and 133.91 eV can be attributed to P2p3/2 and P2p1/2, respectively. The fitting of the P2p has shown 137.9 eV that is unclear/unknown [76, 77].

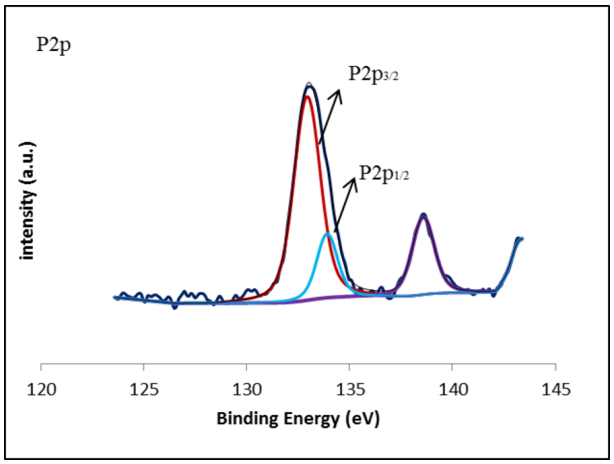


Figure 4.18 High-resolution spectra of phosphate peaks (P2p) for APA/Ti.

- **XPS Analysis of GO/Ti and RGO/Ti nanocomposites**

GO and RGO deposited on APA/Ti surfaces were analyzed by using XPS. Also, the deconvoluting the C1s binding energies of the functional groups were examined because of the variations of the chemical states after chemical reduction.GO sheets were easily immobilized on APA/Ti owing to S_N2 nucleophilic reactions between the epoxy groups of GO surface and the amine groups of APA molecules [35, 41]. XPS Survey Analysis of GO/Ti was shown in Figure 4.19. The changes of C1s, O1s, Ti2p, P2p and N1s peaks were distinctly observed.

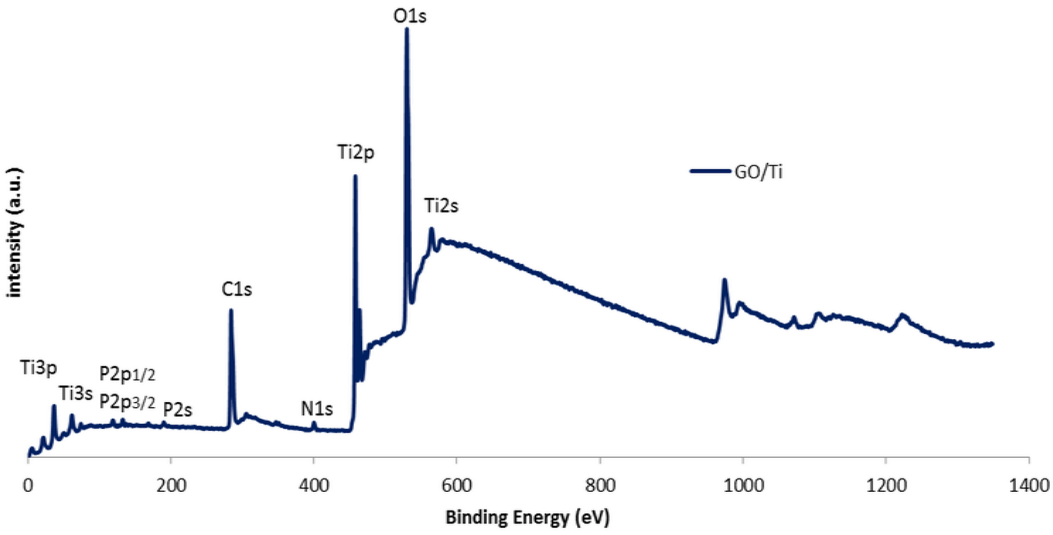


Figure 4.19 XPS Survey Analysis of GO/Ti.

Elemental analysis measurements were performed by XPS analysis to define the atomic ratio of carbon to oxygen (C/O). Table 4.7 has shown the atomic percentages of GO coating APA/Ti surface.

Table 4.7
Atomic percentages of GO coating APA/Ti surface.

Atoms	Atomic%
C1s	41.83
O1s	41.56
Ti2p	9.62
P2p	1.95
N1s	1.91

The C1s core-level spectra of GO/Ti surface was resolved into five peak components at 283.57eV, 284.25 eV, 286.03eV, 286.51 eV, and 288.1eV assigned to C-Ti/C=C, C-C, C-O/C-O-C, C-OH and O=C-OH, respectively and shown in Figure 4.20 [41, 78, 79, 80]. Atomic percentages of C1s bonds were detected (Table 4.8).

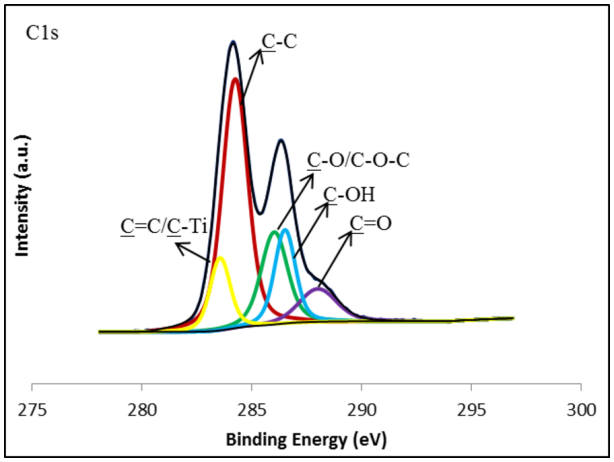


Figure 4.20 High-resolution spectra of carbon peaks (C1s) for GO/Ti.

Table 4.8
Parameters of GO/Ti showing binding energy (eV), full width at half maximum (FWHM, eV), relative % concentration and chemical bonds.

Element	Binding Energy(eV)	FWHM	Relative Conc. (Atomic%)	Bond Assign Assignment (Chemical State)
C1s	284.25	1.37	47.17	C-C
	286.03	1.42	18.15	C-O/C-O-C
	288.01	2.01	9.21	C=O
	286.51	1.13	14.58	C-OH
	283.57	1.09	10.89	C-Ti/C=C

During chemical reduction process, the oxygen-containing functional groups such as epoxide, carbonyl and carboxyl groups were removed from GO flakes modified on APA/Ti surface. XPS survey was shown the reduction effect in detail in Figure 4.20 that is clear since the presence of oxygen atoms of RGO significantly decreased compared with GO (Figure 4.19) and also the level of N1s increased because of chemical reduction process (Figure 4.21).

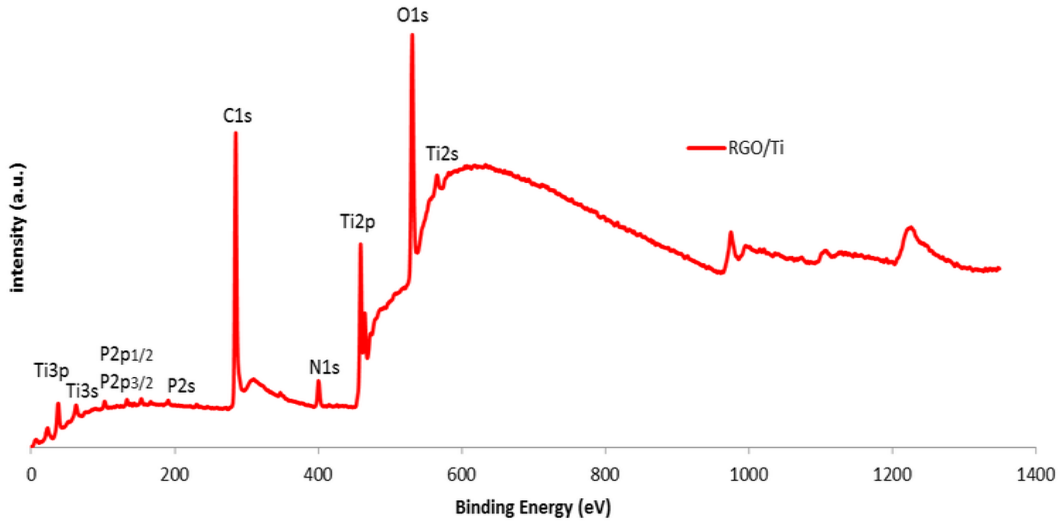


Figure 4.21 XPS Survey Analysis of RGO/Ti.

Table 4.9
Atomic percentages of RGO/Ti surface.

Atoms	Atomic%
C1s	61.08
O1s	24.00
Ti2p	5.93
P2p	1.83
N1s	4.22

The elemental composition were shown in Table 4.9 to detect C/O ratio. Moreover, the deconvolution of C1s spectra of RGO incorporated APA/Ti surface was appeared at 283.98 eV , 284.7 eV, 285.82 eV, 286.73 eV,and 289.26 eV attributable to C-Ti/C-H, C-C, C-N/C-O, C-OH and O=C-OH peaks, respectively and was shown in the Figure 4.22 [41, 48, 78, 79, 80]. Atomic percentages of C1s bonds were demonstrated (Table 4.10).

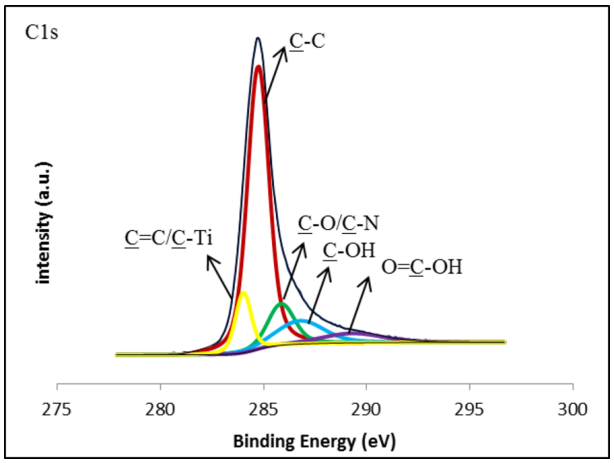


Figure 4.22 High-resolution spectra of carbon peaks (C1s) for RGO/Ti.

Table 4.10
Parameters of RGO/Ti showing binding energy (eV), full width at half maximum (FWHM, eV), relative % concentration and chemical bonds.

Element	Binding Energy(eV)	FWHM	Relative Conc. (Atomic%)	Bond Assign Assignment (Chemical State)
C1s	284.7	1.37	47.17	C-C
	285.82	1.42	18.15	C-N/C-O
	286.73	2.01	9.21	C-OH
	289.26	1.13	14.58	O=C-OH
	283.98	1.09	10.89	C-Ti/C=C

• XPS Analysis of Fmoc amino acids modified on RGO/Ti nanocomposites

The XPS survey spectrums of Fmoc amino acids modified on RGO/Ti surface were analyzed by using Thermo Scientific K-Alpha XPS and were shown in Figure 4.23 and Figure 4.25.

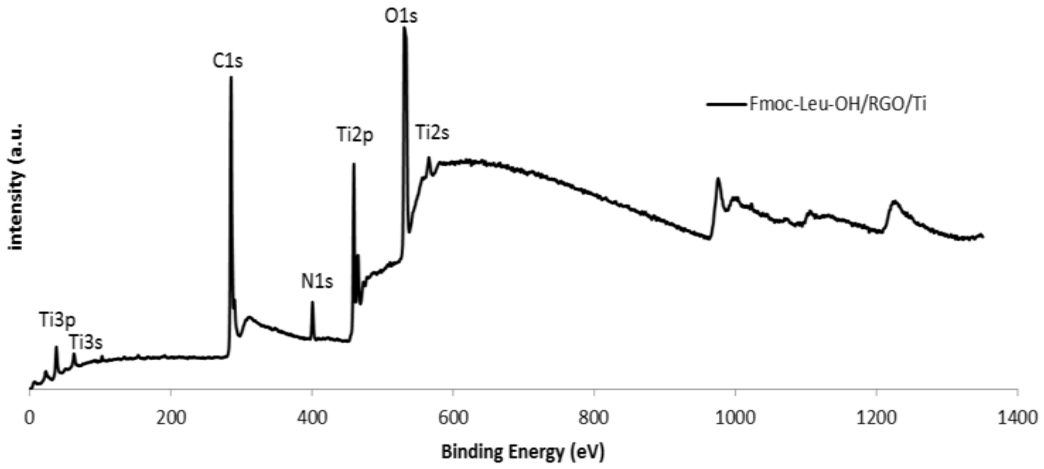


Figure 4.23 XPS Survey Analysis of Fmoc-Leu-OH modified on RGO/Ti.

Table 4.11
Atomic percentages of Fmoc-Leu-OH/RGO/Ti.

Atoms	Atomic%
C1s	59.74
O1s	29.71
Ti2p	5.16
P2p	4.09

In XPS survey in Figure 4.23, the atomic percentages of C1s, O1s and N1s were presented after Fmoc-Leu-OH amino acids ($C_{21}H_{23}NO_4$) modified on RGO/Ti surface (Table 4.11) [81]. The C1s spectrum can be curve fitted into five different peaks that were found the binding energies at 284.46 eV, 284.88 eV, 286.7 eV and 289.72 eV, the corresponding to C-C, C-C/C-H, C-O/C-N, and O=C-OH bonds (Table 4.12) [80, 81]. In the analysis of C1s core level, the $\pi - \pi$ stacking interaction between the Fmoc conjugated amino acids and RGO/Ti was shown as 292.04 eV bond. (Figure 4.24).

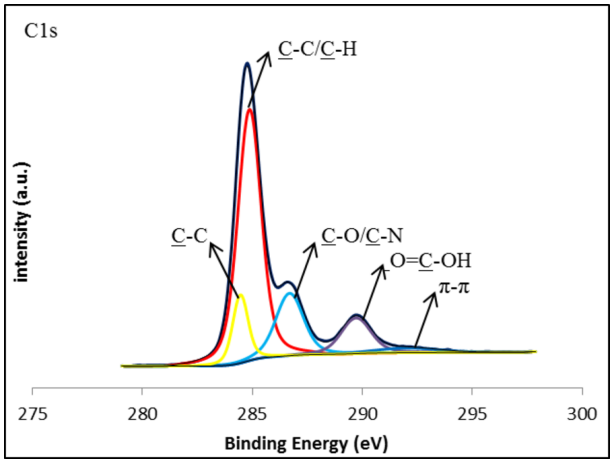


Figure 4.24 High-resolution spectra of carbon peaks (C1s) for Fmoc-Leu-OH/RGO/Ti.

Table 4.12
Parameters of Fmoc-Leu-OH/RGO/Ti showing binding energy (eV), full width at half maximum (FWHM, eV), relative % concentration and chemical bonds.

Element	Binding Energy(eV)	FWHM	Relative Conc. (Atomic%)	Bond Assign Assignment (Chemical State)
C1s	284.88	1.25	58.67	C-C/C-H
	286.7	1.48	17.24	C-N/C-O
	289.72	1.59	10.36	O=C-OH
	292.04	3.37	2.89	$\pi - \pi$
	283.46	0.83	10.56	C-C

In XPS survey, Fmoc-Ser-OH amino acids ($C_{18}H_{17}NO_5$) were modified on RGO/Ti surface.(Figure 4.25) The atomic percentages of Fmoc-Ser-OH/RGO/Ti were detected and shown in Table 4.13

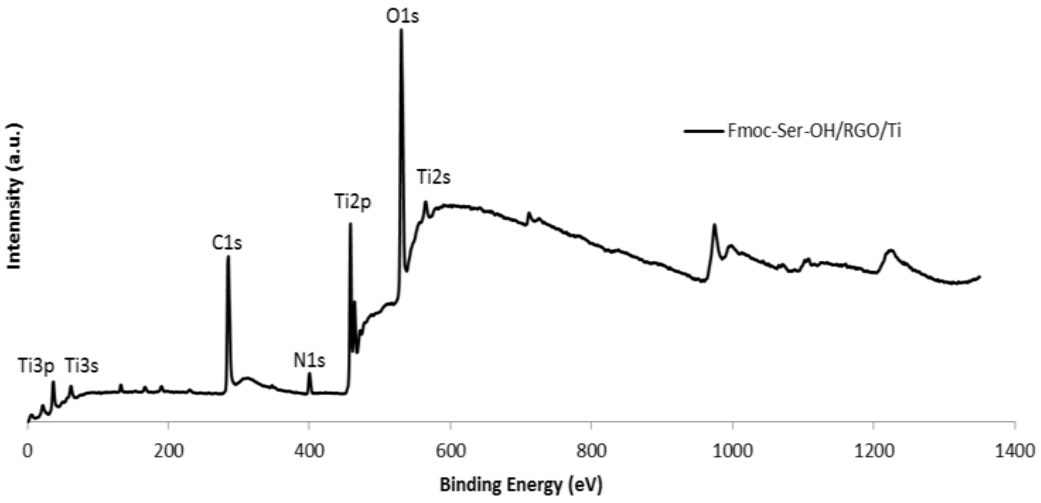


Figure 4.25 XPS Survey Analysis of Fmoc-Ser-OH modified on RGO/Ti.

Table 4.13
Atomic percentages of RGO/Ti surface.

Atoms	Atomic%
C1s	61.08
O1s	24.00
Ti2p	5.93
P2p	1.83
N1s	4.22

The atomic percents of C1s and O1s were measured to be as 48.24% and 36.18% in XPS survey in Table 4.13.The adsorption effect of Fmoc-Ser-OH amino acids on RGO/Ti was clearly indicated due to increasing the content of oxygen (O) atoms. The deconvolution of C1s spectra was resolved into five different peaks at 284.23eV, 284.94eV, 286.32eV, 287.98 eV and 290.56 eV attributable to C-C/C-H,C-H, C-OH/C-O, O=C-NH and O=C-OH or $\pi - \pi$ bonds (Figure 4.26) [80, 82].

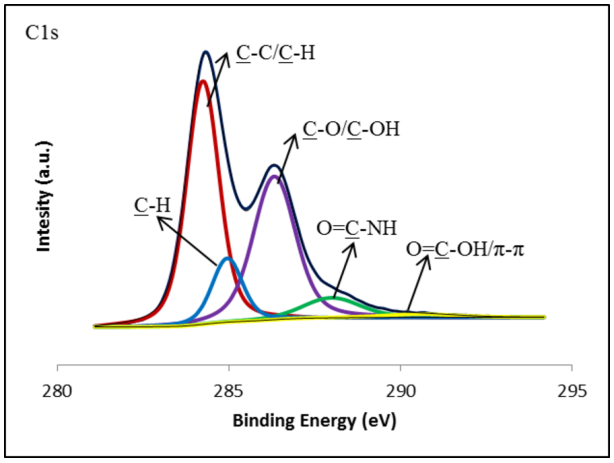


Figure 4.26 High resolution spectra of carbon peaks (C1s) for Fmoc-Ser-OH/RGO/Ti.

Table 4.14
Parameters of Fmoc-Ser-OH/RGO/Ti showing binding energy (eV), full width at half maximum (FWHM, eV), relative% concentration and chemical bonds.

Element	Binding Energy(eV)	FWHM	Relative Conc. (Atomic%)	Bond Assign Assignment (Chemical State)
C1s	284.23	1.13	45.81	C-C
	286.32	1.46	34.98	C-OH
	287.98	1.97	6.63	O=C-NH
	284.94	1.05	11.23	C-H
	290.56	2.52	1.35	O=C-OH/$\pi - \pi$

4.1.5 Raman Spectroscopy

- **Raman Spectroscopy of Activated Ti surface**

The Raman scattering signal from unmodified and modified Ti surface was recorded by using an excitation wavelength of 532 nm. The presence of three modes was represented to formation of TiO_2 coated glass. The major peaks located at about 606 cm^{-1}, 418 cm^{-1}, and 283 cm^{-1} were measured and shown in Figure 4.27 [83], [84], [85].

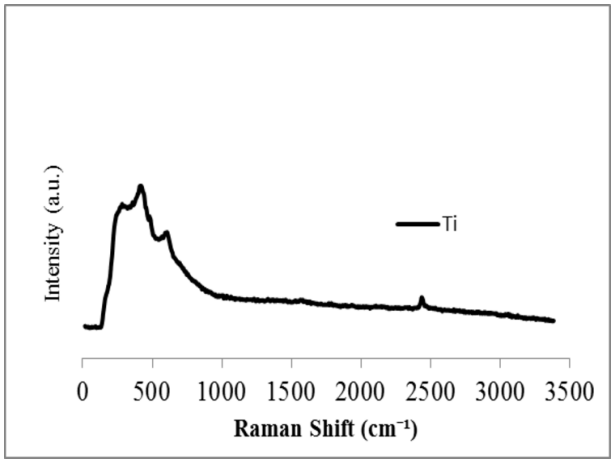


Figure 4.27 Raman spectra of Bare Ti surface.

• **Raman Spectroscopy of GO/Ti and RGO/Ti nanocomposites**

Raman spectras of GO and RGO deposited on APA/Ti surfaces were investigated to understand the signatures and the structural disorder with the Id/Ig ratio before and after reduction. The D band is related to the structural imperfections that originate from the presence of functional groups such as hydroxyl, epoxy on the carbon skeleton [45, 86, 87]. Moreover, the oxidation process effects the size of the in-plane sp2 domains. The G band associated with the first-order scattering of the E2g mode of sp2 domain of carbon atoms [86, 88]. As shown in the Raman spectrum of GO/Ti, the curves display two main peaks at around 1351 cm^{-1} and 1575 cm^{-1} corresponding to the D peak and G peak, respectively (Figure 4.28). After chemically reduction of GO/Ti, the G peak was downshifted from 1575 cm^{-1} to 1571 cm^{-1}. In the Raman spectrum of GO, the D peak was also broadened and shifted to 1346^{-1} (Figure 4.28). Two other peaks at around 2674 cm^{-1} and 2910 cm^{-1} corresponding to 2D and D+G mode were clearly found. This increase in Id/Ig is described to the extent of defects or disorder in the carbon material or carbon ratio of sp2/sp3 [86, 88]. The Id/Ig intensity ratio of RGO/Ti was measured to be as 1.03 which is compare to value of the Id/Ig ratio of GO which was found to be 1.00.

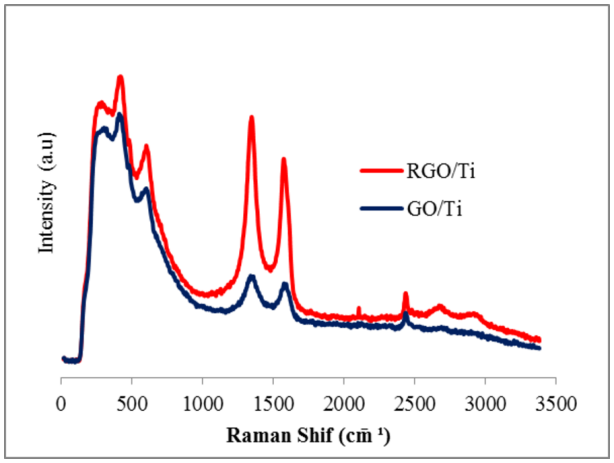


Figure 4.28 Raman spectra of GO/Ti and RGO/Ti surface.

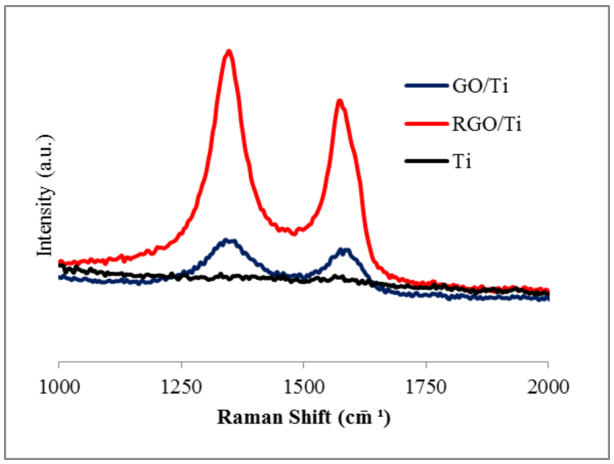


Figure 4.29 Raman spectras of Ti, GO/Ti and RGO/Ti surface.

• **Raman Spectroscopy of Fmoc amino acids modified on RGO/Ti nanocomposites**

The Raman spectrums of Fmoc amino acids modified RGO/Ti surfaces were investigated by using an excitation wavelength of 532 nm. In the Raman spectrum of Fmoc-Ser-OH amino acids modified RGO/Ti surface, G and D peaks appeared 1346 cm^{-1} and 1583 cm^{-1}, respectively. Figure 4.30 shown that Fmoc-Ser-OH molecules affected the G peak shifted compared to that of RGO/Ti surface. As depicted in Figure 4.30, Id/Ig ratio was slightly decreased from 1.02 to 1.01. The G band of RGO/Ti at 1571 cm^{-1} upshifted to 1579 cm^{-1} after modification of Fmoc-Leu-OH amino acids on RGO/Ti surface. The Raman spectra, presented in Figure 4.30, demonstrated that D peaks appeared at around 1346 cm^{-1}. The Id/Ig ratio was changed from 1.02 to 1.01.

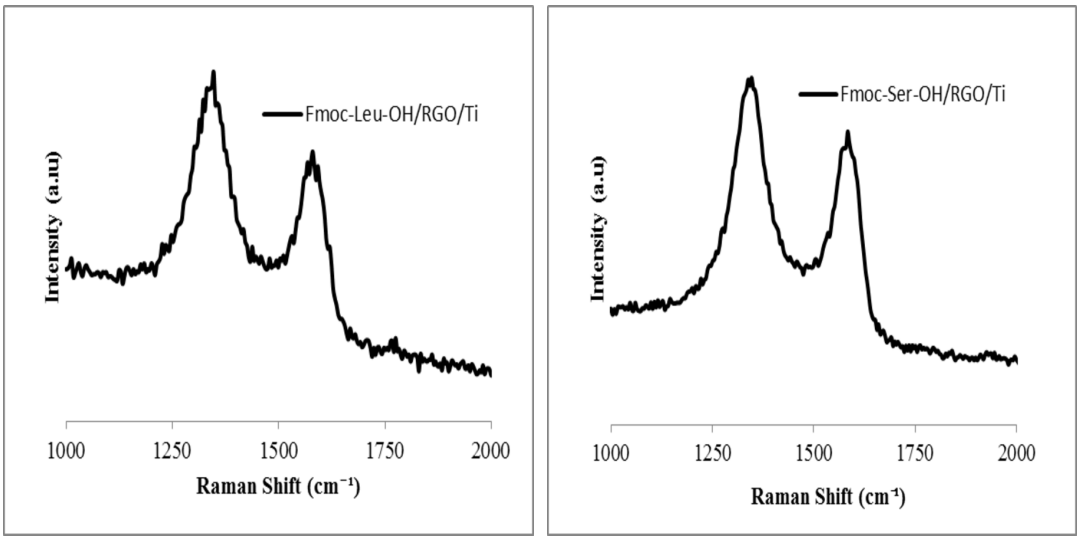


Figure 4.30 Raman spectras of Fmoc Amino Acids on RGO/Ti surfaces.

4.2 Cell Studies

4.2.1 MTT Assay of unmodified and modified Ti surface

The effects of surface modification on cell viability were investigated by using MTT assay. Osteoblast cells were seeded and cultured on unmodified, modified Ti surfaces and tissue culture polystyrene (TCPS) plates. In order to detect cellular viability and cytotoxicity of chemicals on the experimental groups, MTT assay was used and evaluated after being incubated for 1st, 3rd and 5th days. Activated Ti surface was chosen as control group in all experimental setup. Data were plotted as mean ± S.E. (n=9).

At 1st day, the result of MTT assay was shown in Figure 4.31. The metabolic activities of cells on experimental groups were measured and calculated to be as 106.3% ± 2.4%, 125.6% ± 3.8%, 114.5% ± 2.2%, 132.4% ± 1.8%, 122.7% ± 4.2% and 124.3% ± 4.1% corresponding to APA/Ti, GO/Ti, RGO/Ti, Fmoc-Ser-OH/RGO/Ti, Fmoc-Leu-OH/RGO/Ti, TCPS, respectively according to Ti control group (99% ± 2.5%). Experimental groups were significantly different when compare to Ti and APA treated group (df=6, F=24.520, Sig.=0,000). There were observed that carbon structures of both GO and RGO positively affected the osteoblast cell viability. Moreover, the

results suggested that hydrophilic areas of the modified Ti surfaces were more prone to augment the viable osteoblast cell number.

At 3rd day, the result of MTT assay was indicated in Figure 4.32. The increase in the number of viable cell was observed except to RGO/Ti surface. According to Ti control group (101.6% ± 3.3%), the percentages of viable cell number on experimental groups were measured and calculated to be as 122.6% ± 7.3%, 135.4% ± 4.3%, 113% ± 3.5%, 147.6% ± 7%, 140.5% ± 6.3% and 136% ± 5.1%, respectively. Experimental groups showed significant different when compare to Ti and APA treated group. (df=6, F=9.437, Sig.=0,000).

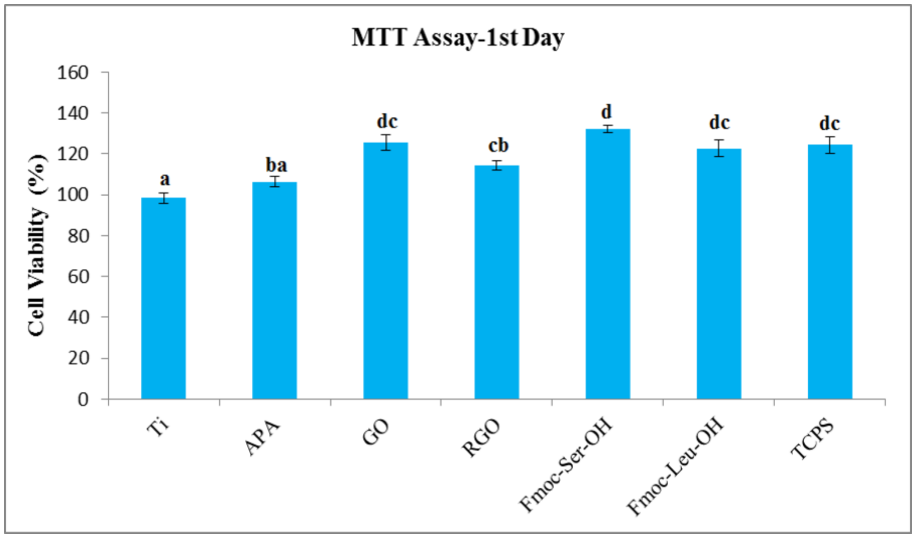


Figure 4.31 MTT assay results at 1st day. Data is expressed in means ± SE and represent the results of three independent experiments ($p < 0.05$).

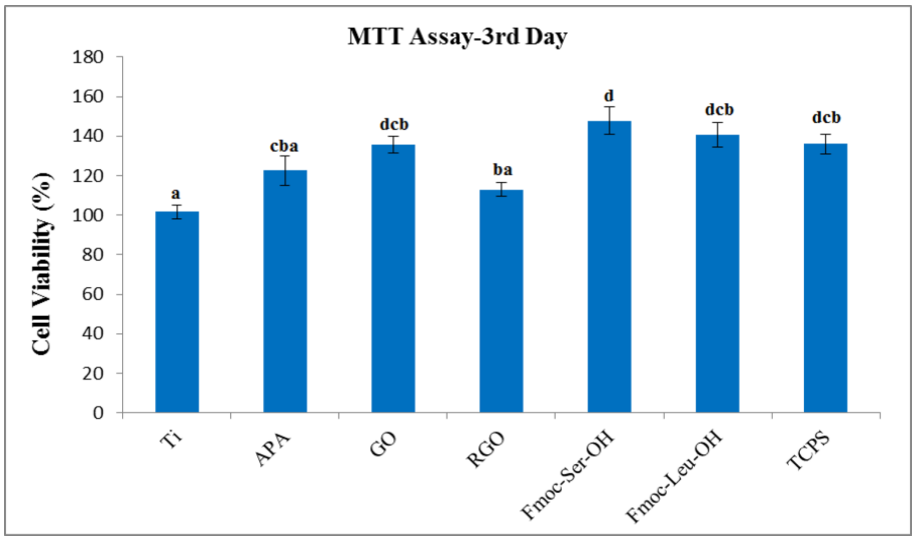


Figure 4.32 MTT assay results at 3rd day. Data is expressed in means ± SE and represent the results of three independent experiments ($p < 0.05$).

At 5th day, the MTT assay indicated the metabolic activities of osteoblast cells among all groups. As shown in Figure 4.33, all experimental groups have shown higher cell viability than Ti control group and MTT results of first and third days. The viable cell number on Ti control and other experimental groups were calculated to be as 100% ± 4.3%, 169% ± 10.9%, 217.8% ± 8.7%, 179.4% ± 9%, 228.2% ± 8.2%, 207% ± 8.6% and 204.1% ± 14.2%, respectively. It was observed that the cell number increased with increasing culture incubation period. The cellular viability was better on GO/Ti than RGO/Ti. The highest increase in the number of viable cells was found after being treated with Fmoc-Ser-OH amino acids on RGO/Ti surface ($p < 0.05$; df=6, F=20.759, Sig.=0,000).

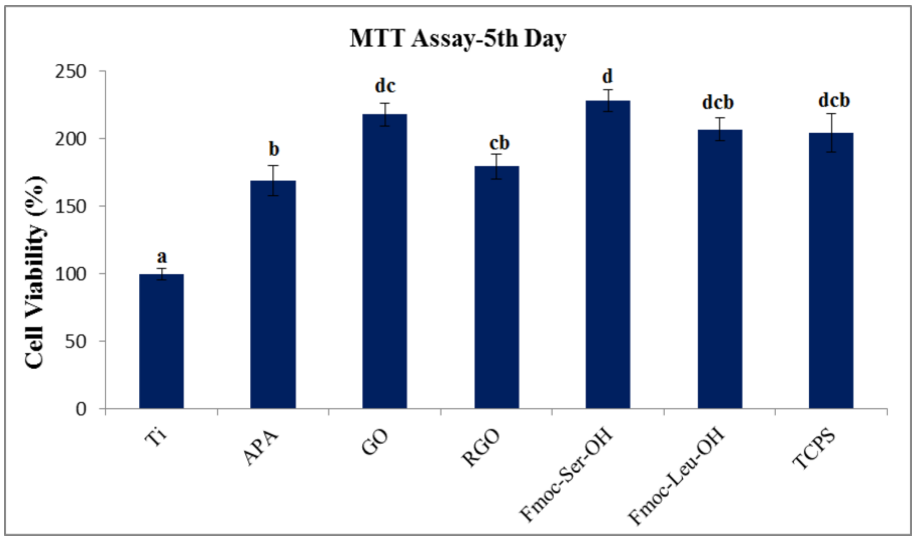


Figure 4.33 MTT assay results at 5th day. Data is expressed in means ± SE and represent the results of three independent experiments ($p < 0.05$).

MTT results among all experimental groups were matched with each other. According to the data shown in Fig.4.34, the viable cell number increased with culture time. The viabilities of the cells on Fmoc-Ser-OH/RGO/Ti surface were higher than surfaces of all experimental groups following 24h, 72h and 120h of application ($p < 0.05$).

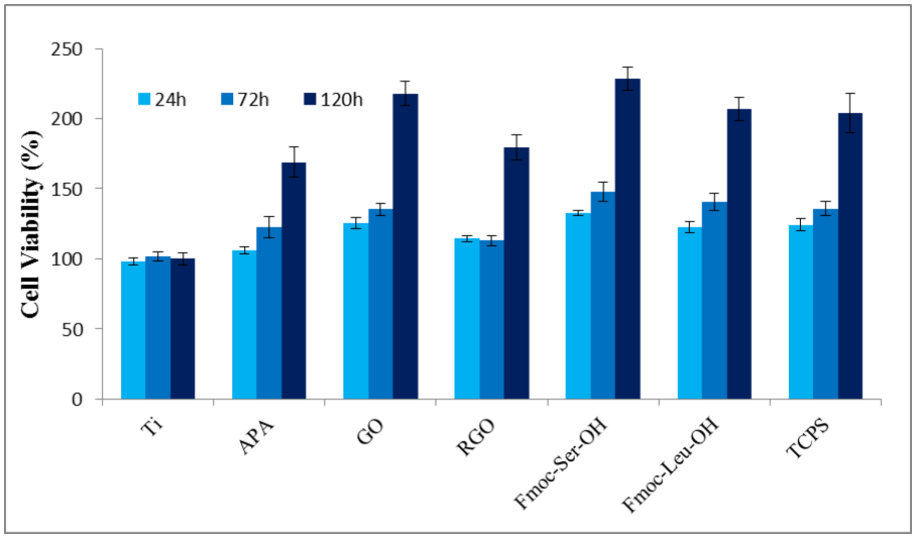


Figure 4.34 MTT assay for assessing cellular viability of osteoblasts on all experimental groups after 24h, 72h and 120h of application.

4.2.2 Alamar Blue Assay of unmodified and modified Ti surface

The Alamar Blue (AB) assay which is a noncytotoxic reduction oxidation (redox) indicator was used to measure and compare cell proliferation on unmodified, modified Ti surfaces and TCPS at 1st, 3rd, and 5th days after cell seeding and culturing. Absorbance is described as the proportional to the number and metabolic activity of the cells. Two equations were used to calculate the percent reduction and the percent difference between treated and control cells in cytotoxicity/proliferation experiments. Nonseeded wells and activated Ti surface were used as a negative control and positive control groups, respectively. Figure 4.35 and Figure 4.36 demonstrated the results of AB assay for 1st day. AB assay demonstrated higher cell population with respect to negative control and positive control groups. All the data were expressed as means ± SE and n=15. According to negative control group (28% ± 1.1%), the percentages of reduction of Alamar Blue were measured then calculated to be as 36.6% ± 1%, 50.3% ± 1.2%, 54.3% ± 0.9%, 51.3% ± 1.1%, 64% ± 1.5%, 53% ± 0.7% and 55.7% ± 1.3% that introduced APA/Ti, GO/Ti, RGO/Ti, Fmoc-Ser-OH/RGO/Ti, Fmoc-Leu-OH/RGO/Ti and TCPS, respectively (Figure 4.35). The percentages of AB reduction gave preliminary information about cell proliferation. When the AB results were compared to the positive control group (100% ± 2.7%) at 1st day, the cell proliferation rates for all experimental group were calculated to be as 137.5% ± 3.2%, 148.3% ± 3.1%, 140.1% ± 3.1%, 174.9% ± 4.2%, 144.8% ± 1.8% and 152.1% ± 3.6%, respectively and shown in Figure 4.37. There was a statistically significant difference among all experimental groups for proliferating osteoblast cells on Fmoc-Ser-OH modified on RGO/Ti surface ($p < 0.05$; df=6, F=52.884, Sig.=0,000).

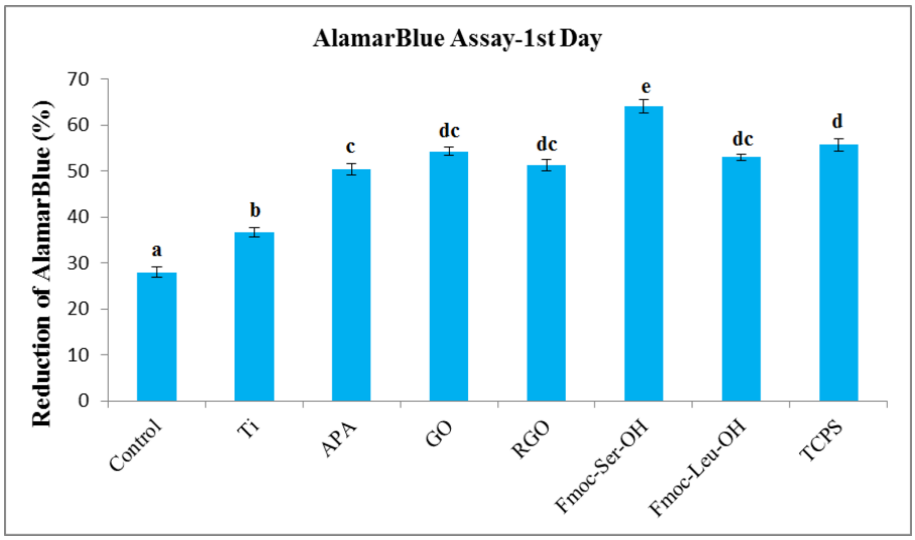


Figure 4.35 Alamar Blue assay results at 1st day. Data are presented as mean ± standard error of percentage viability compared to negative control (n=15, $p < 0.05$).

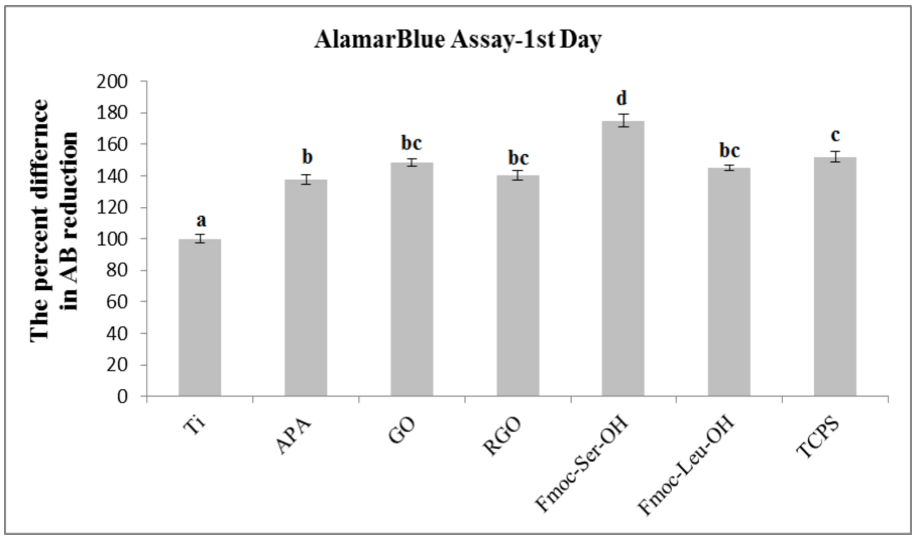


Figure 4.36 Alamar Blue assay results at 1st day. Data are presented as mean ± standard error of percentage viability compared to positive control (n=15, $p < 0.05$).

According to AB results on 3rd day, all experimental groups have shown an increase ratio in cell proliferation in Figure 4.37 and Figure 4.38 and the highest proliferation percentage was observed on Fmoc-Ser-OH modified RGO/Ti surfaces compared to proliferation rates of other experimental groups. When we sort all experimental data according to negative control group assignable to 27.4% ± 0.2, the cell proliferation on Ti, APA/Ti, RGO/Ti Fmoc-Leu-OH/RGO/Ti, GO/Ti, TCPS and Fmoc-Ser-OH/RGO/Ti surfaces were calculated to be as 52.5% ± 1.1%, 62.8% ± 2%, 62.3% ± 1.6%, 64.8% ± 1.7%,69.2% ± 1.1%, 71.9% ± 2.6% and 80.3%±3%, respectively. Moreover, the percent differences between control and treated cells in proliferation experiment, shown in Figure 4.38, found to be as 100% ±2.2%, 119.6% ± 3.7%, 131.7% ± 2.1%, 118.5% ± 3.1%, 152.9% ± 5.7%, 123.3%±3.2% and 136.8% ± 4.9%, respectively. The significant different of experimental groups was demonstrated when compare to Ti group ($p<0.05$; df=6, F=18.080, Sig.=0,000). A significant increase in basic data of cell studies on Ti was observed from 1st day to 3rd day; therefore, it caused a decrease in the relative percentages among other experimental groups. Also, the maintain of same trend in experimental groups was observed at 3rd as the first day.

At 5th day, results of AB reduction, shown in Figure 4.39 were calculated to be as 50.3%±1.2%, 62.4% ± 1.2%, 71.6% ± 2.3%, 62.9% ± 1.6%, 83.2% ± 2.3%, 65% ± 2% and 80% ± 1.2% with respect to negative control group attributable to 24.3% ± 0.4%. The similar trend was shown that cell proliferation on all experimental groups increased from 1st day to 5th day except to Ti surface. When compared to the positive control (100% ± 2.3%) at 5th day, the results of the percent difference in AB reduction was found to be as 124% ± 2.4%, 137.7% ± 3.5%, 125% ± 3.2%, 165.3% ± 4.6%, 129.2% ± 4% and 155.8% ± 2.6%, respectively and displayed in Figure 4.40 ($p<0.05$; df=6, F=42.488, Sig.=0,000).

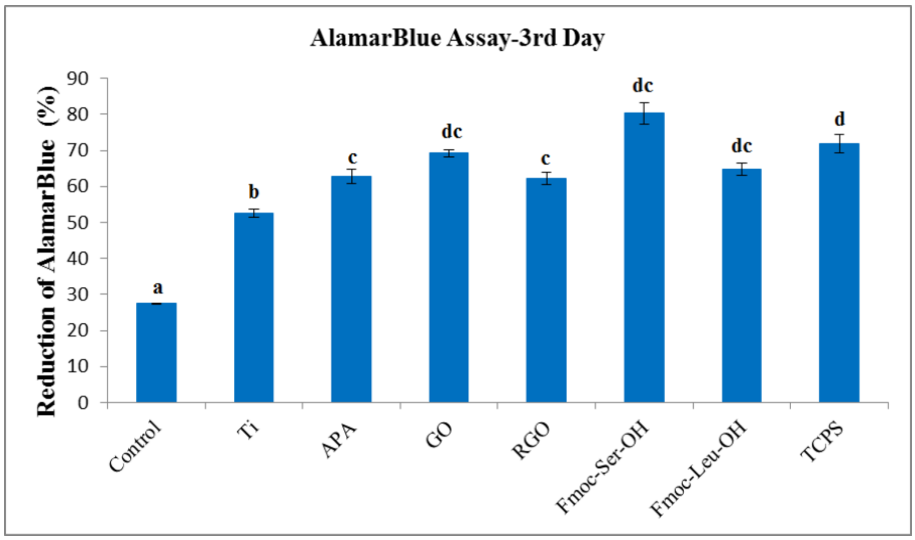


Figure 4.37 Alamar Blue assay results at 3rd day. Data are presented as mean ± standard error of percentage viability compared to negative control (n=15, $p < 0.05$).

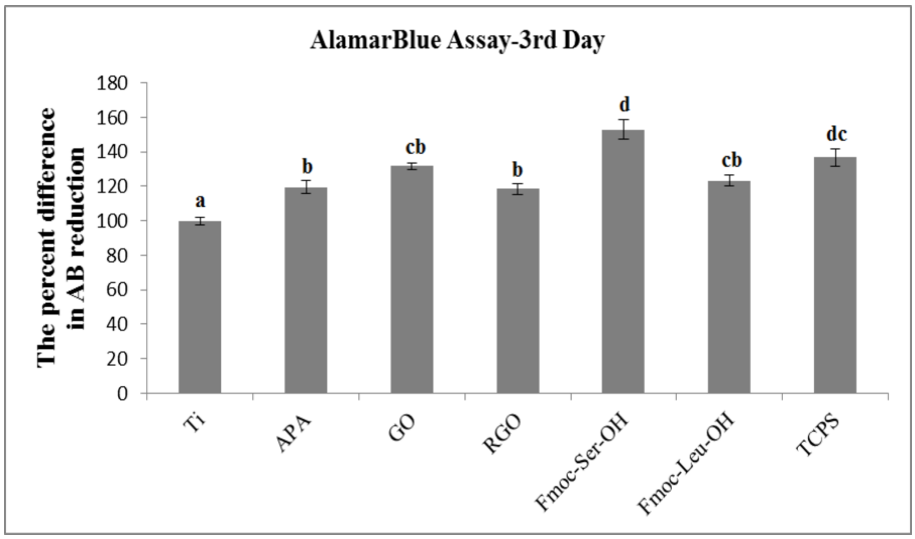


Figure 4.38 Alamar Blue assay results at 3rd day. Data are presented as mean ± standard error of percentage viability compared to positive control (n=15, $p < 0.05$).

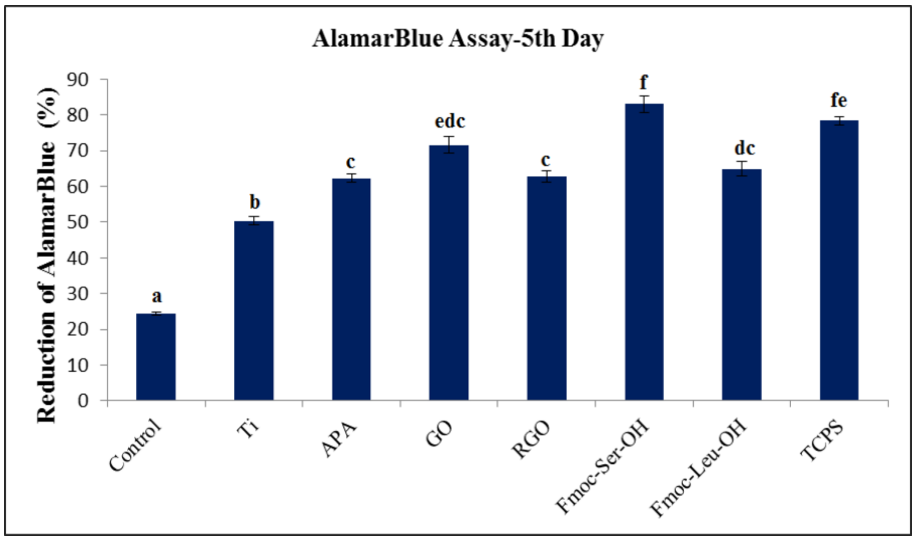


Figure 4.39 Alamar Blue assay results at 5th day. Data are presented as mean ± standard error of percentage viability compared to negative control (n=15, $p < 0.05$).

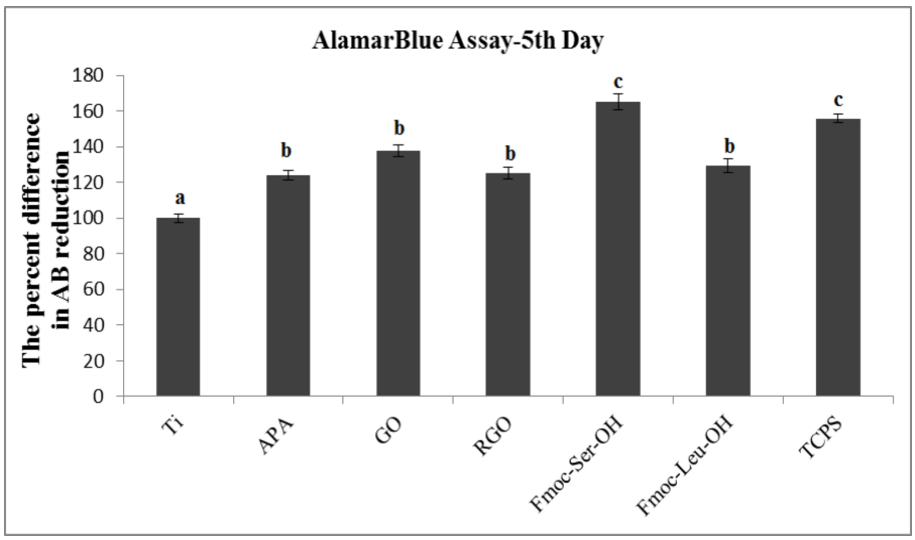


Figure 4.40 Alamar Blue assay results at 5th day. Data are presented as mean ± standard error of percentage viability compared to positive control (n=15,$p < 0.05$).

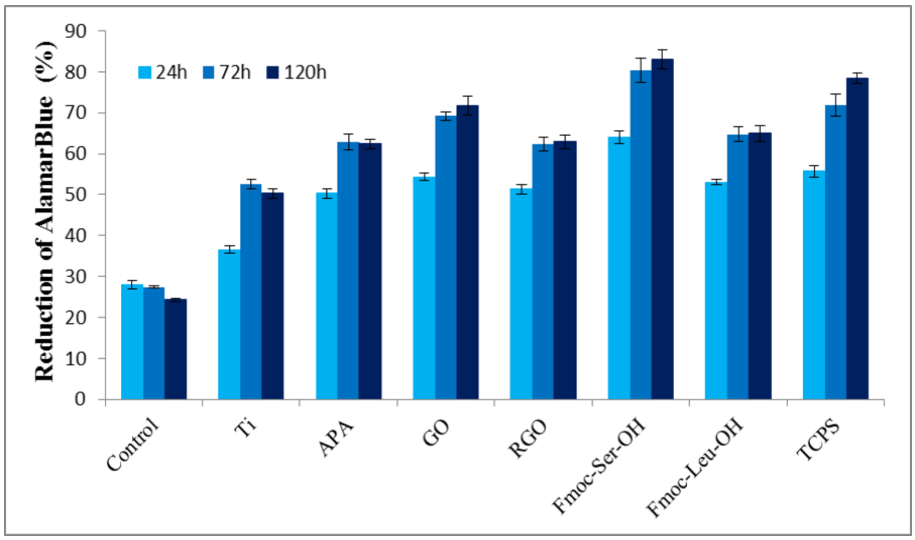


Figure 4.41 Alamar Blue assay for evaluating proliferation of osteoblasts compare to negative control group after 24h, 72h and 120h of incubation.

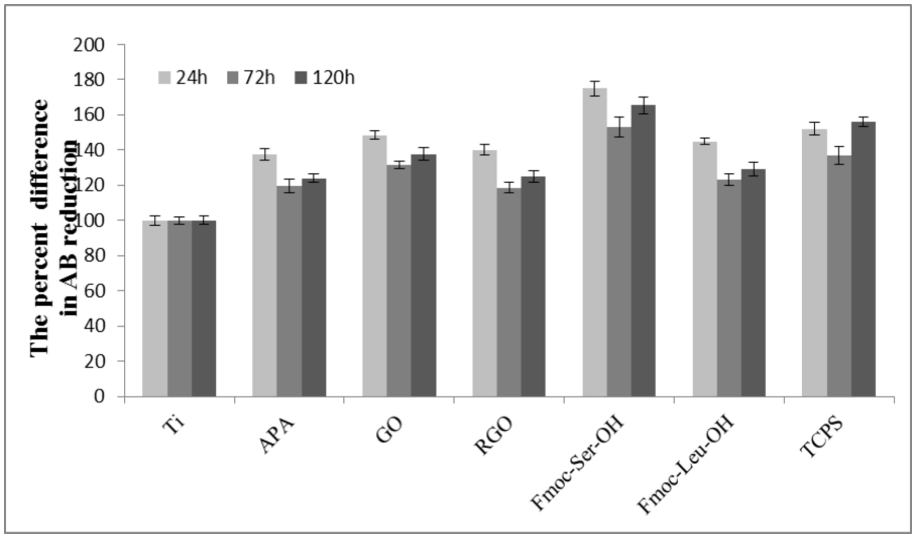
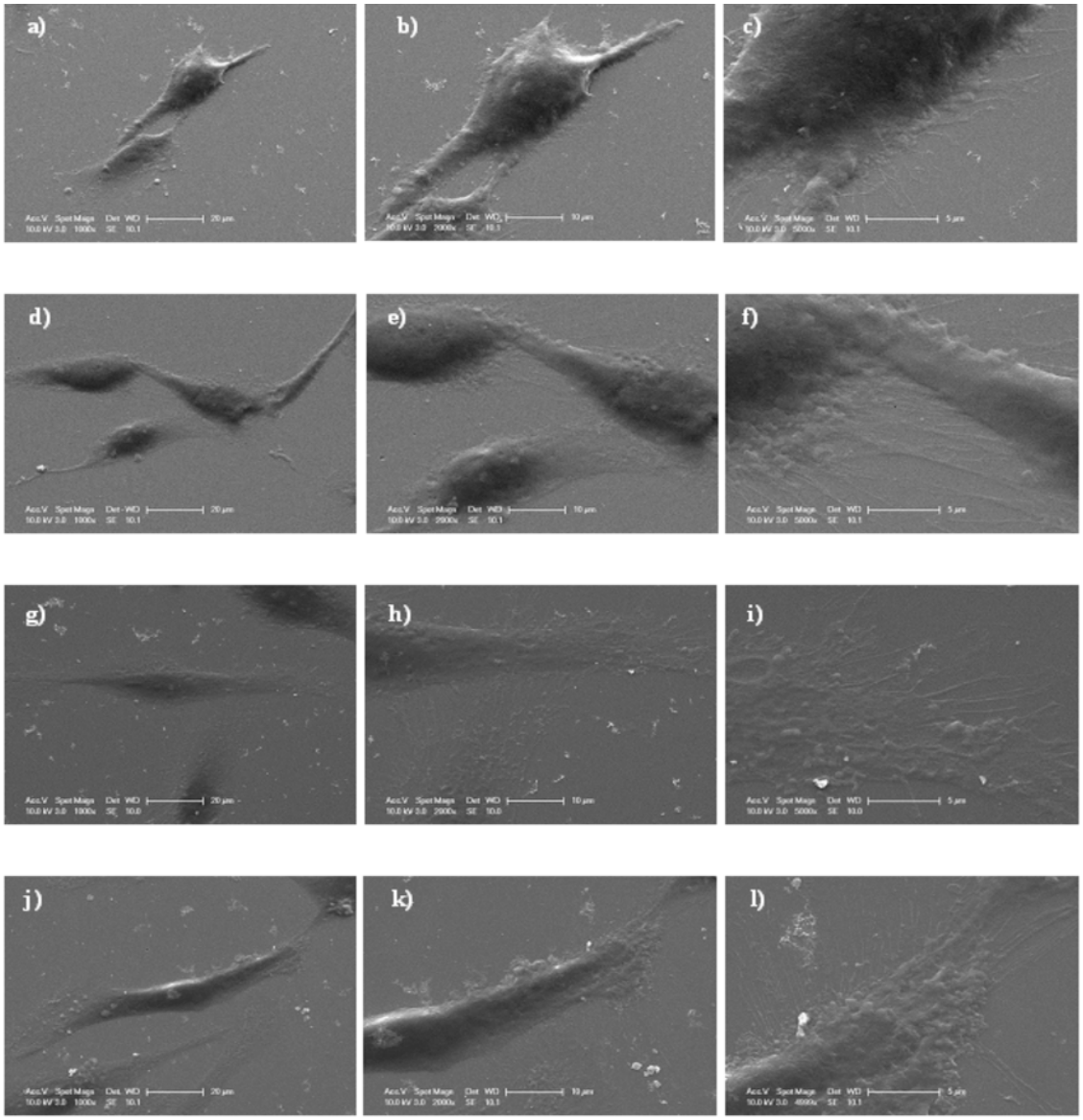


Figure 4.42 Alamar Blue assay for evaluating proliferation of osteoblasts compare to positive control group after 24h, 72h and 120h of incubation.

Figure 4.41 and Figure 4.42 showed the proliferation of osteoblast cells compare to negative and positive control groups after 24h, 72h and 120h of incubation. It is important result that cell proliferation was greater for Fmoc amino acids than the control ones. Figure 4.41 indicated percentages of AB reduction accreted from 1st day to 3rd day with respect to negative control group; on the other hand, percent difference in AB reduction slowed down from 1st day to 3rd day because of increasing cell proliferation on Ti surface at 3rd (Figure 4.42). However, the same trend of cell proliferation among groups was observed in all experimental periods. At 1st and 5th day, the cell proliferation rates approached each others. The results of basic data supported that cell proliferation on Ti surface was less than on other groups at 1st day; therefore, relative cell proliferation showed the highest value at 1st day when compare to 3rd day. Also, cell proliferation on Ti was almost stable value from 3rd day and 5th day while increasing cell proliferation on other groups maintained, so the percentages of relative cell proliferation augmented.

4.2.3 Cell Adhesion and Morphology of unmodified and modified Ti surface

SEM at an acceleration voltage in the range 5-10kV was used to visualize osteoblast cell morphology on unmodified and modified Ti surfaces and to assess cell-substrates affinity by the aid of responses of cellular components (filopodia and lamellipodia). Cellular attachments to unmodified and modified Ti surfaces were shown in Figure 4.43 after osteoblast cells were incubated for 24h.



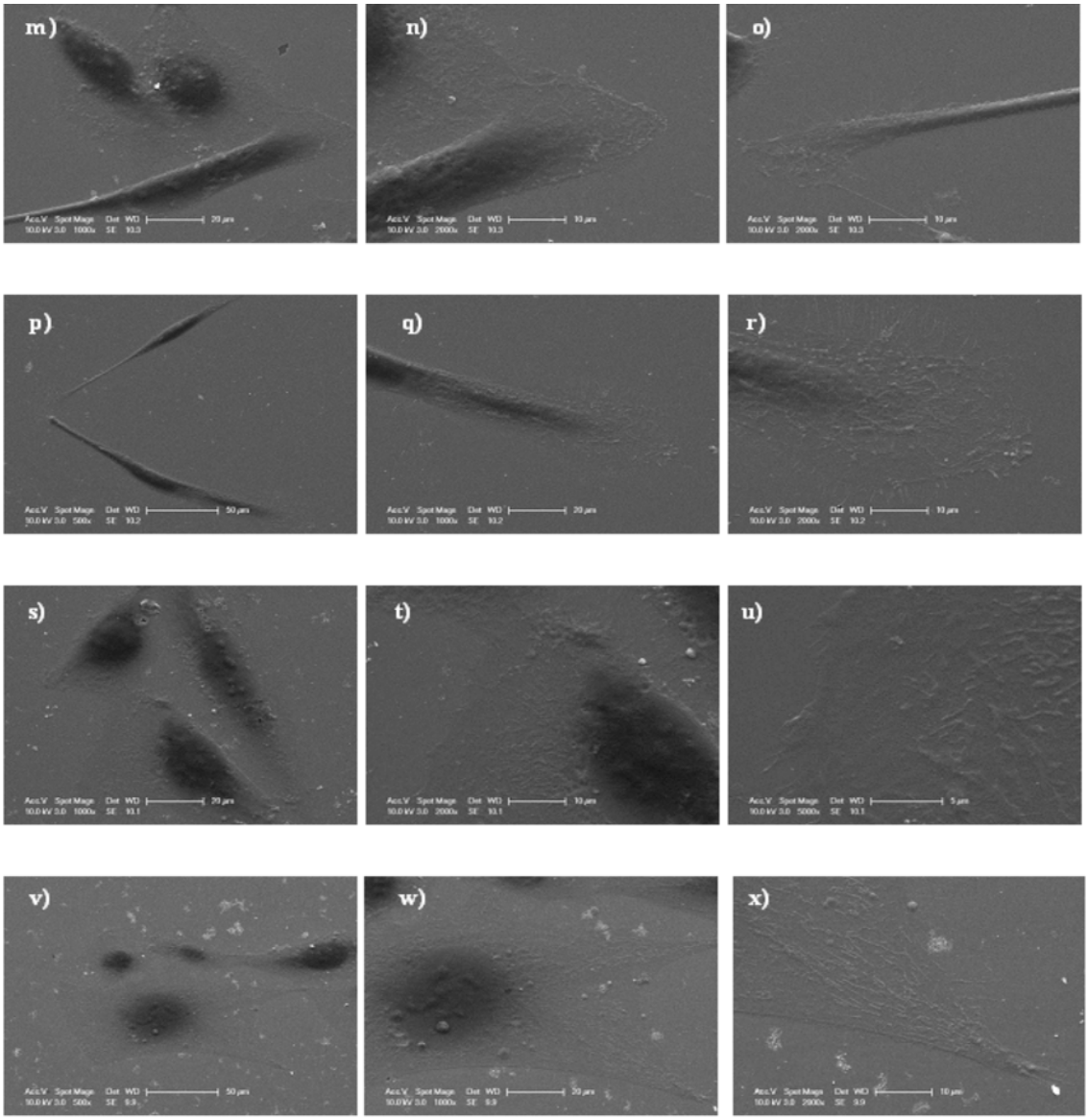


Figure 4.43 SEM images of cell morphologies on Ti (a,x1000; b,x2000; c,x5000 magnification), APA/Ti (d,x1000; e,x2000; f,x5000 magnification),GO/Ti (g,x1000; h,x2000; i,x5000 magnification), RGO/Ti (j,x1000; k,x2000; l,x5000 magnification), Fmoc-Leu-OH/RGO/Ti (m,x1000; n,x2000; o,x5000 and p,x1000; qx2000; r,x5000 magnification) and Fmoc-Ser-OH/RGO/Ti (s,x1000; t,x2000; u,x5000 and v,x500; w,x1000; x,x2000 magnification) after 1st day of culture.

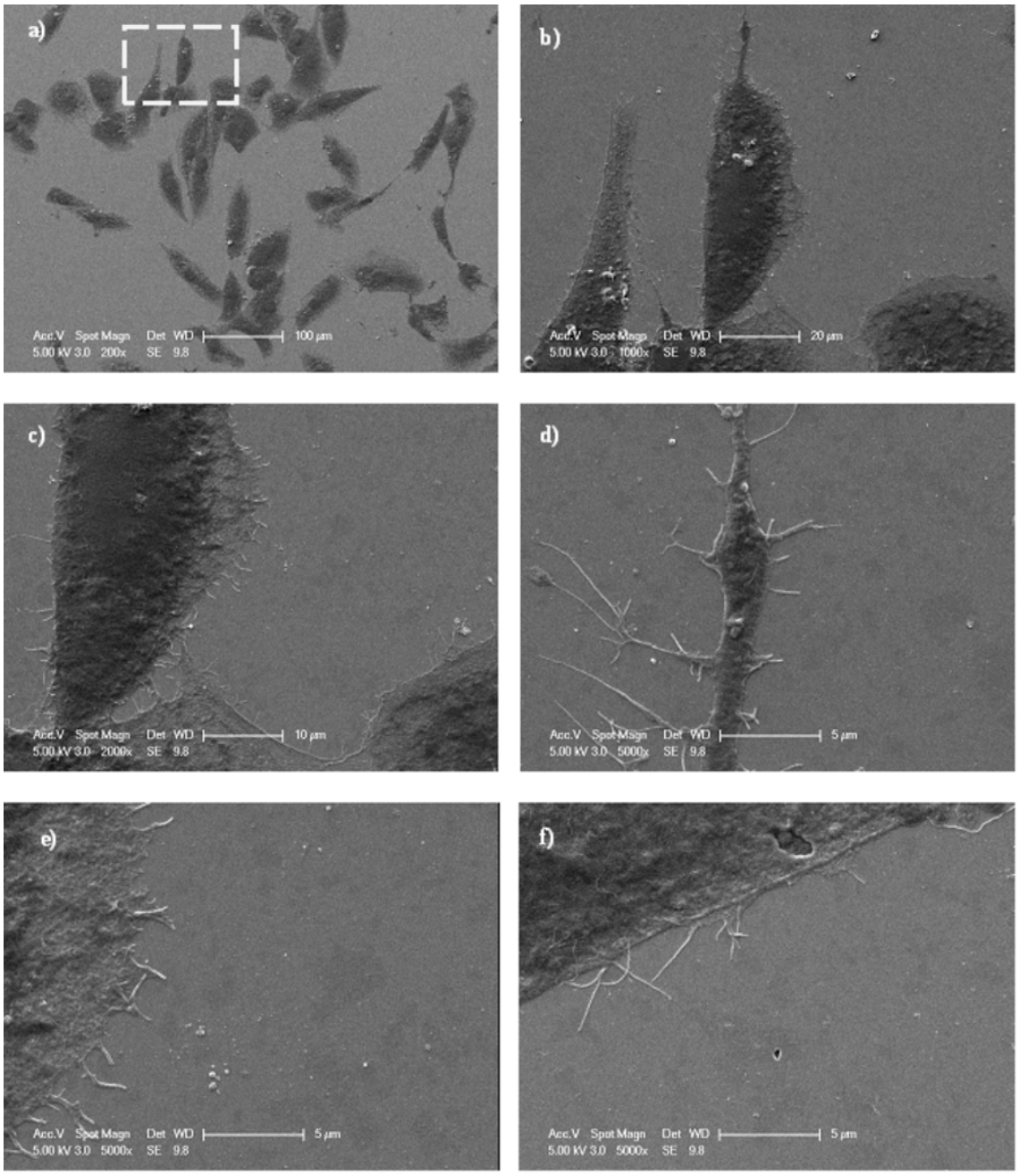


Figure 4.44 SEM images of GO flakes modified on Ti surfaces (a,x200; b,x0100; c,x2000; d,e,f x5000 magnification) after 1st day of cell culture.)

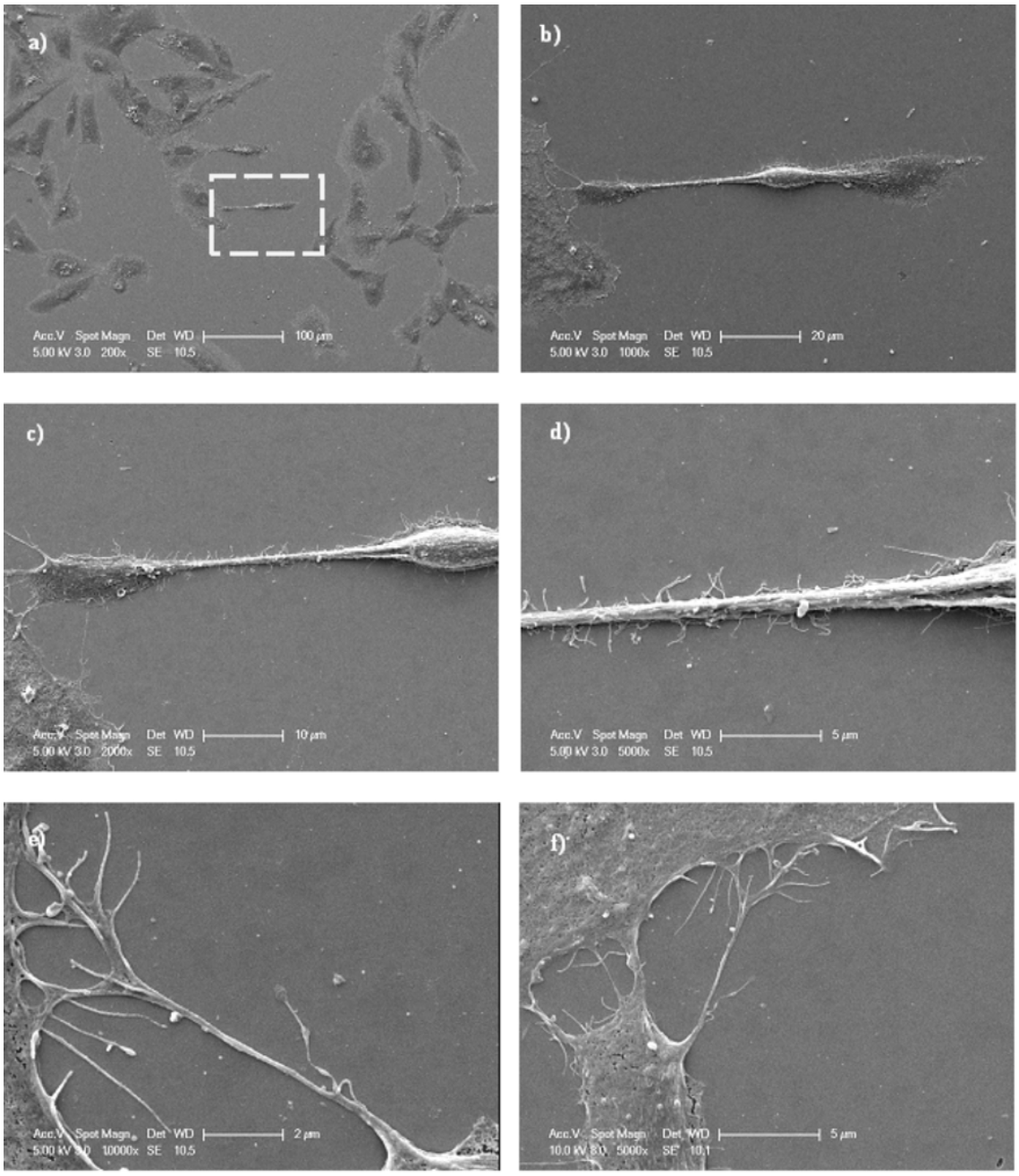


Figure 4.45 SEM images of RGO flakes modified on Ti surfaces (a,x100; b,x1000; c,x2000; d,x5000; e,x10.000; f,x5000 (10kV) magnification) after 1st day of cell culture.

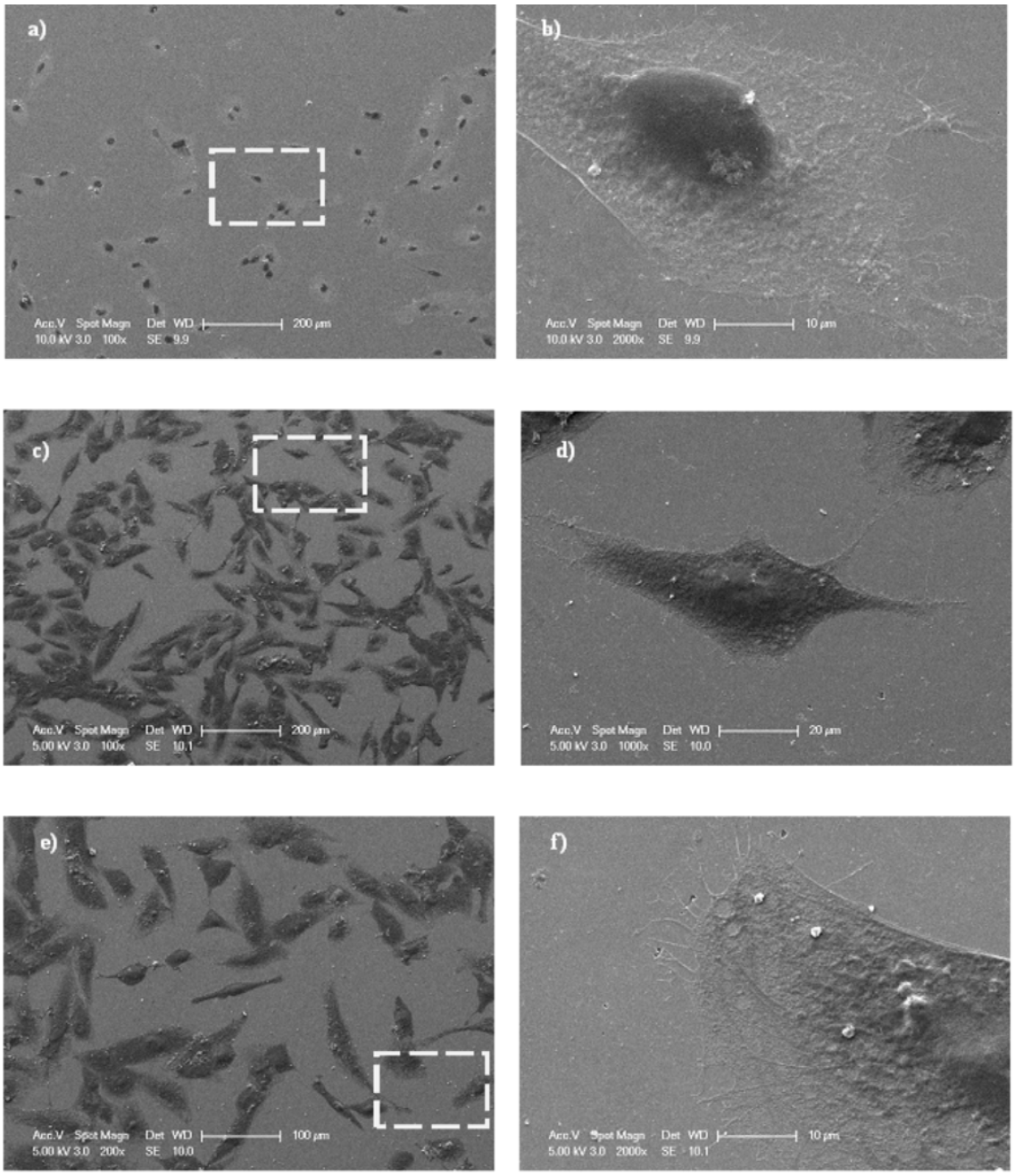


Figure 4.46 SEM images of cell morphologies on Ti (a,x100; b,x2000 magnification), APA/Ti (c,x100; d,x1000 magnification) and GO/Ti (e,x200; f,x2000 magnification) surfaces after 3rd day of culture.

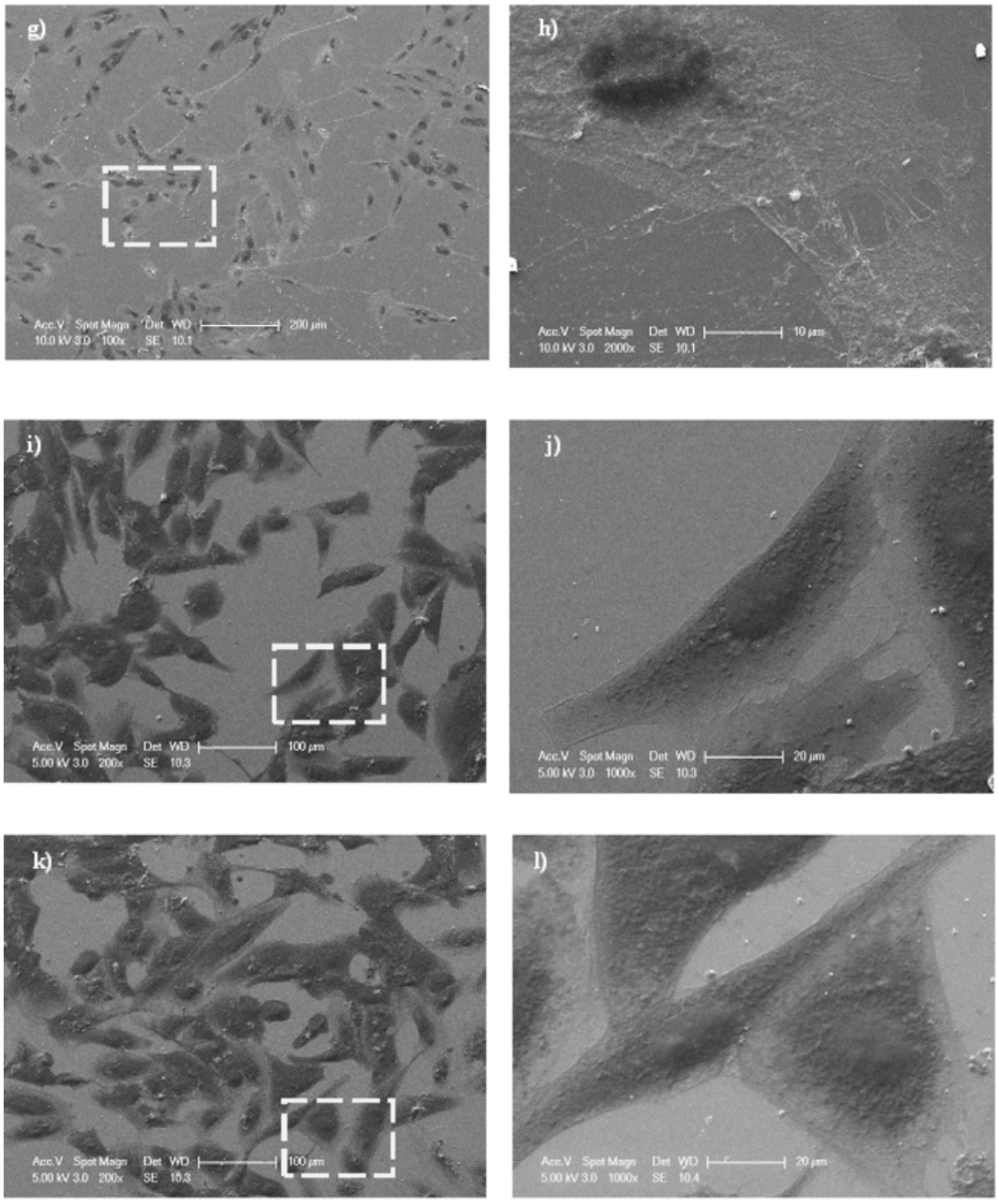


Figure 4.47 SEM images of cell morphologies on RGO/Ti (g,x100; h,x2000 magnification), Fmoc-Ser-OH/RGO/Ti (i,x200; j,x1000 magnification), Fmoc-Leu-OH/RGO/Ti (k,x200; l,x1000 magnification) surfaces after 3rd day of culture.

5. DISCUSSION

Biomaterials play a critical roles in the fields of tissue engineering and regenerative medicine. Upon implantation of material as smart interface, the first interaction can provide an advanced step to create a new tissue surrounding the implant surface. Therefore, functionalization and modification with bioactive molecules on the substrate surface are substantially required to enhance the surface biocompatibility and bioactivity. In this study, GO, RGO and their chemically modified graphene based-surfaces (CMGs) including an outstanding potentials for cell behaviour were deposited on Ti surfaces (Figure 3.1.schematic representation of unmodified and modified Ti surfaces). In order to obtain information about surface chemistry and morphology of unmodified and modified Ti surfaces, common techniques including SEM, AFM, WCAs, XPS and Raman spectroscopy were used before cellular behaviour to these surfaces were investigated.

SEM was used to observe shape and morphology of samples because of rapid, non-invasive and effective imaging technique. Here, we observed GO and RGO flakes on APA/Ti surfaces and Fmoc amino acids modified on RGO/Ti surfaces by using SEM. The lateral width of GO flakes coating APA/Ti surface were clearly shown in Figure 4.2 and Figure 4.3. The self assembly of GO flakes or nanosheets density at surfaces depends on controlling SAM modification of APA molecules on the surface and the ratio of GO density in water and physiological environments. It was observed that APA/Ti surface was covered with a uniform layer of GO flakes. The contrast difference between GO flakes and Ti surface could be clearly distinguished at low accelerating voltage (2kV). We investigated well-distinguished GO flakes on APA/Ti surface after doping Au particles (Figure 4.4). The approximate thickness of GO flakes can be estimated with SEM image color contrast.

As shown in Figure 4.2, Figure 4.3 and Figure 4.5, GO and RGO flakes deposited APA/Ti surfaces were observed to be as transparent features. The chemical reduction

led to changes in GO morphology in addition to chemical structure [37]. The morphology of GO flakes seems thin curtain. It is expected that the morphology of RGO surface can seems strongly folded curtain due to the loss of hydrophilic groups after reduced process [86]. This observation suggested that RGO flakes on APA/Ti surface were overlapped rather than aggregated. Moreover, the planar structure of RGO flakes on APA/Ti surface after chemical reduction was observed to be able to the maintain of successful modification. The morphology and structure of surfaces were investigated by using SEM and shown in Figure 4.6 and Figure 4.7 after RGO/Ti surface modified with Fmoc amino acids.

For more detailed structural information, Atomic force microscopy (AFM) topographic image and magnification of RGO on APA/Ti surface are shown in Fig.4.8 and Figure 4.9, respectively. AFM is the most alternative way to identify thickness of graphene and graphene derivatives [41, 86]. The tapping or contact mode AFM was used to scan 5x5 μm^2 area.The lateral width and thickness were found as 0,667 μm, 2.828 nm and 0.481μm, 1.669 nm ,respectively before modification of Fmoc amino acids. The overlapped RGO flakes on APA/Ti were clearly observed in the AFM images.

Water contact angle (WCAs) measurements for bare, activated Ti and modified Ti surfaces were carried out by using contact angle device (CAM 100,USA). Meanwhile plasma treatment controls the hydrophilicity of the surface to enhance adhesion for easily modification of functional groups [89]. After plasma treatment of Ti coating glass, WCA value dramatically decreased from 71.85° ± 2.76° to 0° which was not measured due to the abundant hydroxyl groups on Ti surface (Fig.4.10) [65, 90]. Self-assembled monolayers of APA molecules modified on Ti surface to generate amine (-NH_2) groups [63, 65]. GO flakes were immobilized on APA/Ti surface. WCAs of APA/Ti and GO/Ti were calculated to be 33.45° ± 3.3° and 21.1° ± 4.3°, respectively [65, 91]. It was found that GO coating APA/Ti surface was more hydrophilic than APA modified Ti surface due to the presence of the oxygen functionalities such as epoxy, carbonly, carboxyl and hydroxyl groups. After process of chemically reduced GO modified APA/Ti surface, WCA value of surface was increased from 21.1 ° ± 4.3° to 69.96 ° ± 0.1° because of the removal of oxygen-containing functional groups (Fig.4.11)

[41, 91]. To obtain more successful cell interaction on nanocomposite surface, adsorption of Fmoc amino acids with increasing dipping times (2h-24h) was investigated by using WCA measurement system. It was know that Fmoc aromatic groups were shown to be effective molecular gelators [57, 58, 59, 61]. As shown in Table 4.3, WCAs of Fmoc-Leu-OH on RGO/Ti surface range from 75.91° ± 3.51° to 55.57° ± 4.17° for different dipping times (2h-24h). For adsorption of Fmoc-Ser-OH on RGO/Ti surface, water contact angles gradually measured from 63.58 ° ± 2.33° to 30.24° ± 3.17° for different time intervals (2h-24h) and presented in Table 4.4. To provide successful orientation or monolayer of Fmoc amino acids on surfaces, dipping time was limited to be as 24h. As can be seen in Figure 4.12 and Figure 4.13, Fmoc-Ser-OH amino acids formed more hydrophilic area than Fmoc-Leu-OH amino acids after modification of Fmoc amino acids. The supervision of increasing dipping times suggested that the successful displacement of Fmoc amino acids was consistent with the water contact angle results. The graphene tends to protect properties of the natural structure. Therefore, compared with covalent functionalization, the noncovalent interactions such as $\pi - \pi$ and hydrophobic interactions are preferred by biomolecules and carbon family such as carbon nanotube, graphene etc. [60]. As a consequence of this natural selection, RGO coating surface easily modified with aromatic fluorenyl rings of Fmoc amino acids. The remarkable decrease in contact angle was assigned to the upgrade hydrophilicity of the surfaces as a consequence of the carboxylic acid and hydroxyl group of the successful adsorbed Fmoc amino acids on reduced graphene (Figure 4.14).

To get more reliable results, the chemical analysis of Ti surfaces prior and after the modifications were investigated by using X-rays Photoelectron Spectroscopy (XPS). As seen from Fig.4.15 and Fig.4.16, the C1s,O1s, Ti2p and N1s levels of Ti and APA /Ti surface could be noticeable. The XPS survey show that the O1s and Ti2p levels decreased and C1s level increased due to the modification of APA molecules on Ti surface. Figure 4.15 demonstrated that the high intensity of N1s signal also exhibited significant changes after modification of APA on Ti because of effect of the NH_2 "tailgroup". Table.4.5 summarized the percentages of C1s, O1s, P2p and N1s peaks arising from APA molecules ($H_2N(CH_2)_3P(O)(OH)_2$).The deconvolution of O1s peaks was presented in Figure 4.17 and Table 4.6. The possible binding energies at

the O1s region was resolved into three contributions due to oxide at around 529-530 eV, hydroxide at around 531.5 eV, and phosphate at about 530-532 eV [92], [72]. The expected interactions of APA molecules on the Ti surface [73] was shown in terms of the formations of covalent Ti, P-O-Ti/P=O [74, 75] and P-OH [74, 72] bonds that assigned at the binding energies of 529.96 eV, 531 eV and 531.98 eV. The fitting of the P2p exhibited three peaks at 132.94 eV, 133.91 eV and 138.57 eV in Figure 4.18. The P2p3/2 and P2p1/2 peaks was represented to be at 132.94 eV, 133.91 eV due to the presence of phosphate and oxygen bindings. The peak at 138.57 eV is unknown [76, 77].

GO sheets were easily immobilized on APA/Ti owing to S_N2 nucleophilic reactions between the epoxy groups of the surface of GO and the amine groups of APA [35] In XPS survey in Fig.4.19, the atomic percentages of C1s, O1s, Ti2p, P2p and N1s were detected to be as approximately 41.83%, 41.56%, 9.62%, 1.95% and 1.91%. The C1s region of GO shows possible functional groups including aromatic C=C and aliphatic C-C; hydroxyl carbon C-OH; epoxy carbon C-O; carboxyl carbon O=C-OH [41]. In the deconvoluted C1s spectra in the Fig.4.20, the peak centered at 284.25 eV was assigned to the C-C bonds. Moreover, a peak emerges at 283.57 eV which could be contributed by the chemical bonding between titanium and carbon or sp2 peak [78], [79]. The other peaks appeared at 286,03 eV, 286,51 eV and 288,1 eV which were assigned to C-O/O-C-O, C-OH and C=O, respectively [41, 80]. Table 4.8 has shown that atomic percentages of C1s bonds were found to be as 47.17%, 18.15%, 14.58%, 10.89% and 9.21% assigned to C-C, C-OH, C-O/O-C-O, C-Ti/C=C and C=O bonds, respectively. GO flakes on APA/Ti chemically reduced by using the hydrazine monohydrate and XPS survey was indicated in Figure 4.21. Elemental analysis measurements were observed in Table 4.7 and Table 4.9 to describe C/O ratio of both GO/Ti and RGO/Ti. The XPS survey has shown that the elemental composition including C1s, O1s, Ti2p, P2p and N1s that were detected to be as approximately 61.08%, 24%, 5.93%, 1.83% and 4.22%, respectively. Herein, the increment in level of N1s and the decrement in level of oxygen atoms emerged because of chemical reduction process in Figure 4.20. It was clearly shown that five peaks appeared after chemically RGO/Ti. The deconvolution of C1s spectra of RGO incorporated APA/Ti surface was appeared at 283.98 eV,

284.7 eV, 285.82 eV, 286.73 eV and 289.26 eV [78, 79, 41, 48, 80] which were assigned to C-Ti/C=C, C-C, C-O/C-N, C-OH and O=C-OH peaks, respectively and was shown in the Figure 4.22 and Table 4.10.

The adsorption of Fmoc conjugated amino acids on RGO/Ti surface with the $\pi - \pi$ stacking interaction were investigated by using XPS and exhibited in Figure 4.23 and Figure 4.25. For modification of Fmoc-Leu-OH ($C_{21}H_{23}NO_4$) and Fmoc-Ser-OH ($C_{18}H_{17}NO_5$) amino acids, the reaction conditions such as applying an excess concentration and reaction time were specified in this study. The elementary composition of surface layers with depths of about 8-10 nm was determined by using XPS. It is known that chemical shifts in spectra permit polar bonds to be ascertained. In order to assess the degree of modification of amino acids, the elemental information was summarized in Table 4.11 and Table 4.13, respectively. The atomic percentages of C1s, O1s, Ti2p and N1s for Fmoc-Leu-OH/RGO/Ti were measured to be as 59.74%, 29.71%, 5.16% and 4.09% [81]. There may be formed in gel form such as surfactants. The atomic percentages of C1s, O1s, Ti2p, P2p and N1s for Fmoc-Ser-OH/RGO/Ti were detected to be as 48.24%, 36.18%, 6.95%, 1.77% and 3.72%, respectively. The formation of Fmoc-Leu-OH on RGO/Ti was confirmed with the increase of carboxyl group (O=C-OH) and the presence of amine bond (C-N) and was shown in Figure 4.24 [80, 81, 93]. Further evidence of the adsorption of Fmoc-Ser-OH amino acids was obtained by high-resolution XPS spectra of carbon peaks (C1s) indicating amide (O=C-NH) and hydroxyl (C-OH) bonds (Figure 4.26) [80, 82]. It was clearly shown that the $\pi - \pi$ stacking interaction appeared for the adsorption of Fmoc conjugated amino acids on RGO/Ti surface. The literature binding energy for the $\pi - \pi$ peak ranges from 290 eV to 292 eV because of the π electrons of the aromatic ring [68, 94]. As shown the deconvoluted C1s peaks of Fmoc-Leu-OH and Fmoc-Ser-OH in Fig.4.24 and Fig.4.26, a peak was emerged at 292.04 eV and 290.56 eV, the corresponding to $\pi - \pi$ interaction [95, 96]. Also, peak at 290.56 eV can be O=C-OH bond [97].

Raman spectroscopy is a well-known non-destructive method based on inelastic scattering of monochromatic light. The unmodified and modified Ti surfaces were further investigated by using Raman spectroscopy. As it is seen in Fig.4.27. Raman

spectra of TiO_2 coated glass was investigated. The peaks at about 606 cm^{-1}, 418 cm^{-1}, and 283 cm^{-1} were observed [83, 84, 85]. The evidence of GO coating Ti surface was also shown by aid of raman spectroscopy measurement. Raman spectra of GO/Ti, shown in Figure 4.28, appeared two prominent peaks at around 1351 cm^{-1} and 1575 cm^{-1} corresponding to the D (mode of κ-point photons of A1g symmetry) and G peaks (the E2g mode of sp2 carbon atoms), respectively. As mentioned in the literature, the G band is appeared due to the vibration of sp2 bonded carbon, whereas the D band is induced by disordered structure or the breakdown of translational symmetry [86, 87]

Raman spectroscopy was performed to verify the chemical reaction onto GO/Ti surface which was shown in Figure 4.29. The chemical reduction would give rise to the change of surface chemistry and nanostructure in GO coating substrate [37]. In the Raman spectra of RGO/Ti surface, the G peak was downshifted from 1575 cm^{-1} to 1571 cm^{-1} and the D peaks was shifted to 1346 cm^{-1}. The Id/Ig ratio was slightly increased from 1 to 1.03. The slight increase may be related to the removal of the functional groups upon reduction and the subsequent creation of defects [86, 87].

The binding ability of Fmoc amino acids on RGO/Ti surface were further investigated using Raman spectroscopy. Upon functionalization of Fmoc-Ser-OH amino acids on RGO/Ti surface, the both of G-band peak and D-band peak were observed. The D band was found to be as 1583 cm^{-1}. The G band was measured to be as 1346 cm^{-1}. Choi et al. reported that G peak was increased for noncovalent functionalization of reduced graphene in benzene [98]. The surface functionalization of RGO/Ti surface was confirmed by the shift of one characteristic peaks and the change of Id/Ig ratio. After modification of Fmoc-Leu-OH amino acids, D and G peaks of RGO/Ti at around 1346 cm^{-1} and 1575 cm^{-1} were measured. As mentioned in the literature [96, 99, 100]. The D peak increased and the Id/Ig intensity ratio decreased.

The $\pi - \pi$ stacking interaction between RGO/Ti and Fmoc conjugated amino acids was evaluated by raman spectroscopy to be as complementary characterization technique. WCA, XPS and Raman Spectroscopy results suggested that adsorption of Fmoc amino acids was successfully carried out.

The physico-chemical changes of substrate surface such as chemistry, morphology and energy influence the adsorption of proteins and cellular responses on the implant [11, 13]. In this study, the effects of unmodified and modified graphene based materials on cellular adhesion, proliferation and morphology were focused. The MTT and Alamar Blue Assay were applied to investigate and control the osteoblast cell behavior on modified Ti surfaces and TCPS. Cell viability was evaluated by using MTT assay after culturing 1st, 3rd and 5th days, respectively. After 1st day of culture, the results of MTT assay contributed to evaluate the early cell attachment on all experimental groups. Also, the results of MTT assay could be used to estimate the cell growth and proliferation at 3rd and 5th days according to chosen control group.

At 1st, 3rd and 5th days, the change of MTT results arising from surface functional groups and morphology was shown in Figure 4.34. Activated Ti surface was chosen as control group. Hydroxyl (-OH) functional groups of activated Ti surface exhibits neutral and hydrophilic properties on Ti surface. Amine group (-NH_2) functionality of APA forms a positive charge on Ti surface. Previous studies shown that amine groups promoted proliferation for several cells (myoblast, endothelial and osteoblast) [101, 102]. Herein, Increase in viable cell number was observed after modification of APA molecules on Ti surface. However, the MTT results difference were not statistically significant on 1st and 3rd days compare to Ti control group (Figure 4.31 and Figure 4.32). APA molecules on Ti led to increase in viable cell number after 5th day of incubation and statistically significant with respect to Ti control group (Figure 4.33).

The excellent cell viability of GO deposited APA/Ti surfaces was derived from the presence of the oxygen functionalities (hydroxyl (-OH) and epoxy groups on the surface and carboxyl (-COOH) groups at the edges) and effect of a flat monolayer of carbon structure [103, 104]. The MTT results have suggested that negatively charged surfaces of GO accelerated osteoblast cell-biomaterial interactions compare to Ti control group and APA/Ti. As seen in Figure 4.34, the number of cell viability on RGO/Ti surface was more less than GO/Ti but the increment in the number of viable cells on RGO/Ti was observed compare to Ti control group for all culture periods despite of its surface chemistry with poor hydrophilicity. It is evident that not only hydrophilicity

but also carbon structure of two dimensional graphene derivatives substantially affect cell behaviour. The results displayed that difference of viable cell number ratio between GO/Ti and RGO/Ti was not statistically significant for 1st and 5th days.

The first response is certainly the most critical issue for creating a new tissue surrounding the implant surface. It is determined that adhesion of osteoblast is a major step to subsequent cell functions such as adhesion, proliferation etc [11, 46, 47]. It is well-known that the conformation of adhesive proteins is changed by effect of the hydrophobic surface where limits the acceleration of cell adhesion [17]. Keselowsky et al. reported that surfaces modified differently chargeable functional groups, which was arranged impact levels to be as hydroxyl $>$ carboxyl $=$ amino $>$ methyl, influenced adhesion of MC3T3-E1 [105]. Therefore, hyrophilic areas of designed material surfaces were effectuated by using GO and Fmoc amino acids, respectively. Fmoc amino acids having different the hydropathy indexes were chosen to investigate initial cell behaviour on substrate surfaces. MTT results shown that the Fmoc-Ser-OH was more effective amino acid to increase the viability of osteoblast cells due to its chemical properties. (Figure 4.34). Also, there were no significant differences between Fmoc-Ser-OH/RGO/Ti and GO/Ti at 1st, 3rd and 5th days ($p < 0.05$). However, there were the highest cell viability on Fmoc-amino acids/RGO/Ti compare to control group and other experimental groups.

Alamar Blue (AB) assay was used to figure out impacts of surface modification on cell proliferation. It is a non-destructive assay which based on detection of metabolic activity of the osteoblast cells. After osteoblast cells were seeded and cultured on unmodified, modified and TCPS for 1st, 3rd and 5th days, AB assay was applied. In order to display cell proliferation ratios at all culture periods, negative and positive control groups corresponding to nonseeded wells and Ti surface were used. At 1st day, the early cell response on designed substrate surface was clearly indicated (Figure 4.35 and Figure 4.36). All AB results showed that the similar trend of cell proliferation at 3rd and 5th days was observed as the first day. The percentages of AB reduction, showed in Fig.4.41, increased from 1st day and 5th day for all groups except to Ti group which caused nearly cell proliferation rate at 3rd and 5 th days. This setup gave

preliminary information about cell proliferation.

The percent difference in AB reduction was shown in Fig.4.42. Especially, the cell proliferation rates on the different experimental groups were the highest values at 1st day in comparison to other culture time (Figure 4.36). A significant increase in basic data of cell studies for Ti were observed from 1st day to 3rd day. It was observed that basic data of cell studies for Ti in the third and fifth days had almost the same value while increasing cell proliferation on other experimental groups continued. Therefore, percent difference in AB reduction increased at 1st day and decreased at 3rd day, then again increased 5th day ($p < 0.05$). Moreover, the trend between experimental groups was not changed at 1st, 3rd and 5th days. As a result of these, early cell proliferation could be improved by using graphene derivatives and biomolecules and also cell viability was protected during experimental procedures.

According to AB results on 1st and 3rd day shown in Figure 4.36 and Figure 4.38, Fmoc-Ser-OH amino acids on RGO/Ti have significantly higher amount of proliferating cells compared to all experimental groups ($p < 0.05$). There was a significant difference between Fmoc-Ser-OH/RGO/Ti and GO/Ti but no significant difference between RGO/Ti and GO/Ti surfaces ($p < 0.05$). Moreover, the adsorption of Fmoc-Leu-OH amino acids on RGO/Ti had a positive effect on cell proliferation when compared with effect of RGO/Ti, GO/Ti APA/Ti, Ti surfaces but no statistical difference from these groups. At 5th day, the cell proliferation rates on Fmoc-Ser-OH/RGO/Ti surface were the highest values in comparison to all experimental group (except to TCPS) and statistically significant result. Furthermore, cell proliferation on GO/Ti and Fmoc-Leu-OH/RGO/Ti had a significant difference when compared with RGO/Ti. (Figure 4.40).

The overall MTT results indicated that the percentage of live cells augment with increasing culture incubation period compare to Ti control group. Alamar Blue results appeared to be consistent with the MTT results according to effects of substrates on cell behavior. The quantitative cell proliferation results and were also proved by using SEM.

SEM images of osteoblast cells cultured on unmodified and modified Ti surfaces demonstrated that cells adhered to these surfaces exhibited the response of cellular components (filopodia and lamellipodia). Previous studies show that adhesion of cells to substrate is based on the physico-chemical surface properties such as the surface chemistry, charge, hydrophilicity and surface morphology [11, 101]. In order to promote the initial cell attachment with subsequent cell spreading and proliferation, the presence of surface chemistry is a critical factor. After being cultured for 24h, the development of filopodia presented on Ti and APA/Ti surfaces where ruffles and lamellipodia was not observed. Fig.4.43 (a, b, c; d, e) [106]. The protrusion of actin-rich structures are commonly called as lamellipodium [107]. Figure 4.44 indicated that less distinct lamellipodia spread with protruding filopodia because of influences of a flat monolayer of carbon atoms and the negatively charged GO coating Ti surface and the change of surface properties thus provided acceleration of osteoblast cell attachment and spreading. Osteoblast cells did not clearly present lamellipodia on RGO/Ti surface owing to the decrease of oxygen-containing functional groups Fig.4.43 (j,k,l).

The $\pi - \pi$ stacking interaction occurs between RGO coating Ti surface and aromatic residues of Fmoc amino acids to increase biocompatibility of RGO/Ti surfaces. The physico-chemical surface properties influenced the adhesion and extension of filopodia and lamellipodia. Results proved that the effects of Fmoc-Ser-OH and Fmoc-Leu-OH having different the hydropathy indexes enhanced the initial cellular adhesion. The effects of the hydrophobic or hydrophilic properties of side chains of amino acids significantly showed different results at the cell-biomaterial interface after modification of Fmoc amino acids. Figure.4.43 (m, n, o; p, q, r) demonstrated that the actin-rich lamellipodium spread on Fmoc-Leu-OH/RGO/Ti where displayed short filopodia growing from lamellipodia. The well-developed lamellipodia highly extended on Fmoc-Ser-OH/RGO/Ti Fig.4.43 (s, t, u; v, w, x). On the first day of culture, the effects of Fmoc amino acids were considered as a leading factor to promote cell adhesion and proliferation because of accelerated lamellipodia formation and cell spreading on substrate surface.

SEM images (Fig.4.44, Fig.4.45) at voltage (5kV) have shown graphene oxide derivatives coating surfaces after being cultured for 1st day. In addition to cell maturation and progression, GO and RGO flakes on these surfaces were clearly indicated. Cell morphology and adhesion were evaluated for 3rd day. The SEM images in Fig.4.46 and Fig.4.47 illustrated cell attachment on unmodified and modified Ti surfaces after being incubated for 3rd day. According to time-dependent lamellipodia and filopodia formation, osteoblast cell morphologies on the modified Ti surfaces displayed significantly cell attachment and spreading with large lamellipodia extensions compare to unmodified Ti surfaces where cells appeared filopodia and lamellipodia extensions. The in vitro studies supported that cell responses could be influenced by the presence of nanometric surface roughness and surface chemistry.

5.1 Future Studies

In this study, the results of characterization and cell studies supported that designed materials and methodology are promising for bone tissue engineering. In further studies, antimicrobial activity will be assessed and modification of several Fmoc amino acids on graphene based materials will be investigated to figure out different surface properties and subsequently their effects on cell behaviour. The impacts of interface changes will be also applied in stem cell research.

REFERENCES

1. Zhu, Y., S. Murali, W. Cai, X. Li, J. W. Suk, J. R. Potts, and R. S. Ruoff, "Graphene and graphene oxide: Synthesis, properties, and applications," *Advanced Materials*, Vol. 22, no. 35, pp. 3906–3924, 2010.

2. Chung, C., Y.-k. Kim, D. Shin, S.-r. Ryoo, B. H. E. E. Hong, and D.-h. Min, "Biomedical application of graphene and graphene oxide," *Accounts of Chemical Research*, Vol. 46, no. 10, pp. 2211–2224, 2013.

3. Zhang, Y., T. R. Nayak, H. Hong, and W. Cai, "Graphene: a versatile nanoplatform for biomedical applications," *Nanoscale*, Vol. 4, no. 13, p. 3833, 2012.

4. Bressan, E., L. Ferroni, C. Gardin, L. Sbricoli, L. Gobbato, F. Ludovichetti, I. Tocco, A. Carraro, A. Piattelli, and B. Zavan, "Graphene based scaffolds effects on stem cells commitment," *Journal of Translational Medicine*, Vol. 12, no. 1, p. 296, 2014.

5. Nebe, J. G. B., F. Luethen, R. Lange, and U. Beck, "Interface interactions of osteoblasts with structured titanium and the correlation between physicochemical characteristics and cell biological parameters," *Macromolecular Bioscience*, Vol. 7, no. 5, pp. 567–578, 2007.

6. Lincks, J., B. D. Boyan, C. R. Blanchard, C. H. Lohmann, Y. Liu, D. L. Cochran, D. D. Dean, and Z. Schwartz, "Response of mg63 osteoblast-like cells to titanium and titanium alloy is dependent on surface roughness and composition," *Biomaterials*, Vol. 19, pp. 2219–2232, 1998.

7. Albrektsson, T., and C. Johansson, "Osseointegration, osteoconduction, osteoinduction," *Europen Spine Journal*, Vol. 10, no. 2, pp. 96–101, 2001.

8. Georgakilas, V., M. Otyepka, A. B. Bourlinos, V. Chandra, N. Kim, K. C. Kemp, P. Hobza, R. Zboril, and K. S. Kim, "Functionalization of graphene: Covalent and noncovalent approaches, derivatives and applications," *Chemical Reviews*, Vol. 112, no. 11, pp. 6156–6214, 2012.

9. Wang, Y., Z. Zhang, L. Xu, X. Li, and H. Chen, "Hydrogels of halogenated fmoc-short peptides for potential application in tissue engineering," *Colloids and Surfaces B : Biointerfaces*, Vol. 104, pp. 163–168, 2013.

10. Adhikari, B., and A. Banerjee, "Short peptide based hydrogels : incorporation of graphene into the hydrogel," *Soft Matter*, Vol. 7, no. 19, p. 9259, 2011.

11. O'Brien, F. J., "Biomaterials scaffolds for tissue engineering," *Materials Today*, Vol. 14, no. 3, pp. 88–95, 2011.

12. Bauer, S., P. Schmuki, K. von der Mark, and J. Park, "Engineering biocompatible implant surfaces. part i: Materials and surfaces," *Progress in Materials Science*, Vol. 58, no. 3, pp. 261–326, 2012.

13. Dohan Ehrenfest, D. M., P. G. Coelho, B. S. Kang, Y. T. Sul, and T. Albrektsson, "Classification of osseointegrated implant surfaces: Materials, chemistry and topography," *Trends in Biotechnology*, Vol. 28, no. 4, pp. 198–206, 2010.

14. Chen, Q., and G. A. Thouas, "Metallic implant biomaterials," *Materials Science and Engineering: R: Reports*, Vol. 87, pp. 1–57, 2015.

15. Sul, Y.-t., C. B. Johansson, S. Petronis, A. Krozer, A. Wennerberg, and T. Albrektsson, "Characteristics of the surface oxides on turned and electrochemically oxidized pure titanium implants up to dielectric breakdown : the oxide thickness , micropore configurations , surface roughness , crystal structure and chemical composition," *Biomaterials*, Vol. 23, pp. 491–501, 2002.

16. Yang, Y., J. Tian, L. Deng, and J. L. Ong, "Morphological behavior of osteoblast-like cells on surface-modified titanium in vitro," *Biomaterials*, Vol. 23, no. 5, pp. 1383–1389, 2002.

17. Ku, Y., C. P. Chung, and J. H. Jang, "The effect of the surface modification of titanium using a recombinant fragment of fibronectin and vitronectin on cell behavior," *Biomaterials*, Vol. 26, no. 25, pp. 5153–5157, 2005.

18. Pittrof, A., S. Bauer, and P. Schmuki, "Micropatterned tio2 nanotube surfaces for site-selective nucleation of hydroxyapatite from simulated body fluid," *Biomaterials*, Vol. 7, no. 1, pp. 424–431, 2011.

19. Pittrof, A., S. Bauer, and P. Schmuki, "Evaluating mechanical adhesion of sol-gel titanium dioxide coatings containing calcium phosphate for metal implant application.," *Biomaterials*, Vol. 21, no. 21, pp. 2193–2201, 2000.

20. Bsat, S., S. Yavari, M. Munsch, E. Valstar, and A. Zadpoor, "Effect of alkali-acid-heat chemical surface treatment on electron beam melted porous titanium and its apatite forming ability.," *Materials*, Vol. 8, no. 4, pp. 1612–1625, 2015.

21. Khor, K. A., Y. W. Gu, D. Pan, and P. Cheang, "Microstructure and mechanical properties of plasma sprayed ha/ysz/ti-6al-4v composite coatings," *Biomaterials*, Vol. 25, no. 18, pp. 4009–4017, 2004.

22. Ajami, E., and K.-F. Aguey-Zinsou, "Functionalization of electropolished titanium surfaces with silane-based self-assembled monolayers and their application in drug delivery," *Journal of Colloid and Interface Science*, Vol. 385, no. 1, pp. 258–267, 2012.

23. Ulman, A., "Formation and structure of self-assembled monolayers," *Chemical Reviews*, Vol. 96, no. 4, pp. 1533–1554, 1996.

24. Haensch, C., S. Hoeppener, and U. S. Schubert, "Chemical modification of self-assembled silane based monolayers by surface reactions.," *Chemical Society Reviews*, Vol. 39, no. 6, pp. 2323–2334, 2010.

25. Paz, Y., "Self-assembled monolayers and titanium dioxide: From surface patterning to potential applications," *Beilstein Journal of Nanotechnology*, Vol. 2, no. 1, pp. 845–861, 2011.

26. Faucheux, N., R. Schweiss, K. Lutzow, C. Werner, and T. Groth, "Self-assembled monolayers with different terminating groups as model substrates for cell adhesion studies," *Biomaterials*, Vol. 25, no. 14, pp. 2721–2730, 2004.

27. Cai, K., M. Frant, J. Bossert, G. Hildebrand, K. Liefeith, and K. D. Jandt, "Surface functionalized titanium thin films: Zeta-potential, protein adsorption and cell proliferation," *Colloids and Surfaces B: Biointerfaces*, Vol. 50, no. 1, pp. 1–8, 2006.

28. Mazzocchetti, L., T. Tsoufis, P. Rudolf, and K. Loos, "Enzymatic synthesis of amylose brushes revisited: Details from x-ray photoelectron spectroscopy and spectroscopic ellipsometry," *Macromolecular Bioscience*, Vol. 14, no. 2, pp. 186–194, 2014.

29. Aissaoui, N., L. Bergaoui, J. Landoulsi, J. F. Lambert, and S. Boujday, "Silane layers on silicon surfaces: mechanism of interaction, stability, and influence on protein adsorption," *Langmuir*, Vol. 28, no. 1, pp. 656–665, 2012.

30. Badley, E. M., J. Chatt, and R. L. Richards, "Isonitrile complexes of platinum(ii) and their reactions with alcohols and amines to give carbene complexes," *J. Chem. Soc. A*, pp. 21–25, 1971.

31. Zoulalian, V., S. Monge, S. Zurcher, M. Textor, J. J. Robin, and S. Tosatti, "Functionalization of titanium oxide surfaces by means of poly (alkyl-phosphonates)," *Journal of Physical Chemistry B*, Vol. 110, no. 51, pp. 25603–25605, 2006.

32. Silverman, B. M., K. a. Wieghaus, and J. Schwartz, "Comparative properties of siloxane vs phosphonate monolayers on a key titanium alloy," *Langmuir*, Vol. 21, pp. 225–228, 2005.

33. Gawalt, E. S., M. J. Avaltroni, N. Koch, and J. Schwartz, "Self-assembly and bonding of alkanephosphonic acids on the native oxide surface of titanium," *Langmuir*, Vol. 17, no. 19, pp. 5736–5738, 2001.

34. Dubey, M., T. Weidner, L. J. Gamble, and D. G. Castner, "Structure and order of phosphonic acid-based self-assembled monolayers on si(100)," *Langmuir*, Vol. 26, no. 18, pp. 14747–14754, 2010.

35. Dreyer, D. R., S. Park, C. W. Bielawski, and R. S. Ruoff, "The chemistry of graphene oxide.," *Chemical Society Reviews*, Vol. 39, no. 1, pp. 228–240, 2010.

36. Some, S., Y. Kim, Y. Yoon, H. Yoo, S. Lee, Y. Park, and H. Lee, "The chemistry of graphene oxide.," *Scientific Reports*, Vol. 3, no. 1, p. 1929, 2013.

37. Pei, S., and H. M. Cheng, "The reduction of graphene oxide.," *Carbon*, Vol. 50, no. 9, pp. 3210–3228, 2012.

38. Bai, S., and X. Shen, "Graphene inorganic nanocomposite," *RSC Advances*, Vol. 2, no. 1, p. 64, 2012.

39. Nayak, T. R., H. Andersen, V. S. Makam, C. Khaw, S. Bae, X. Xu, P. L. R. Ee, J. H. Ahn, B. H. Hong, G. Pastorin, and B. Ozyilmaz, "Graphene for controlled and accelerated osteogenic differentiation of human mesenchymal stem cells," *ACS Nano*, Vol. 5, no. 6, pp. 4670–4678, 2011.

40. Gao, J., K. Shen, F. Bao, J. Yin, D. Wang, R. Ma, C. Yan, T. Chen, G. Wang, X. Liu, X. Zhang, and D. Zhang, "Preparation and characterization of a graphene oxide film modified by the covalent attachment of polysiloxane," *Polymer-Plastics Technology and Engineering*, Vol. 52, no. 6, pp. 553–557, 2013.

41. Ku, S. H., and C. B. Park, "Myoblast differentiation on graphene oxide.," *Biomaterials*, Vol. 34, pp. 2017–2023, 2013.

42. Mittal, V., "Functional polymer nanocomposites with graphene : A review.," *Macromolecular Materials and Engineering*, Vol. 299, no. 8, pp. 906–931, 2014.

43. Ryoo, S. R., Y. K. Kim, M. H. Kim, and D. H. Min, "Behaviors of nih-3t3 fibroblasts on graphene/ carbon nanotubes : Proliferation, focal adhesion, and gene transfection studies.," *American Chemical Society*, Vol. 4, no. 11, pp. 6587–6598, 2010.

44. Lee, W. C., C. H. Y. X. Lim, H. Shi, L. Tang, Y. Wang, C. T. Lim, and K. P. Loh, "Origin of enhanced stem cell growth and differentiation on graphene and graphene oxide," *ACS Nano*, Vol. 5, no. 9, pp. 7334–7341, 2011.

45. Park, S. Y., J. Park, S. H. Sim, M. G. Sung, K. S. Kim, B. H. Hong, and S. Hong, "Enhanced differentiation of human neural stem cells into neurons on graphene," *Advanced Materials*, Vol. 23, no. 36, pp. 263–267, 2011.

46. Kalbacova, M., A. Broz, J. Kong, and M. Kalbac, "Graphene substrates promote adherence of human osteoblasts and mesenchymal stromal cells," *Carbon*, Vol. 48, no. 15, pp. 4323–4329, 2010.

47. Biris, A. R., M. Mahmood, M. D. Lazar, E. Dervishi, F. Watanabe, T. Mustafa, G. Baciut, M. Baciut, S. Bran, S. Ali, and A. S. Biris, "Novel multicomponent and biocompatible nanocomposite materials based on few-layer graphenes synthesized on a gold/hydroxyapatite catalytic system with applications in bone regeneration," *Journal of Physical Chemistry C*, Vol. 115, no. 39, pp. 18967–18976, 2011.

48. Chen, G.-Y., D. W.-P. Pang, S.-M. Hwang, H.-Y. Tuan, and Y.-C. Hu, "A graphene - based platform for induced pluripotent stem cells culture and differentiation," *Biomaterials*, Vol. 33, no. 2, pp. 418–427, 2012.

49. Lee, W. C., C. H. Lim, Kenry, C. Su, K. P. Loh, and C. T. Lim, "Cell-assembled graphene biocomposite for enhanced chondrogenic differentiation," *Small*, Vol. 11, no. 8, pp. 963–969, 2015.

50. Agarwal, S., X. Zhou, F. Ye, Q. He, G. C. K. Chen, J. Soo, F. Boey, H. Zhang, and P. Chen, "Interfacing live cells with nanocarbon substrates," *Langmuir*, Vol. 26, no. 4, pp. 2244–2247, 2010.

51. Akhavan, O., and E. Ghaderi, "Flash photo stimulation of human neural stem cells on graphene/tio2 heterojunction for differentiation into neurons.," *Nanoscale*, Vol. 5, no. 21, pp. 10316–10326, 2013.

52. Gawande, M. B., and P. S. Branco, "An efficient and expeditious fmoc protection of amines and amino acids in aqueous media," *Green Chemistry*, Vol. 13, no. 12, p. 3355, 2011.

53. Kyte, J., and R. F. Doolittle, "A simple method for displaying the hydropathic character of a protien," *J. Mol. Biol.*, Vol. 157, pp. 105–132, 1982.

54. Cousins, B. G., A. K. Das, R. Sharma, Y. Li, P. Mcnamara, I. H. Hillier, I. A. Kinloch, and R. V. Ulijn, "Enzyme-activated surfactants for dispersion of carbon nanotubes," *Small*, Vol. 5, no. 5, pp. 587–590, 2009.

55. Orbach, R., L. Adler Abramovich, S. Zigerson, I. Mironi-harpaz, and D. Seliktar, "Self-assembled fmoc - peptides as a platform for the formation of nanostructures and hydrogels," *Biomacromolecules*, Vol. 10, pp. 2646–2651, 2009.

56. Frith, W. J., A. M. Donald, D. J. Adams, and A. Aufderhorst-roberts, "Gels formed from amino-acid derivatives , their novel rheology as probed by bulk and particle tracking rheological methods," *Journal of Non-Newtonian Fluid Mechanics*, Vol. 222, pp. 1–8, 2014.

57. Cheng, G., V. Castelletto, C. M. Moulton, G. E. Newby, and I. W. Hamley, "Hydrogelation and self-assembly of fmoc-tripeptides : Unexpected influence of sequence on self-assembled fibril structure , and hydrogel modulus and anisotropy," *Langmuir*, Vol. 10, no. 19, pp. 4990–4998, 2010.

58. Wang, Y., Z. Zhang, L. Xu, X. Li, and H. Chen, "Hydrogels of halogenated fmoc-short peptides for potential application in tissue engineering," *Colloids and Surfaces B : Biointerfaces*, Vol. 104, pp. 163–168, 2013.

59. Jayawarna, V., S. M. Richardson, A. R. Hirst, N. W. Hodson, A. Saiani, J. E. Gough, and R. V. Ulijn, "Introducing chemical functionality in fmoc-peptide gels for cell culture," *Acta Biomaterialia*, Vol. 5, no. 3, pp. 934–943, 2009.

60. Zong, X., N. Kong, J. Liu, W. Yang, M. Cao, and J. J. Gooding, "The influence of graphene on the electrical communication through organic layers on graphite and gold electrodes," *ELECTROANALYSIS*, Vol. 26, pp. 84–92, 2014.

61. Jayawarna, V., M. Ali, T. A. Jowitt, A. F. Miller, A. Saiani, J. E. Gough, and R. V. Ulijn, "Nanostructured hydrogels for three-dimensional cell culture through self - assembly of fluorenylmethoxycarbonyl â dipeptides," *Advanced Materials*, Vol. 18, pp. 611–614, 2006.

62. Liu, S., T. H. Zeng, M. Hofmann, E. Burcombe, J. Wei, R. Jiang, J. Kong, and Y. Chen, "Antibacterial activity of graphite, graphite oxide, graphene oxide, and reduced graphene oxide: Membrane and oxidative stress," *ACS Nano*, Vol. 5, no. 9, pp. 6971–6980, 2011.

63. Weng, Y. J., F. Qi, N. Huang, J. Wang, J. Y. Cheng, and Y. X. Leng, "Photochemical immobilization of bovine serum albumin on ti-o and evaluations in vitro and in vivo," *Applied Surface Science*, Vol. 255, no. 2, pp. 489–493, 2008.

64. Park, J. W., Y. J. Kim, J. H. Jang, T. G. Kwon, Y. C. Bae, and J. Y. Suh, "Effects of phosphoric acid treatment of titanium surfaces on surface properties, osteoblast response and removal of torque forces.," *Acta Materialia*, Vol. 6, no. 4, pp. 1661–1670, 2010.

65. Lei, L., C. Li, P. Yang, and N. Huang, "Photo-immobilized heparin micropatterns on ti-o surface: Preparation, characterization, and evaluation in vitro," *Journal of Materials Science*, Vol. 46, no. 21, pp. 6772–6782, 2011.

66. Weng, Y. J., J. R. Ren, N. Huang, J. Wang, J. Y. Chen, Y. X. Leng, and H. Q. Liu, "Surface engineering of ti-o films by photochemical immobilization of gelatin," *Materials Science and Engineering C*, Vol. 28, no. 8, pp. 1495–1500, 2008.

67. Mi, Y., Z. Wang, X. Liu, S. Yang, H. Wang, J. Ou, Z. Li, and J. Wang, "A simple and feasible in-situ reduction route for preparation of graphene lubricant films applied to a variety of substrates," *Green Chemistry*, Vol. 22, no. 16, p. 8036, 2012.

68. Li, Y., B. G. Cousins, R. V. Ulijn, and I. A. Kinloch, "A study of the dynamic interaction of surfactants with graphite and carbon nanotubes using fmoc-amino acids as a model system," *Langmuir*, Vol. 25, no. 19, pp. 11760–11767, 2009.

69. Riss, T. L., R. A. Moravec, A. L. Nile, H. A. Benink, T. J. Worzella, L. Minor, D. Storts, and Y. Reid, "Cell viability assays assay guidance manual," *Assay Guidance Manual*, pp. 1–23, 2015.

70. Riss, T. L., A. L. Niles, and L. Minor, "Cell viability assays assay guidance manual," *Assay Guidance Manual*, pp. 1–23, 2004.

71. Garipcan, B., S. Odabas, G. Demirel, J. Burger, S. S. Nonnenmann, M. T. Coster, E. M. Gallo, B. Nabet, J. E. Spanier, and E. Piskin, "In vitro biocompatibility of n-type and undoped silicon nanowires," *Advanced Engineering Materials*, Vol. 13, no. 1-2, pp. 3–9, 2011.

72. Adden, N., L. J. Gamble, H. A. Castner, D. G., G. Gross, and B. Forschung, "Phosphonic acid monolayers for binding of bioactive molecules to titanium surfaces.," *Langmuir*, Vol. 19, p. 8197â8204, 2006.

73. Yoon, I. K., J. Y. Hwang, W. C. Jang, H. W. Kim, and U. S. Shin, "Natural bone-like biomimetic surface modification of titanium.," *Applied Surface Science*, Vol. 301, pp. 401–409, 2014.

74. Mani, G., D. M. Johnson, D. Marton, V. L. Dougherty, M. D. Feldman, D. Patel, and C. Mauli Agrawal, "Stability of self-assembled monolayers on titanium and gold.," *Langmuir*, Vol. 24, no. 13, p. 6774â6784, 2008.

75. Bhure, R., T. M. Abdel-Fattah, and A. Mahapatro, "Stability of phosphonic self assembled monolayers (sams) on cobalt chromium (coâcr) alloy under oxidative conditions," *Applied Surface Science*, Vol. 257, no. 13, pp. 5605–5612, 2011.

76. Ramasahayam, S. K., U. B. Nasini, V. Bairi, A. U. Shaikha, and T. Viswanathan, "Microwave assisted synthesis and characterization of silicon and phosphorous co-doped carbon as an electrocatalyst for oxygen reduction reaction," *RSC Adv.*, Vol. 4, pp. 6306–6313, 2014.

77. Metok, N. i., L. Liu, E. Beilis, N. Eliaz, and D. Mandler, "Preparation and characterization of alkylphosphonic acid self-assembled monolayers on titanium alloy by chemisorption and electrochemical deposition.," *Langmuir*, Vol. 30, no. 23, pp. 6791–6799, 2014.

78. Akhavan, O., and E. Ghaderi, "Differentiation of human neural stem cells into neural networks on graphene nanogrids.," *J. Mater. Chem. B*, Vol. 1, pp. 6291–6301, 2013.

79. Boutchich, M., A. Jaffre, D. Alamarguy, J. Alvarez, A. Barras, Y. Tanizawa, R. , Tero, H. Okada, T. V. Thu, K. J. P, and S. A, "Characterization of graphene oxide reduced through chemical and biological processes," *Journal of Physics Conference Series*, Vol. 433, 2013.

80. Bratt, A., and A. R. Barron, "Xps of carbon nanomaterials," *Measurement*, no. 1-16, 2011.

81. Kalaskar, D., R. Ulijn, J. Gough, M. R. Alexander, D. J. Scurr, W. W. Sampson, and S. Eichhorn, "Characterisation of amino acid modified cellulose surfaces using tof-sims and xps," *Cellulose*, Vol. 17, pp. 747–756, 2010.

82. Yu, J.-C., F.-G. Zhao, W. Shao, C.-W. Ge, and W.-S. Li, "Shape-controllable and versatile synthesis of copper nanocrystals with amino acids as capping agents," *Nanoscale*, Vol. 7, pp. 8811–8818, 2015.

83. Hardcastle, F., "Raman spectroscopy of titania (tio2) nanotubular water splitting catalysts," *Journal of the Arkansas Academy of Science*, Vol. 65, 2011.

84. Henderson, M., A. Gibaud, J.-F. Bardeau, and J. White, "An x ray reflectivity study of evaporation induced self-assembled titania based films," *J. Mater. Chem.,*, Vol. 16, pp. 2478–2484, 2006.

85. Cai, C.-J., M.-W. Xu, S.-J. Bao, C.-C. Ji, Z.-J. Lu, and D.-Z. Jia, "A green and facile route for constructing flower shaped tio2 nanocrystals assembled on graphene oxide sheets for enhanced photocatalytic activity," *Nanotechnology*, Vol. 24, no. 27, p. 275602, 2013.

86. Sobon, G., J. Sotor, J. Jagiello, R. Kozinski, M. Zdrojek, M. Holdynski, P. Paletko, J. Boguslawski, L. Lipinska, and K. M. Abramski, "Graphene oxide vs reduced graphene oxide as saturable absorbers for er-doped passively mode-locked fiber laser.," *Optics Express*, Vol. 20, no. 17, pp. 19463–19473, 2012.

87. Wojtoniszak, M., X. Chean, R. J. Kalenczuk, A. Wajda, J. Lapczuk, M. Kurzewski, M. Drozdzik, P. K. Chu, and E. Borowiak-Palena, "Synthesis, dispersion, and cytocompatibility of graphene oxide and reduced graphene oxide," *Colloids and Surfaces B: Biointerfaces*, Vol. 89, pp. 79–85, 2012.

88. Miroshnikov, Y., G. Grinbom, G. Gershinsky, G. D. Nessim, and Z. David, "Do we need covalent bonding of si nanoparticles on graphene oxide for li - ion batteries?," *The Royal Society of Chemistry*, Vol. 173, pp. 391 – 402, 2014.

89. Wolf, R., and A. C. Sparavigna, "Role of plasma surface treatments on wetting and adhesion," *Engineering*, Vol. 2, no. 6, 2010.

90. Oberg, E., "Machineryâs handbook 29th ed.," p. 324, 2012.

91. Ou, J., J. Wang, S. Liu, B. Mu, J. Ren, H. Wang, and S. Yang, "Tribology study of reduced graphene oxide sheets on silicon substrate synthesized via covalent assembly," *Langmuir*, Vol. 26, no. 20, pp. 15830–15836, 2010.

92. Kowalski, K., I. Glazowska, and Z. Gora, "Electrochemical formation of bioactive surface layer on titanium," *Journal of Achievements in Materials and Manufacturing Engineering*, Vol. 18, no. 1, p. 147â150, 2006.

93. Catetoa, C. A., and A. Ragauskas, "Amino acid modified cellulose whiskers," *RSC Adv.*, Vol. 1, pp. 1695–1697, 2011.

94. Terzyk, A. P., "The influence of activated carbon surface chemical composition on the adsorption of acetaminophen (paracetamol) in vitro part ii. tg, ftir, and xps analysis of carbons and the temperature dependence of adsorption kinetics at the neutral ph," *Colloids and Surfaces A: Physicochemical and Engineering Aspects*, Vol. 177, pp. 23–45, 2001.

95. Feng, W., W. Luoa, and Y. Fenga, "Photo-responsive carbon nanomaterials functionalized by azobenzene moieties: structures, properties and application," *Nanoscale*, Vol. 4, no. 20, pp. 6118–6134, 2012.

96. Teng, C.-C., C.-C. M. Ma, C.-H. Lu, S.-Y. Yang, S.-H. Lee, M.-C. Hsiao, M.-Y. Yen, K.-C. Chiou, and T.-M. Lee, "Thermal conductivity and structure of non-covalent functionalized graphene/epoxy composites," *Carbon*, Vol. 49, pp. 5107–5116, 2011.

97. Papagelis, K., M. Kalyva, D. Tasis, J. Parthenios, A. Siokou, and C. Galiotis, "Covalently functionalized carbon nanotubes as macroinitiators for radical polymerization," *Physica status solid (b)*, Vol. 244, no. 11, pp. 4046–4050, 2007.

98. Choi, E.-Y., T. H. Han, J. Hong, J. E. Kim, S. H. Lee, H. W. Kima, , and S. O. Kim, "Noncovalent functionalization of graphene with end-functional polymers," *J. Mater. Chem.,*, Vol. 20, pp. 1907–1912, 2010.

99. Kim, M., N. S. Safron, C. Huang, M. S. Arnold, and P. Gopalan, "Light-driven reversible modulation of doping in graphene," *Nano Lett.*, Vol. 12, no. 1, pp. 182–187, 2012.

100. Piao, L., Q. Liu, Y. Li, and C. Wang, "Adsorption of l-phenylalanine on single-walled carbon nanotubes," *J. Phys. Chem. C*, Vol. 112, no. 8, pp. 2857–2863, 2008.

101. Thevenot, P., W. Hu, and L. Tang, "Surface chemistry influenc implant biocompatibility," *Curr Top Med Chem.*, Vol. 8, no. 4, pp. 270–280, 2008.

102. Li, J., N. Kawazoe, and G. Chen, "Gold nanoparticles with different charge and moiety induce differential cell response on mesenchymal stem cell osteogenesis," *Biomaterials*, Vol. 54, pp. 226–236, 2015.

103. Zhao, C., X. Lu, C. Zanden, and J. Liu, "The promising application of graphene oxide as coating materials in orthopedic implants: preparation, characterization and cell behavior," *Biomed. Mater.*, Vol. 10, no. 1, p. 15019, 2015.

104. Depan, D., B. Girase, J. Shah, and R. Misra, "Structue process property relationship of the polar graphene oxide-mediated cellular response and stimulated growth of osteoblasts on hybrid chitosan network structure nanocomposite scaffolds," *Acta Biomateria*, Vol. 7, no. 9, pp. 3432–3445, 2011.

105. Keselowsky, B. G., D. M. Collard, and A. J. Garcia, "Surface chemistry modulates fibronectin conformation and directs integrin binding and specificity to control cell adhesion," *J Biomed Mater Res A*, Vol. 66, no. 2, pp. 247–259, 2003.

106. Mattila, P. K., and P. Lappalainen, "Filopodia: molecular architecture and cellular functions," *Nat. Rev. Mol. Cell. Bio.*, Vol. 9, no. 6, pp. 446–454, 2008.

107. Le Clainche, C., and M.-F. Carlier, "Regulation of actin assembly associated with protrusion and adhesion in cell migration," *Physiol Rev.*, Vol. 88, no. 2, pp. 489–513, 2008.